Synthesis and Characterization of Host-Guest Complexes: Metal-Organic Nanocapsules Using Aryl-Substituted Pyrogallol[4]arenes

---

A Dissertation

Presented to

The Faculty of the Graduate School

University of Missouri-Columbia

In Partial Fulfillment

Of the Requirements for the Degree

Doctor of Philosophy

By

Andrew K. Maerz

Dr. Jerry L. Atwood, Dissertation Supervisor

July 2011

The undersigned, appointed by the dean of the Graduate School, have examined the dissertation entitled

Synthesis and Characterization of Host-Guest Complexes: Metal-Organic Nanocapsules Using Aryl-Substituted Pyrogallol[4]arenes

Presented by **Andrew K. Maerz**

A candidate for the degree of doctor of philosophy of **Chemistry**,

And hereby certify that, in their opinion, it is worthy of acceptance

Professor Jerry L. Atwood (CHAIR)

_____

Professor Peter A. Tipton (OUTSIDE MEMBER)

_____

Professor Jason W. Cooley (MEMBER)

_____

Professor Carol A. Deakyne (MEMBER)

_____

Professor Paul A. Sharp (MEMBER)

_____

ACKNOWLEDGMENTS

TABLE OF CONTENTS

2 Synthesis and Characterization of Aryl-substituted Pyrogallol[4]arenes

3 Formation of Metal-Organic Nanocapsules (MONCs) Through Conformational Flipping

4 The Use of Mixed Macrocycles in New and Diverse Supramolecular Architecture Via Solvent Mediation

LIST OF TABLES

LIST OF FIGURES

LIST OF SCHEMES

ABSTRACT

The desire to synthesize and control self-assembly of molecular nanocapsules has long been a focus within the supramolecular community due to the nanocapsules' potential applications as tools for encapsulation and delivery of host molecules, catalytic media sites, and gas sorption agents. Resorcin[4]arenes (RsC) and pyrogallol[4]arenes (PgC) have received considerable attention due to their preference to form the all-*cis* cone-shaped (*rccc*) structure, thus allowing dimeric and hexameric nanocapsule formation through complementary and structurally distinct intermolecular hydrogen bonding interactions or metal coordination. However, the preference of pyrogallol[4]arenes to form these *rccc* all-*cis* "bowl-like" structures only holds true for alkyl-substituted analogs, which lack cooperative intermolecular hydrogen bonding and aryl-group π-π interactions.

By changing the lower rim R-group, one drastically alters the chemical environment. *C*-arylresorcin[4]arenes, for example, adopt a more kinetically stable *cis-trans-trans* chair stereostructure (*rctt*), but show interconversion to the thermodynamic product, the all-*cis rccc* cone. In contrast, our studies of the *C*-arylpyrogallol[4]arenes unexpectedly suggest that the *cis-trans-trans* chair stereostructure is the thermodynamic product.

Taking advantage of the generally favorable shape of the alkyl-substituted PgC macrocycle, researchers have combined zinc complexes with these cone-shaped macrocycles to produce dimeric metal-seamed nanocapsules. However, due to the lack of conformational control and the unfavorable self-assembly associated with the *rctt* chair stereoisomer of PgC, it has attracted significantly less attention in subunit

architectural design. Herein, we show that complexation of zinc and *C*-phenylpyrogallol[4]arene, as well as other benzyl derivatives, induces a conformational flip in these macrocycles from chair to cone. This formation of the zinc-seamed metal-organic nanocapsules has been tracked via NMR, X-ray Diffraction and Mass Spectroscopy studies. The results yield several important trends that can be applied towards both the study of supramolecular self-assembly and the utilization of these host-guest capsular entities for other purposes.

1 Supramolecular Chemistry: The Art of Self-Assembly and Interaction

1.1 Supramolecular Chemistry: By the Book

Supramolecular chemistry has been defined in several different ways over the years. Perhaps it was Jean-Marie Lehn, a Nobel Prize winner in 1987, who best described supramolecular chemistry as being the "chemistry of molecular assemblies and the intermolecular bond,"[1] which has come to be known as "chemistry beyond the molecule."[2] These types of interactions, non-covalent interactions, help direct the self-assembly of unique architectures that would otherwise be difficult to obtain through standard synthetic methods. One needs to only look at nature for confirmation of the complexity of supramolecular chemistry and the usefulness of understanding and exploiting self-assembly. DNA and spherical viruses are examples of natural self-assembly,[3] with the latter framework possessing a cavity capable of entrapment of specific molecular sized guests.

As much a function of pure serendipity as it is a product of novel chemistry, self-assembly and molecular recognition often occur without prior planning. That is, instructions for assembly are written within the shapes of the subunits.[4] Many scientists hesitate to give credit to these "by chance" discoveries for fear of a misrepresentation of the experimental preparation; however, Louis Pasteur once said, "chance favors the prepared mind." By taking that same mentality, researchers in the field of supramolecular chemistry are pushing forward, hoping that through experiment, and a bit of luck, one might harness the intricacies of self-assembly and in doing so gain an understanding of this otherwise unpredictable phenomenon.

If we consider supramolecular chemistry as the act of binding through non-covalent interactions or complexation events, we must first identify what is doing the bonding and to what it is being bound. In this context a molecule (the 'host'), normally a large molecule possessing a sizeable, central hole or cavity, is bound to a uniquely different molecule (a 'guest'), a relatively small-sized species such as a monatomic cation, a simple inorganic anion, or ion pair, creating what is known as a host-guest complex or *supramolecule*. These host-guest complexes are held together by a variety of unique structural relationships, but not, however, by fully covalent bonding between them. Donald Cram defined the host-guest relationship as "molecular complexes which are usually held together by hydrogen bonding, ion pairing, π-acid to π-base interactions, metal-to-ligand binding, van der Waals attractive forces, solvent reorganization, and by partially made and broken covalent bonds." [5]

There are two major classes of hosts within host-guest chemistry, *clathrands* and *cavitands*, both of which are worth defining at this point. Clathrands (**Figure 1.1**) contain extramolecular cavities (the gap between two or more host molecules) where guest interaction is limited to the solid state. An example of a *clathrate*, a clathrand host-guest complexe, is cyclotriveratrylene (CTV) with water. On the other hand, cavitands are hosts possessing permanent cavities which are accessible for guest interaction in both the solution phase and solid state. These molecular containers have an intrinsically curved, concave surface which is generally open at one end allowing for guest interaction, with the resultant complex known as a *cavitate* or *caviplex*. An example of a caviplex is *C*-tert-butylcalix[4]arene with toluene. To summarize, small molecules or subunits combine to form macrocycles or cavitands that combine with guests to form

host-guest complexes or caviplexes.
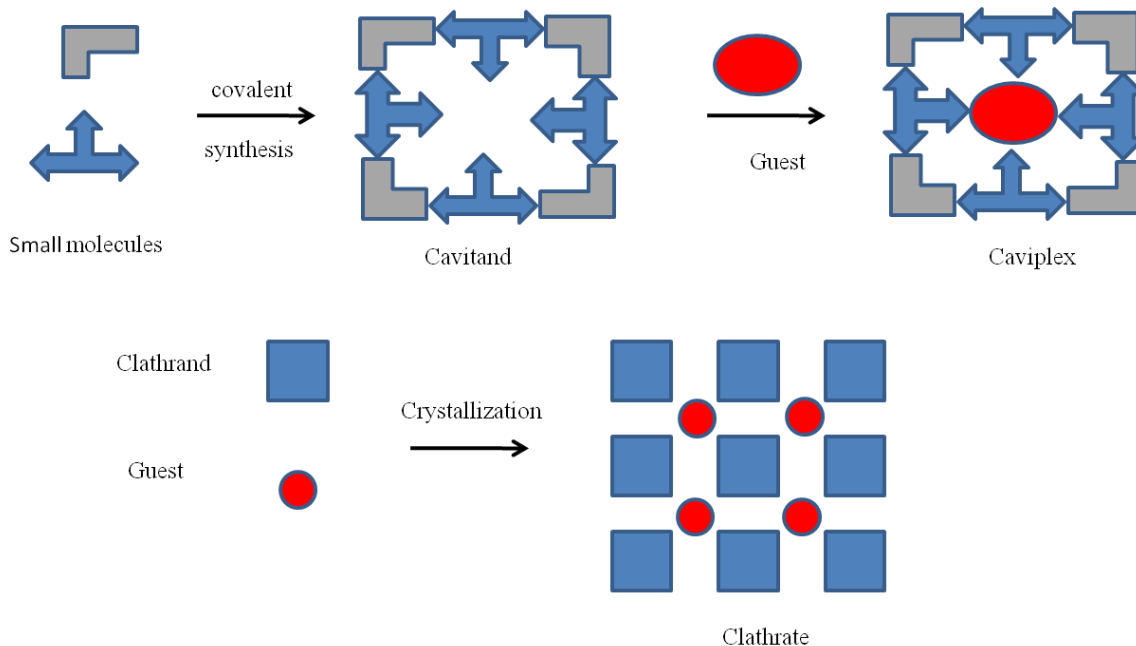
Figure 1.1: a) Schematic representation of the complexation of cavitands into an inclusion host-guest complex known as a caviplex. b) Schematic representation of the complexation of clathrands into an inclusion host-guest complex known as a clathrate, where the gaps between clathrands create the cavity only accessible in the solid-state.

1.1.1 Preorganization and Complementarity

Many of the leading researchers in the area of supramolecular chemistry have found it helpful to assign macrocycles, created synthetically for specific applications, as simple geometric objects in order to determine molecular architecture. It has been said that size, shape, and complementarity are key factors in engineering suitable macrocycles

for self-assembly and host-guest complexation.[6] Molecular architecture, coupled with complementarity, has allowed for increased ease in selection of macrocycles for a particular purpose. Indeed, we see the products of this concept in everyday use: when we look at a basketball and see two hemispheres; when we look at a tennis ball or baseball and see two flexible linear units combining; or when we look at DNA and see two helical strands coming together to form a double helix of complementary base pairs. On a molecular scale, cyclodextrins and calix[4]arenes can likewise act as simple hemispheres or cones, while diphenylglycolurils can act as flexible linear units forming both chemical "basketballs" and chemical "tennis balls".

With respect to host-guest complexation, host preorganization is another important factor. The macrocyclic effect relates not only to chelation of guest by multiple binding sites, but also to the organization of these binding sites prior to guest complexation, known as preorganization.[2] When looking at the noncyclic podands (**Figure 1.2a**) versus the monocyclic corands (**Figure 1.2b**), increased preorganization is responsible for a 10^4 increase in host-guest stability from the podand to the corand, while keeping an equal number of binding sites per host. Similarly, bicyclic hosts such as cryptands (**Figure 1.2d**) are found to be more stable than the monocyclic corands (**Figure 1.2c**). This effect is known as the macrobicyclic effect and is a function of the more rigid, more preorganized macrobicycle. However, increased rigidity and preorganization can lead to slower guest binding kinetics. On the other hand, the faster rate of guest binding for conformationally mobile hosts is accompanied by a faster rate of decomplexation. As with all macrocyclic engineering, the trick is to find the best of both worlds: a rigid yet flexible host allowing for faster guest kinetics and an increase in complex stability.
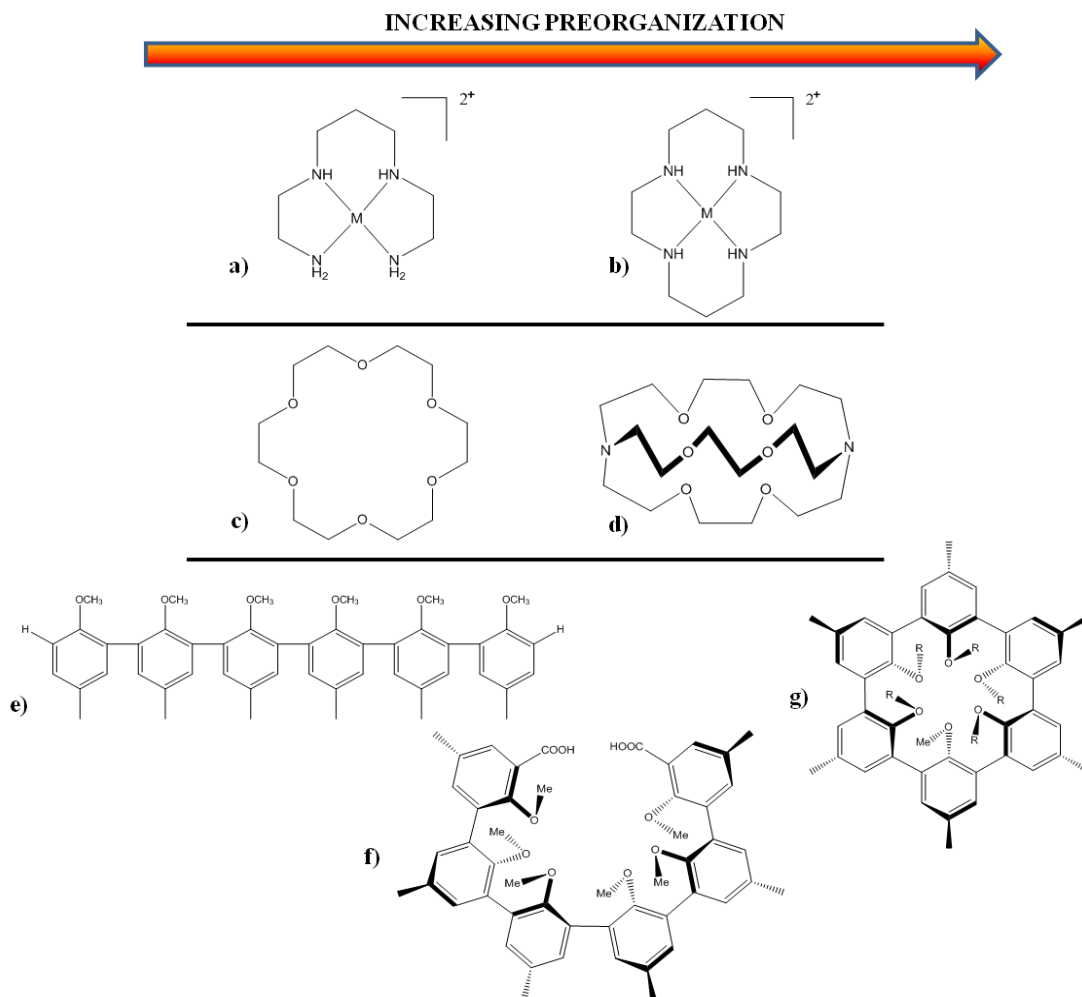
Figure 1.2: Comparison of preorganization effects: **a)** vs. **b)**, macrocyclic; **c)** vs. **d)**, macrobicyclic; and **e)** vs. **f)** vs. **g)**, complementarity.

1.1.2 Building blocks in host-guest chemistry

Several different building blocks have been structurally and functionally well studied to gain further synthetic control over much larger, more complicated architectures. Cyclodextrins, glycourils, triethylbenzenes and kohnkenes are all examples of cavitands capable of forming inclusion complexes and filling a unique role in

supramolecular chemistry. It is important to note that the chemistry of cavitands demonstrates that as the cavity becomes deeper and more rigid, its ability to form caviplexes in solution is enhanced.

When engineered properly for guest complexation, these supramolecular building blocks have a propensity to form inclusion complexes with cationic, anionic, and neutral species, thus giving rise to the use of the building blocks in sensor applications for environmental and biological processes.[7] For example, anionic pollutants such as phosphates, nitrates, and pertechnetate can cause serious harm to the surrounding environment and, therefore, there is a large demand for production of selective anionic receptors.[15] Indicator-displacement assays (IDAs) using triethylbenzene host compounds have proven useful in the detection of analytes[8] such as gallic acid,[9] asparartate,[10] inorganic phosphates,[11] nitrate,[12] citrate,[13] heparin,[14] and tartrate.[15]

1.1.2.1 Cyclodextrins

Cyclodextrins (CDs) are produced from starch by means of enzymatic conversion and typically consist of six (6) (α), seven (7) (β), or eight (8) (γ) glucopyranoside units attached by α-1,4-linkages[16] (**Figure 1.3**). Cyclodextrins have a unique truncated funnel or tapering torus form, which allows for easy host-guest complexation. The empty interior of these host molecules, which is highly hydrophobic, can be accessed by a variety of small guest species, ranging from polar compounds such as alcohols to apolar aliphatic and aromatic hydrocarbons,[17] in either solution or the solid state. Key characteristics of cyclodextrins are given in **Table 1.1**.

Because of cyclodextrin's nontoxicity over a wide range of doses, cyclodextrins have a wide range of applications in the food, cosmetics and pharmaceutical industries.[2] However, because of the weak binding affinity of several pharmaceutical agents to single CDs, research has turned to modification of CDs from monomeric inclusion compounds to dimeric inclusion compounds,[18] polyrotoxanes,[19] and amphiphilic cyclodextrins.[20]
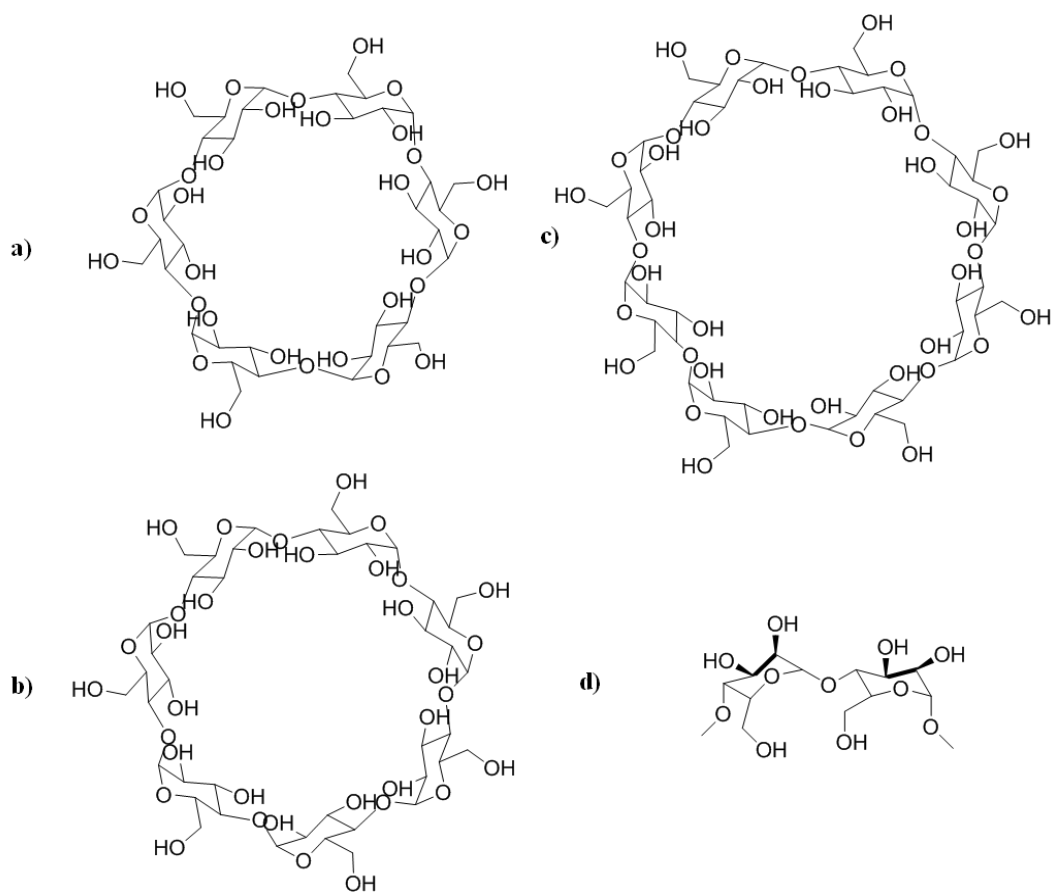
Figure 1.3: a-c) α,β,γ-cyclodextrins consisting of six (6), seven (7), and eight (8) glucose units, respectively. d) 1,4-glycosidic link which joins adjacent D-glucopyranoside units.

Table 1.1: Key characteristics and parameters of α-, β-, and γ-cyclodextrins.[2]

	α	**β**	**γ**
Number of Glucose Units	6	7	8
Internal Cavity Diameter (Å)	4.7-5.3	6-6.6	7.5-8.3
Cavity Volume ($Å^3$)	174	262	427
Common Guest	Benzene, phenol	Naphthalene, 1-amino-8-napthalenesulfonate	Anthracene, crown ethers

1.1.2.2 Gylcoluril-Based Hosts (Specifically Cucurbiturils)

Molecules possessing a funnel shaped architecture are not the only useful three-dimensional building blocks in supramolecular chemistry. Flexible linear subunits such as diphenylglycoluril, a glycoluril-based subunit (**Figure 1.4**), take advantage of multiple hydrogen-bonding interactions to form self-complementary tennis ball assemblies consisting of two intrinsically curved sections.[21]

Cucurbiturils (CB[n]), another gylcoluril-based host composed of *n* glycoluril units (**Figure 1.5**), are thought to occur through a template reaction in which oxonium ions hydrogen bond to the carbonyl groups. Unlike cyclodextrins, cucurbiturils form "barrel-shaped" architectures, capable of forming inclusion complexes with both polar and nonpolar guests. The hydrophobic interior serves as an inclusion site for nonpolar molecules, whereas the polar ureido carbonyl groups allow binding of ions and molecules through charge-dipole and hydrogen-bonding interactions.[22] The cavity of cucurbituril molecules has nanoscale dimensions, which leads to their application as supramolecular host molecules, rotaxane macrocycles,[23] and drug delivery vehicles.[24]
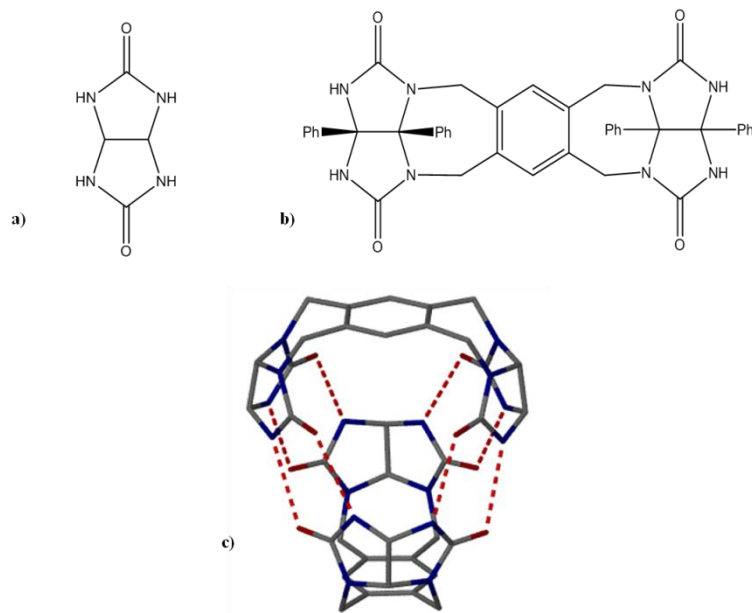
Figure 1.4: Schematic representation of a) glycoluril and b) diphenylglycoluril. c) Crystallographic image of a hydrogen-bonded dimeric sphere based on two (2) diphenylglycoluril units; guest H_2O molecule omitted for clarity.[16]
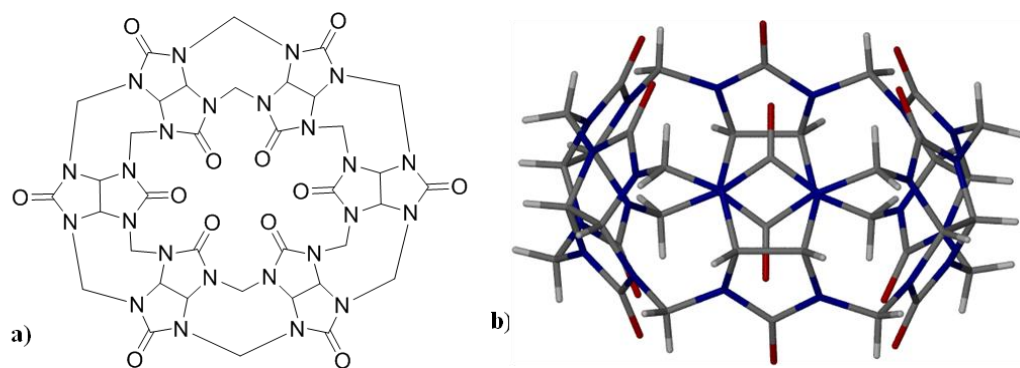
Figure 1.5: a) Schematic representation of a cucurbituril with six (6) glycoluril base units (CB[6]). b) Crystallographic image of CB[6] showing the guest accessible cavity of 5.8 Å in diameter.[19] O: red, C: grey, H: white.

1.1.2.3 1,3,5-triethylbenzene "pinwheel"

Using tripodal hosts (**Figure 1.6**) based on a 1,3,5-trisubstituted-2,4,6- trimethyl- or triethylbenzene scaffold, in which the 1,3,5 positions are directed to one face of the ring, has proven extremely effective at selective anion binding.[15] This rigid and reorganizable scaffold allows for easy alterations at the 1,3,5 positions, depending on the desired application or desired anionic target guest. Due to an enhanced positive charge,
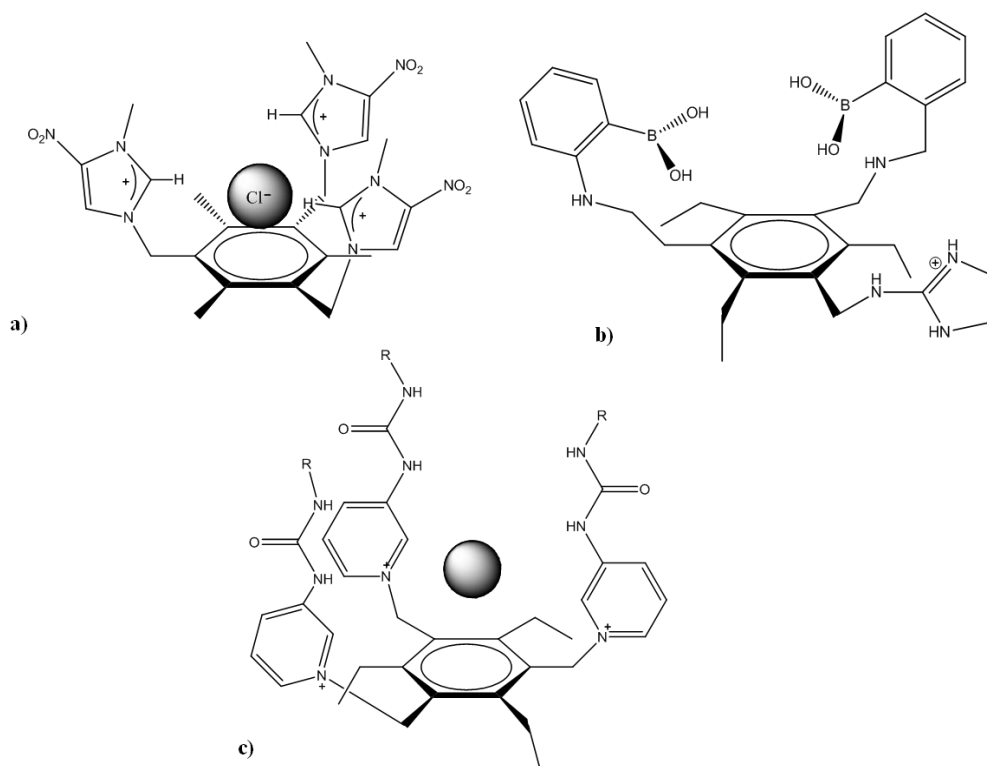
Figure 1.6: Schematic representation of tripodal anionic receptors using a 1,3,5-trisubstituted-2,4,6-trimethyl- or triethylbenzene scaffold. a) Uses three imidazolium rings to enhance binding of anionic guests, b) Uses boronic acid for use in IDAs, c) Uses tripodal tris(urea) cationic receptors for anionic sensors.

specific imidazole derivatives have proven to be highly selective for the chloride over the bromide and iodide anions. The enhanced charge is caused by the addition of a nitro group on the imidazolium ring, which strengthens the $(C-H)^+ \cdots X^-$ electrostatic interaction.[24] Tripodal cationic receptors containing 1-pyridin-3-yl-3-*p*-tolyl-urea (TUP) or 1-octyl-3-pyridin-3-ylurea (OUP) show chemical communication between host and guest, whereby the host geometry is anion dependent and conformationally flexible.[25]

1.1.2.4 Kohnkene

While the previously discussed supramolecular building blocks have been studied in great detail, another less studied group of curved building blocks, the kohnkenes, merits discussion. Kohnkenes (**Figure 1.7**), derived from the reaction of 1,2,4,5-tetrabromobenzene with furan, have a very rigid structure containing an elliptical cavity. However, while the deoxygenated dideoxykohnkene gives rise to an inclusion complex with one water molecule, the standard kohnkenes' small elliptical cavity is unsuitable for guest inclusion, illustrating the difficulty of engineering hosts for host-guest complexation.[2]
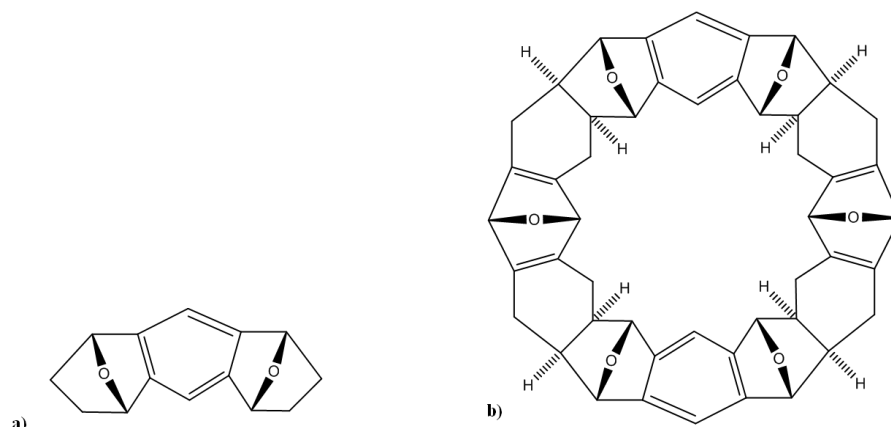
Figure 1.7: Schematic representation of a) kohnkene precursor b) kohnkene.[26]

1.1.2.5 Cyclophanes

Much of the work involving supramolecular host-guest systems has gone into the study of cyclophanes, a group of fused aromatic ring systems, in part due to their unique electronic and structural properties. By definition, cyclophanes must contain at least one macrocyclic ring and achieve closure by some means of curvature. Examples of such supramolecular hosts can be found throughout the scientific literature;[27,28] however, for the sake of comparison, this text will focus on cyclotriveratrylenes (CTV) and calix[4]arenes. One must define cyclophane nomenclature when discussing these supramolecular hosts. In general, any aromatic ring bridged by at least one aliphatic *n*-membered bridge, with *n* ≥ 0, is termed a cyclophane. The number of atoms, *n*, in each bridge is denoted in square brackets before the name. CTV and calix[4]arenes contain a methyl bridge and thus would be appropriately named [1.1.1]orthocyclophane and [1.1.1.1] metacyclophane.

1.1.2.5.1 Cyclotriveratrylenes (CTVs)

Cyclotriveratrylenes are a versatile and readily prepared saucer-shaped supramolecular building block, derived from the acid-catalyzed condensation of formaldehyde and veratrole.[29] CTVs have been studied extensively due to their propensity to form inclusion complexes of the channel variety. They do not exhibit significant binding of small neutral guests; however, larger guests such as buckminsterfullerenes and spherical carboranes show a high affinity for the inherent voids in the solid lattice[30] as well as significant solution binding in non-aqueous solvents.[2]   Because of the limited number of guest molecules acceptable for guest inclusion, application of CTVs in selective isolation of C_{60} and C_{70} from crude mixtures has proven useful and has opened the door to such processes by other macrocycles.

While the isolation of fullerenes is significant, in order to increase the relevance of CTVs as host molecules, it is necessary to expand the molecular cavity to allow for a greater diversity of guest inclusion. Such an expansion has been accomplished by Cram *et al.,*[31] who have synthesized a range of CTV-based cavitands (**Figure 1.8**). While expanding the cavity can lead to an increase in the solution-phase binding of such guests as dimethyl chloride, host-guest affinity can also be enhanced by formation of three-dimensional cryptands.[2]
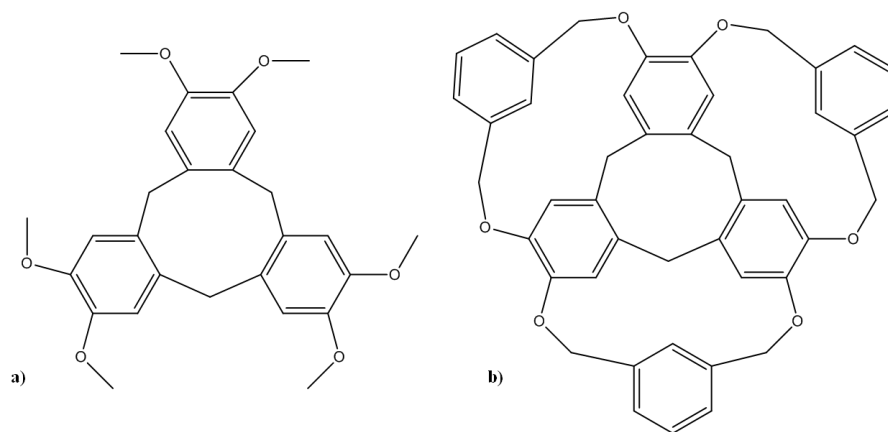
Figure 1.8: Schematic representation of a) cyclotriveratrylene (CTV) and b) expanded CTV-based cavitand.

1.1.2.5.2 Calix[4]arenes

Phenol-formaldehyde chemistry began over a century ago with the work of Adolph von Baeyer[37] and has continued with significant contributions from brilliant chemists along the way. While phenol-formaldehyde chemistry started in the 1870's, it was not until Zinke and Ziegler, in the 1940's, decided to simplify the chemistry by only using *para*-substituted phenols and formaldehyde that the chemistry really started to accelerate. While direct structural elucidation of their products from phenol-formaldehyde condensation could not be determined due to the infancy of both XRD and NMR methods, Zinke's compounds[32] coincided with Niederl and Vogel's proposed cyclic tetramers,[33] and thus, Zinke is given credit for the first synthesis of calix[4]arenes. Later Cornforth and coworkers[34] investigated the strange presence of two distinct compounds, based on different melting points, and suggested the existence of four diastereoisomers, known today as conformers, of the cyclic tetramer (**Figure 1.9**).
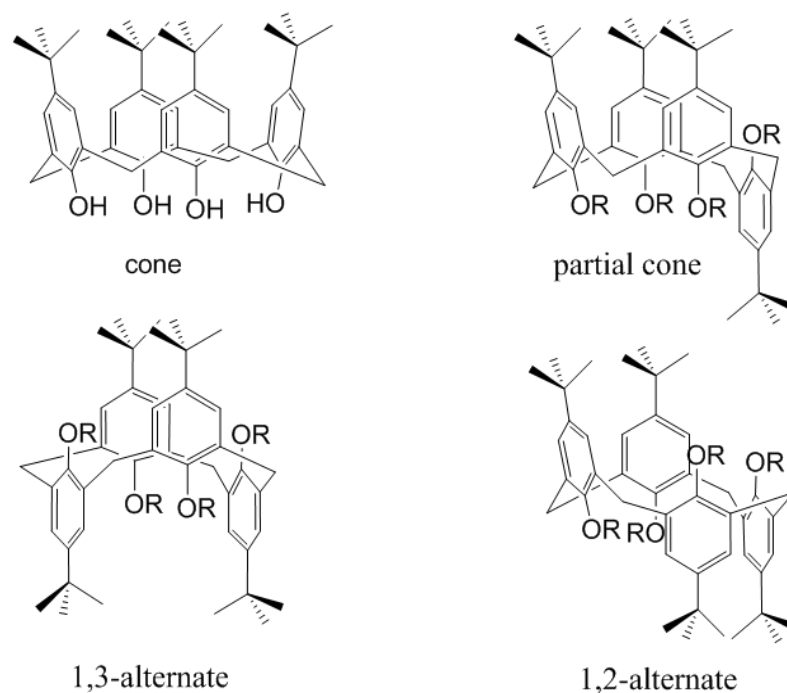
Figure 1.9: Possible conformations of calix[4]arenes.

It was not until the mid 1970's that Gutsche e*t al.*[35] characterized the three major cyclic products in the reaction mixture as a tetramer, a hexamer, and an octamer, with the pentamer and heptamer being minor products.[36] Gutsche also provided the current nomenclature for this group of macrocycles as calix[*n*]arenes[37] (based from the Greek work calyx, meaning "vase" or "chalice"). Here *n* refers to the number of phenolic units within the structure (**Figure 1.10a-d**). Several research groups have gone on to study the functionality of calix[n]arenes,[38] but the remainder of this chapter will focus on their host-guest chemistry.
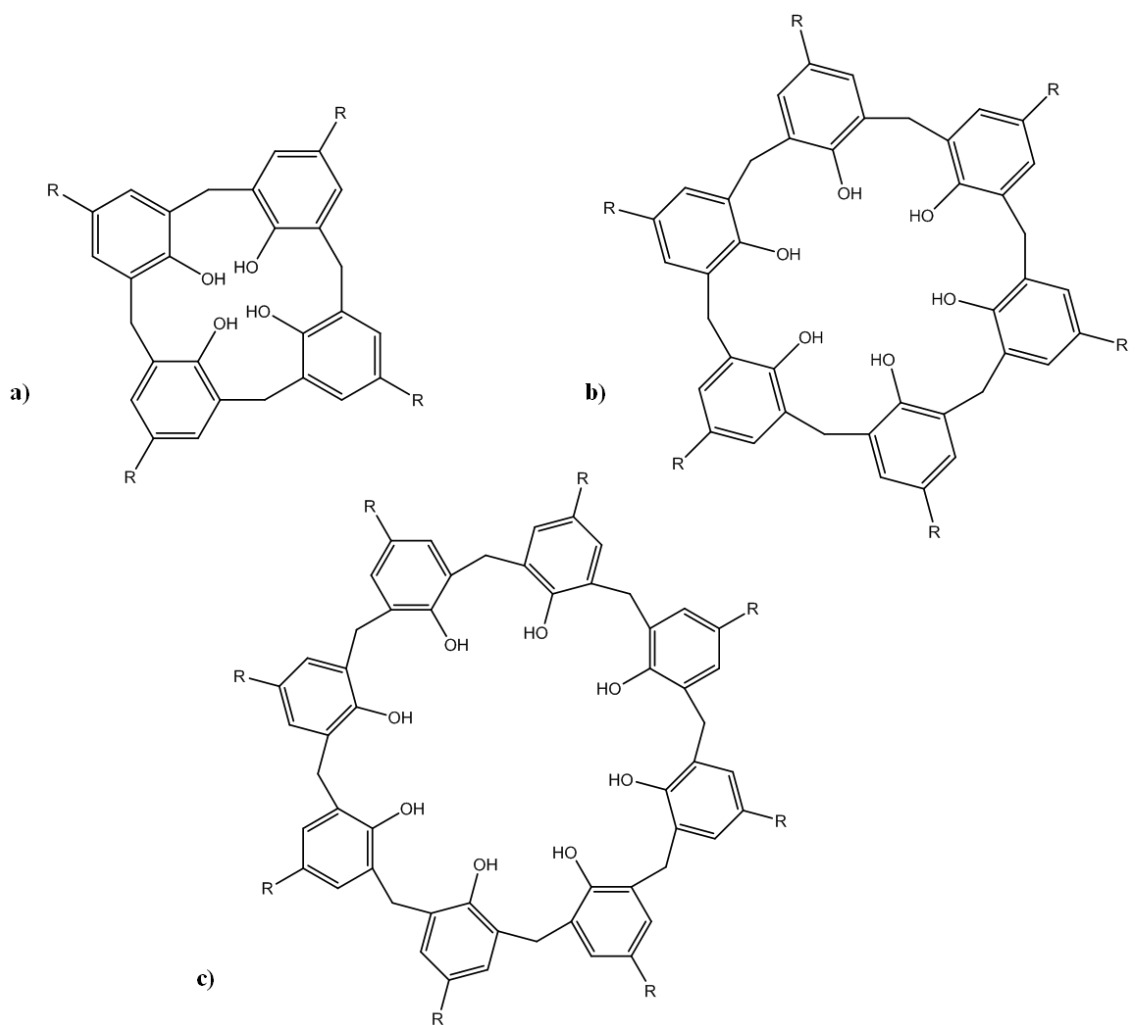
Figure 1.10: Commonly occurring members of the calixarene family: a) calix[4]arene, b) calix[6]arene, and c) calix[8]arene.

Calix[*n*]arenes, specifically calix[4]arenes, have generated significant attention with respect to their host-guest chemistry, due to both the size of the inherent cavity and strong macrocycle-to-macrocycle and macrocycle-to-guest intermolecular forces. It is important to note that while there is interesting host-guest complexation in the solid state, there is little evidence of significant binding of neutral, underivatized calix[4]arenes to

molecular guests in non-aqueous solution.[6] There are, however, several examples of solution-phase complexes with aromatic, aliphatic, and charged guests, in which weak C–H···π,[39] π-π,[40] and cation-π[41-43] interactions stabilize the overall complex.   Simple   1:1 host-guest complexes have been studied for calix[4]arenes and their derivatives resorcin[4]arenes and pyrogallol[4]arenes, due to possible applications in gas storage,[44] catalysis,[45] and sensing.[46-49] However, it is the ability of these arenes to form larger supramolecular entities such as dimeric,[50] trimeric,[51] and hexameric[52] nanostructures that has garnered most of the attention (**Figure 1.11**).

My work has focused on the 1:1 host-guest complexes and larger supramolecular asssemblies formed by resorcin[4]arenes and pyrogallol[4]arenes. These arenes are composed of 1,3-dihydroxy benzenes and 1,2,3-trihydroxybenzenes, respectively. Pyrogallol[4]arenes, in particular, have been investigated much less extensively than have the calixarenes.
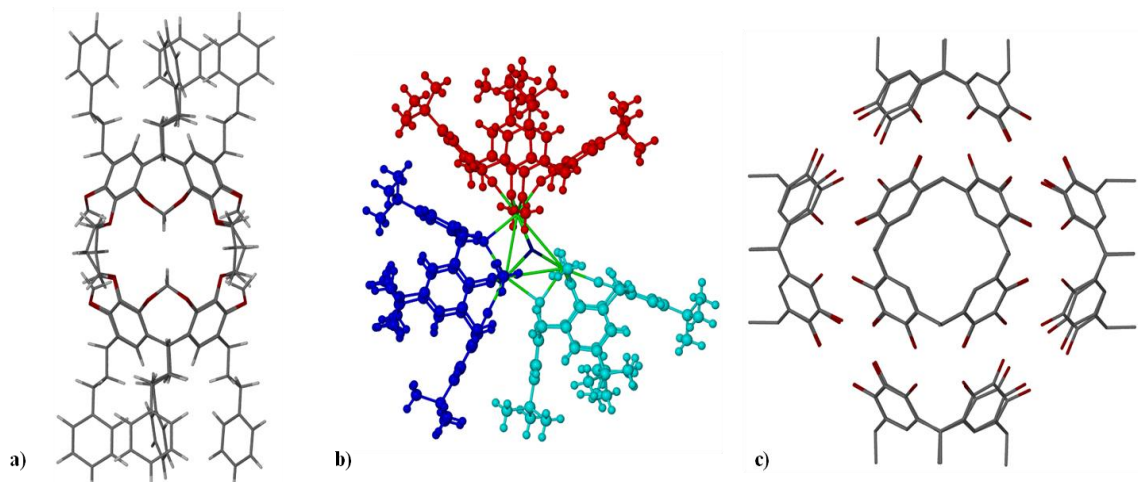
Figure 1.11: a) Crystallographic image of covalently linked dimeric calixarenes. b) Crystallographic image of a trimeric superstructure consisting of three (3) calixarenes, shown in red, blue, and turquoise, linked by samarium in green. c) Hexameric superstructure consisting of six (6) resorcin[4]arenes.

1.2 The Glue that Holds Supramolecular Chemistry Together: Non-covalent Interactions

As previously mentioned, non-covalent interactions are the backbone of supramolecular chemistry. The term "non-covalent" encompasses a wide range of attractive and repulsive forces. These forces are vital to understanding supramolecular complexes, especially host-guest interactions, and must be considered when looking at the stability of the superstructure as a whole. In most cases, individually these non-covalent interactions are weak; however, supramolecular chemistry, and more specifically self-assembly, displays extreme cooperativity by summing up all parts to form powerful overall interactions. Electrostatic (static model) (*i.e.* ion pairing, ion-

18

dipole, and dipole-dipole), induced-dipole, ion-π, hydrogen bonding, and van der Waals interactions will be discussed throughout the text.

1.2.1 Static Model Electrostatic Interactions

The static model of electrostatic interactions considers only coluombic attraction or repulsion between full or partial charges that existed prior to the interaction. Also, the charges remain unchanged after interaction.[53] Thus, ion-ion, ion-dipole, and dipole-dipole interactions all fall within the static model.

Ion pairing is said to exist when a cation and anion are close enough that the energy associated with the electrostatic interaction is stronger than the thermal energy required to separate the ions. While there are several factors that influence the electrostatic interaction energy, solvent properties and the size and shape of the anion and cation play the largest roles.[6] The binding affinity between an anion and a cation ranges from 100-350 kJ/mole. These interactions are by far the strongest of the non-covalent interactions and can be comparable in strength to covalent bonds. Ion-ion interactions play an important role in such host-guest complexes as 1,3,5-trisubstituted-2,4,6-triethylbenzene with halides and tris(diazabicylooctane) with the $[Fe(CN)_6]^{3-}$ anion. .

Ion-dipole interactions can occur when a charged species is dissolved in a polar solvent or when a macrocycle plays the same role as the polar solvent. The strengths of these interactions range between 50-200 kJ/mole. Examples of such interactions are seen between Na^+ and water or crown ethers (**Figure 1.12a**). While these interactions are common in host-guest chemistry, ion-dipole interactions also include coordinative

(dative) bonds found in organometallic complexes such as $[Pd(en)]^{2+}$ (**Figure 1.12b**) or

$[Ru(bpy)_3]^{2+}$ (**Figure 1.12c**).

Polar molecules possess partial positive and negative charges and can align in two

fashions. The alignment of oppositely charged ends from a single pair of dipoles on

adjacent molecules leads to type 1 dipole-dipole interactions (**Figure 1.12d**). The type 2

interactions occur when the partial charges of two parallel dipoles are aligned in opposing

directions (**Figure 1.12e**). The bonding energies associated with these dipole-dipole

interactions lie between 5-50 kJ/mole.
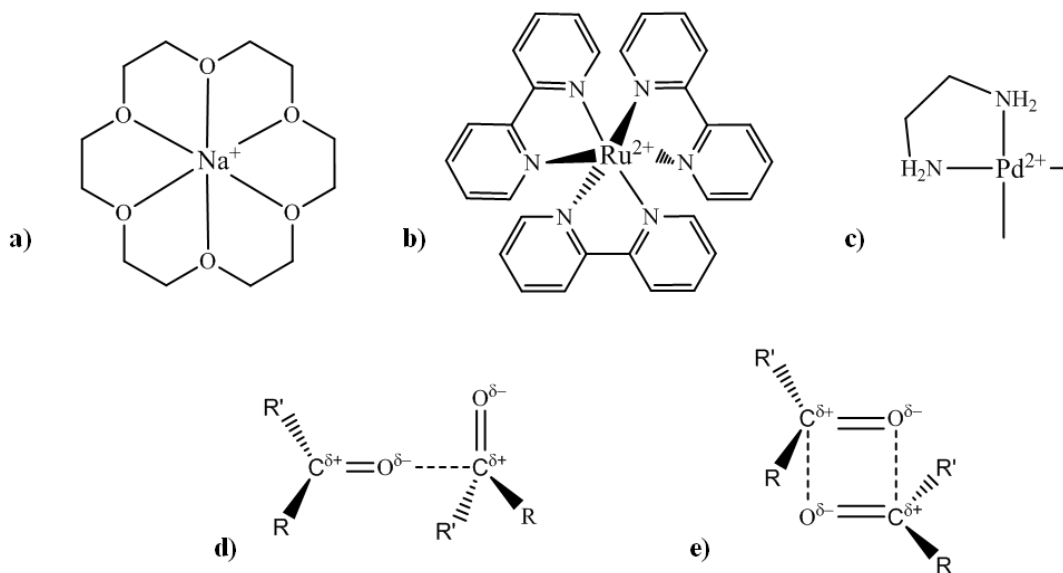
Figure 1.12: Examples of different types of electrostatic interactions a-c) ion-dipole, d)

type 1 dipole-dipole, and e) type 2 dipole-dipole interactions.

1.2.2 Induced-Dipole Interactions

It would be inaccurate to ignore the redistribution of electron density when charged

species interact. As cations move closer to anions, the wavefunctions of the two species

change in response to their proximity; this phenomenon is called polarization. This phenomenon accounts for the attractive interactions between polar and non-polar molecules and between non-polar and non-polar molecules.[6] Such interactions include ion-induced-dipole, dipole-induced-dipole, and induced-dipole-induced-dipole, with the latter interaction being a common way to describe van der Waals or London dispersion forces.

1.2.3 Cation-π, Anion-π, and π-π Interactions

Cation-π, anion-π, and π-π interactions play a pivotal role in the design of supramolecular complexes. These interactions, while sometimes extremely weak, can be as strong as hydrogen bonds, as is the case with certain cation-π interactions. The interactions are due in part to delocalization of the π-electron density enhancing the stabilizing dispersion interactions between aromatic molecules and their neighbors.[54]

Cation-π interactions involving benzene arise from the interaction of the quadrupole moment of benzene with a positively charged species such as an alkaline earth metal, a transition metal, or a non-metallic cation. Examples of complexes displaying cation-π interactions are benzene–K^+ and the cyclopentadiene anion–Fe^{2+} in ferrocene. The stabilization energy of the benzene–K^+ complex is comparable to that of the water–K^+ complex, 75-80 kJ/mol,[6] .

The key to anion-π interactions is using an electron-deficient aromatic system, such as hexafluorobenzene or 1,2,4,5-tetracyanobenzene, to allow for anion complexation. Hay *et al.*[55] and Kochi *et al.*[56] through XRD, as well as MP2/aug-cc-pVDZ

level calculations, have shown stable formation of anion complexes with different electron-deficient benzene systems.

While cation-π and anion-π interactions play a role in the design of supramolecular complexes, it can be argued that π-π interactions, along with hydrogen bonding, account for the majority of supramolecular interactions. Aromatic π-π interactions, often called π-π stacking, fall in two general geometrical categories, offset-face-to-face (OFF) and edge-to-face (EF). Both motifs result in a stabilizing energy of around 9 kJ/mol. On the other hand, a parallel face-to-face geometry yields a repulsive force (**Figure 1.13**).
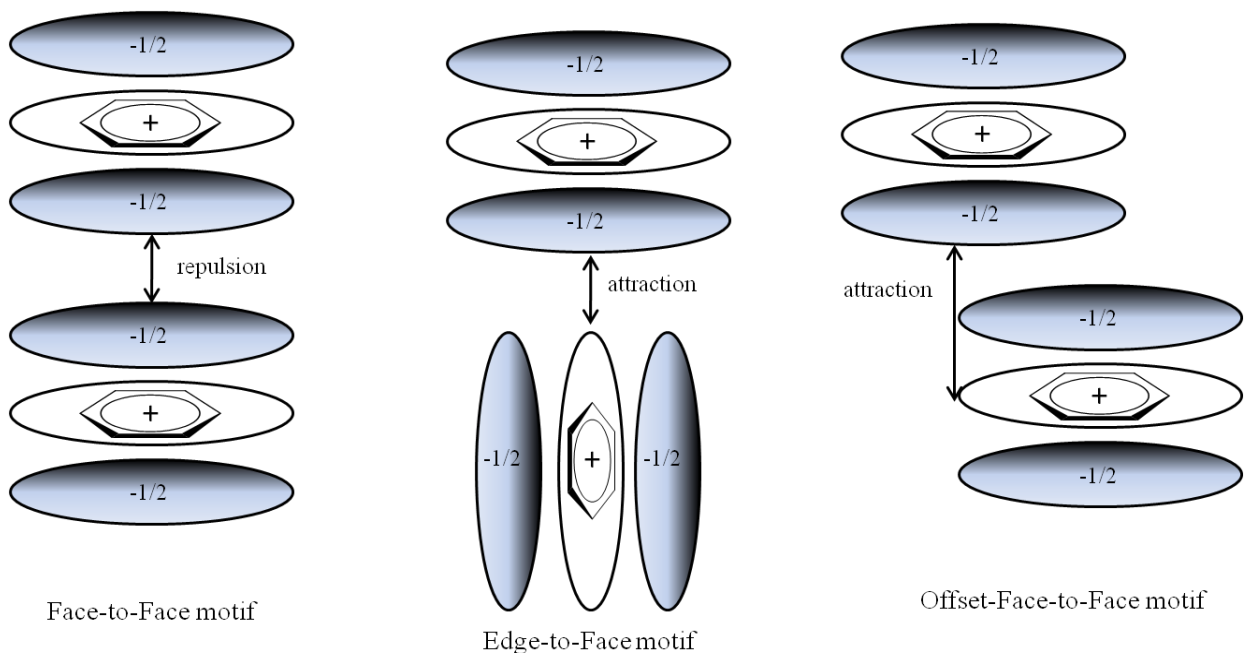
Figure 1.13: Interacting π-quadrupoles illustrating the repulsive and attractive forces associated with different alignment motifs.

1.2.4 Hydrogen Bonding

Hydrogen bonding interactions are found throughout supramolecular chemistry and help contribute to the overall shape and stability of macromolecules. In simplistic terms, conventional hydrogen bonds (e.g., N–H⋯O and O–H⋯O) can be described as a dipole-dipole interaction in which partially positive hydrogen atoms attached to an electron-withdrawing group are attracted to a neighboring dipole. Such a model describes the hydrogen bond as a Coulombic interaction between a polar donor bond ($D^{\delta-}$–$H^{\delta+}$) and an acceptor atom (:$A^{\delta-}$); therefore, hydrogen bonds are often written as D–H⋯A.[7] A more complete description of both conventional and unconventional hydrogen bonds includes the more covalent polarization and charge transfer contributions. In unconventional hydrogen bonds, partially positive hydrogen atoms interact with polar or polarizable ligands. For this type of hydrogen bonding, there is not necessarily significant electron donation from the acceptor into the H⋯A bond. C–H⋯O and C–H⋯π interactions fall within this category.[57] While other interactions might have an effect on the overall stability, hydrogen bonds, because of their relatively strong binding energy and highly directional nature, are often referred to as the 'masterkey interaction in supramolecular chemistry'.[1]

Typical binding energies for conventional hydrogen bonds range from 4-60 kJ/mole, although certain highly acidic compounds such as HF_2^- have bond energies up to 120 kJ/mol.[6] Unconventional hydrogen bonds are typically weaker but can have strengths up to about 100 kJ/mol. Hydrogen bonds have a wide range of bond lengths and angles, and while the electrostatic and delocalization contributions play the major role in

hydrogen-bond strength (**Table 1.2**), geometry also plays a role. In this work, we will only discuss interactions that fall within the cut-offs given in the table.

Table 1.2: Contributions of three (3) distinct hydrogen bonding environments.[2]

D–H⋯A	*Strong*	*Moderate*	*Weak*
	Mainly covalent	Mainly electrostatic	Electrostatic
Bond energy (kJ/mol)	60-120	16-60	<12
Bond lengths (Å)	2.2-2.5	2.5-3.2	3.2-4.0
Bond angles (∘)	175-180	130-180	90-150

2 Synthesis and Characterization of *C*-aryl substituted Pyrogallol[4]arenes

2.1 Introduction: History of Resorcin[4]arenes and Pyrogallol[4]arenes

The endless possibilities for applications of calix[4]arenes helped spur the evolution of new sub-families: resorcin[4]arenes and pyrogallol[4]arenes. Despite the preference of calix[4]arenes is to form the thermodynamically stable cone conformer, the inherent flexibility of these host molecules hinders the stability of the host-guest complex. Modifying calix[4]arenes to form resorcin[4]arenes and pyrogallol[4]arenes adds rigidity and more intramolecular hydrogen bonding, due to the increased number of hydroxyl groups on the upper rim. These properties of the resorcin[4]arenes and pyrogallol[4]arenes not only stabilize guest complexation but also allow formation of nanotubes[58-64] as well as the dimeric and hexameric entities.[65-71]

At this point, it is important to discuss the nomenclature associated with the resorcin[4]arene and pyrogallol[4]arene stereostructures. For these arenes, the five (5) main conformations are the cone, the partial cone, the boat, the saddle (1,3-alternate), and the chair. The orientation of the pendent R-groups is designated *rxxx*. Here *r* is an arbitrary point of reference that has been assigned to the top left corner in **Figure 2.1b**. The *xxx* assigns the stereochemical position (*cis* (*c*) or *trans* (*t*)) of the pendent R-groups with respect to the reference pendent R-group, as one goes counterclockwise. The resulting configurations are *rccc*, *rctt*, *rcct*, and *rtct*.

Even with the increased number of hydroxyl groups on the upper rim, the conformational preferences of both *C*-alkyl- and *C*-arylresorcin[4]arenes closely mimic
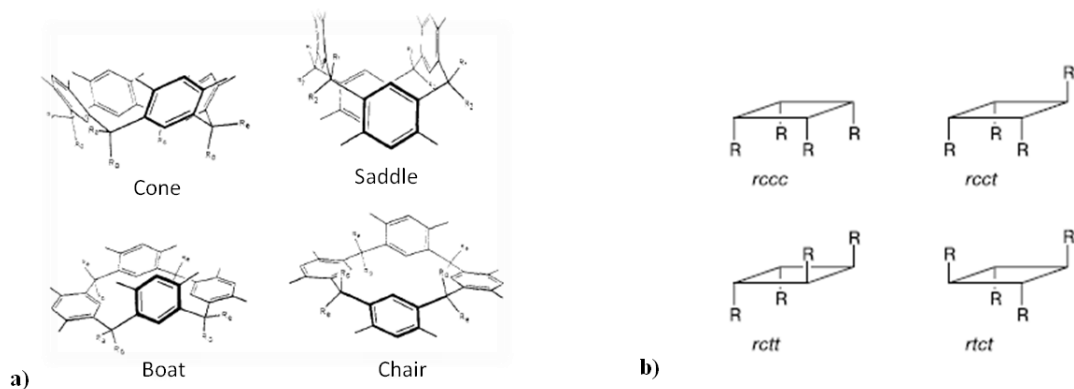
Figure 2.1: a) Possible conformers of resorcin[4]arene. b) Representation of the four (4) principle diastereomers.

those of calix[4]arenes.[72-74] Niederl and Vogel[75] studied the general structural properties of the products formed from reacting resorcinol with aliphatic or aryl aldehydes. These studies later led to structural investigations using x-ray crystallography. The latter analysis showed that these resorcin[4]arenes have the all-*axial*, all-*cis* stereostructure.[76] Intriguing to Hogberg was the possibility of isolating the different stereostructures for resorcin[4]arenes (**Figure 2.1**) and the possible interconversion between stereostructures.[59] Hogberg provided common names for the stereostructures, still used today: *rccc* cone, *rcct* partial cone, *rccc* boat, *rtct* saddle, and *rctt* chair. In Hogberg's study, variable temperature ¹H NMR was used to identify a kinetic product (the *rctt* chair) and a thermodynamic product (the *rccc* cone)[77,78,79] (**Figure 2.2**).. Control of the stereoselectivity is still not well understood, but on the basis of their analysis of alkyl and aryl resorcin[4]arenes, Cram and co-workers[80] have concluded that the R-group is one of the key factors in determining the preferred stereostructure. Other important factors may include reaction conditions, temperature,[81] and solvent effects.[82]

Product Yield vs Reaction Time
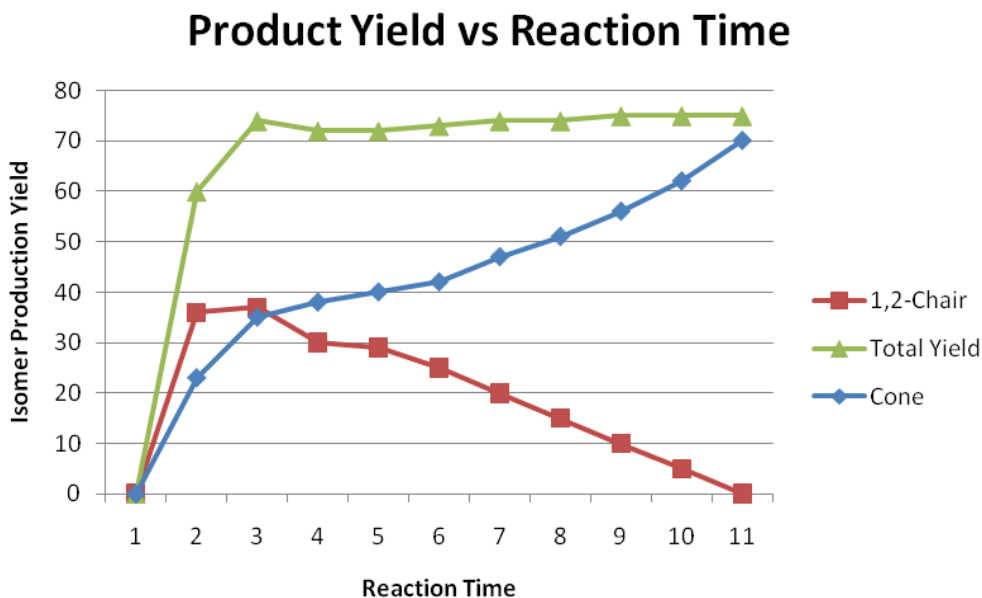
Figure 2.2: The reaction of resorcinol (1.0M) and benzaldehyde (1.0M) in a mixture of ethanol and concentrated HCl (4:1). The yields of the cyclooligomers chair and cone vs. reaction time.

Following Hogberg's investigation,[59] computational studies of conformational isomerism in calix[4]arenes and their analogs received increased attention. In agreement with the experimental results, a molecular mechanics investigation showed that the calix[4]arenes and resorcin[4]arenes favor the C_4 cone conformation.[83]

The main stereoisomeric product for the alkyl-substituted pyrogallol[4]arenes is often the thermodynamically preferred *rccc* cone.[84] The kinetically preferred *rctt* chair stereostructure has also been isolated in good yield, especially when the insolubility of this structure prevents its interconversion to the *rccc* cone. In contrast, *C*-arylpyrogallol[4]arenes have proven difficult to study and are thus relatively unexplored. Prior to my work, the inherent insolubility of the *rctt* chair made it the

27

only known stereostructure for the aryl-substituted pyrogallol[4]arenes. This result raised the question of whether the *rctt* chair stereostructure is a kinetic or thermodynamic product. If it is in fact the thermodynamic product, this will be a substantial change from the other members of the calix[4]arene family. It was this possibility coupled with the lack of evidence for the existence of other C-arylpyrogallol[4]arene stereostructures that spurred my interest in this field of research.

To gain insight into the formation of supramolecular entities from these *C*-arylpyrogallol[4]arenes building blocks, investigation into the building blocks themselves is needed. Also, characterization of these unique macrocycles, with respect to symmetry, stereochemistry and other physical properties, should afford valuable information on their adaptability to specific applications.

2.1.1 Previously reported structures

There are only a few examples of previously reported crystal structures of *C*-arylpyrogallol[4]arenes (**Figure 2.3**). In each of these examples the arene forms the *rctt* chair stereostructure (**Table 2.1**),[85-86] unless alkylation of the hydroxyls is achieved.[87,88]

R = Phenyl
Biphenyl
Naphthyl
4-Hyroxyphenyl
4-Cyanophenyl
4-Fluorophenyl
4-Chlorophenyl
4-Bromophenyl
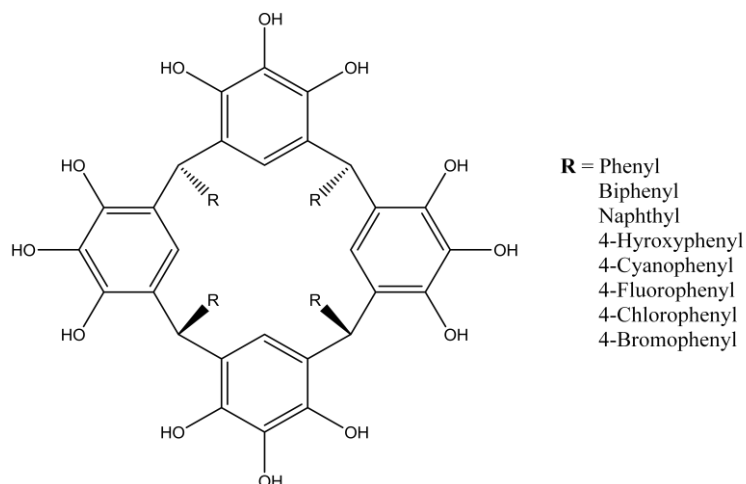
Figure 2.3: Schematic representation of previously reported *C*-arylpyrogallol[4]arene crystallographic structures.[84,86,87,88]

Table 2.1: Previously reported crystal structures of *C*-arylpyrogallol[4]arenes in various solvent systems, each in the chair conformation.[84,86,87]

Pendent R-group	*Solvent System*
Phenyl[86]	DMF
Biphenyl[89]	DMF
Naphthyl[87]	Methanol and Pyrazine
4-Cyanophenyl[84]	DMSO
4-Flurophenyl[84]	DMSO
4-Chlorophenyl[84]	DMSO
4-Bromophenyl[84]	DMSO
4-Methoxyphenyl[86]	DMF

Alshahateet *et al.*[84] reported notable differences in the twist angle (degree of rotation between two eclipsed aryl R-groups) of the product pyrogallol[4]arenes when reactions were carried out at room temperature versus reflux conditions. Synthesizing *C*-4-cyanophenylpyrogallol[4]arene at room temperature produced a twist angle between the two eclipsed phenyl rings of 5.07°; synthesis under reflux conditions produced a twist angle of 21.31°. The authors concluded that the increase in reaction temperature led to an increase in twist angle (**Figure 2.4**). They, however, provided no rationale for this dependence. When comparing *C*-4-fluorophenyl, *C*-4-chlorophenyl, and *C*-4-bromophenyl, the twist angle decreases in the order F > Cl > Br, regardless of the reaction conditions. This trend is consistent with the hydrogen bonding tendencies of the halogens but is inconsistent with their relative covalent radii. It is worth noting that neither the temperature nor the substituent at the *para* position had any noticeable effect on the conformation or configuration of the macrocycle.
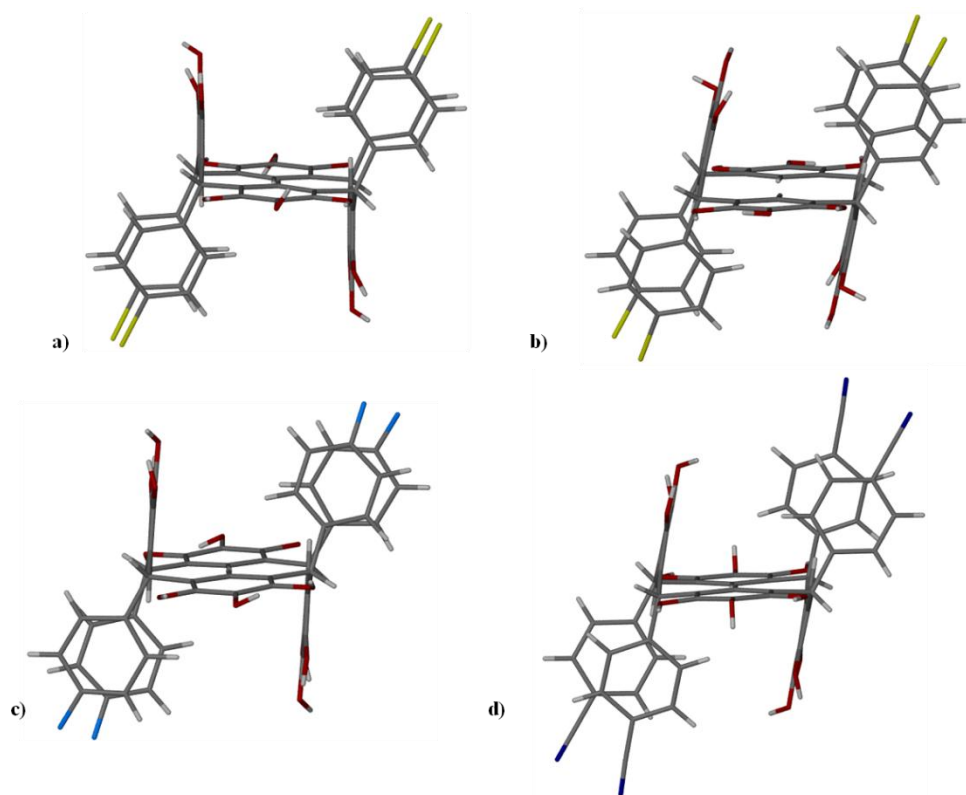
Figure 2.4: Crystallographic images of *para*-substituted a) *C*-4-bromophenylpyrogallol[4]arene, b) *C*-4-chlorophenylpyrogallol[4]arene, c) *C*-4-fluorophenylpyrogallol[4]arene, and d) *C*-4-cyanophenylpyrogallol[4]arene illustrating the increase in twist angle from a-d of $3.0° – 21.31°$. O: red, C: grey, and H: white.

2.2 Thermodynamics: a computational study[90-91]

While it was previously assumed that *C*-arylpyrogallol[4]arenes would follow the kinetic and thermodynamic trends of calix[4]arenes and resorcin[4]arenes, the lack of experimental evidence supporting this claim leads to questions of its validity. In order to test this assumption, quantum mechanical calculations were employed to find the minima

on the potential energy surface of C-phenylpyrogallol[4]arene. Experimental data, in turn, was then used to help strengthen the computational data.

The gas-phase theoretical studies performed with the Gaussian 03 suite of programs[92] gave some very interesting results.[93] In the absence of solvent, calculations at the B3LYP/6-31G(d) level, which does not account for dispersion effects, indicate that the *rctt* chair stereostructure of C-phenylpyrogallol[4]arene with C_1 symmetry is 25.1 kJ/mol higher in enthalpy than the *rccc* cone stereostructure with C_4 symmetry. Of even greater importance is that the *rctt* chair with C_i symmetry lies 70.9 kJ/mol higher in enthalpy than the *rccc* cone. In the C_i chair conformation the 2-position hydroxyl proton on the 1,2,3-trihydroxybenzene rotates out-of-plane, changing the hydrogen-bonding interactions within a given pyrogallol. The destabilization of the chair conformers with respect to the cone conformer originates from the breaking of the cooperative hydrogen-bonding network between the pyrogallols. In the cone conformation of pyrogallol[4]arenes there are twelve (12) possible hydrogen bonds as compared to eight (8) possible hydrogen bonds in the chair conformation. This disruption is not as drastic as that for resorcin[4]arenes, however, for which there is a complete interruption of the hydrogen-bonding network when the cone conformer converts to the chair conformer (**Figure 2.5**)..

The entropy difference among the C-phenylpyrogallol[4]arene stereostructures is stabilizing the *rctt* chair stereostructures with respect to the *rccc* cone (Table 2.2). However, the effect is not large enough at the B3LYP/6-31G(d) level of calculation to change the *rctt* chair to the preferred stereostructure.

At the MP2/6-31G(d) level of calculation, which does account for dispersion effects, there is now a rearrangement in the relative free energies of the stereostructures such that the *rccc* cone is no longer predicted to be most stable (**Table 2.2**). The *rctt* chair C_1 stereostructure is the new global minimum and is more
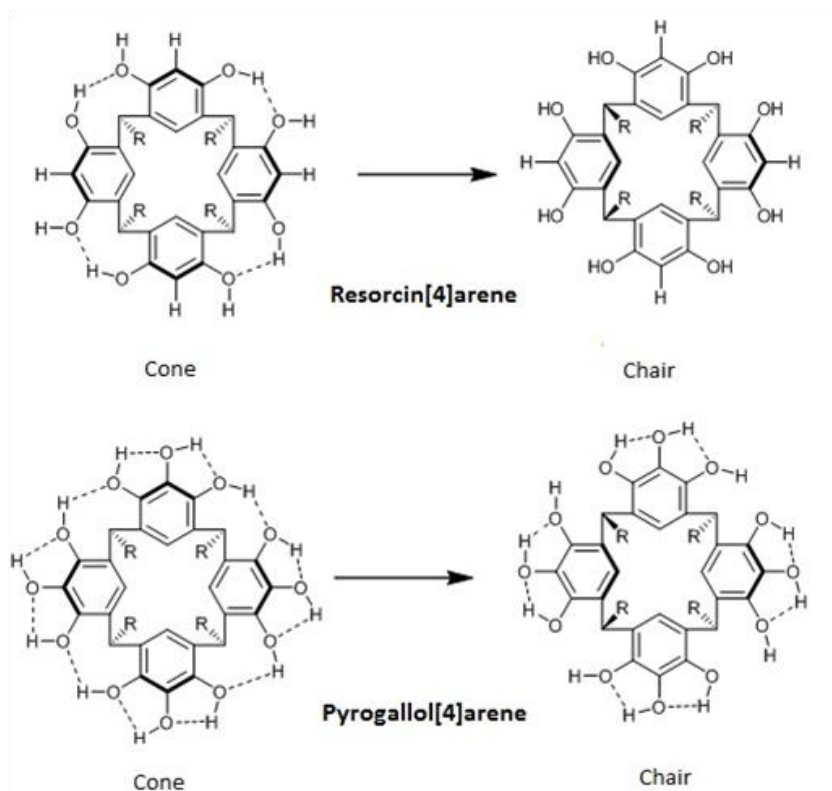
Figure 2.5: Schematic representation of the intermolecular hydrogen-bonding network of resorcin[4]arenes and pyrogallol[4]arenes in two (2) different conformations, explaining some of the differences in thermodynamic stabilization.

stable than the *rccc* cone by 11.0 kJ/mol. The steric decongestion of the phenyl R-groups in the *rctt* chair stereotructures, coupled with accounting for π-π stacking, makes the *rctt* chair more competitive enthalpically with respect to the *rccc* cone (**Figure 2.6** and **Table**

2.2). According to Tsuzuki[93] and Sherrill,[94] π-π interactions contribute between 6.19 and

8.33 kJ/mol of stabilization energy, depending on the level of theory.

Table 2.2: Computational data at both the B3LYP/6-31G(d) and MP2/6-31G(d) levels. Bold lettering indicates the conformers of particular interest, with red numbers indicating the most stable conformer at that particular level of calculation. Reference **Figure 2.6** for conformer identification.

Conformer	*B3LYP/6-31G(d) Δ H kJ/mol*	*B3LYP/6-31G(d) ΔG kJ/mol*	*MP2/6-31G(d) Δ H kJ/mol*	*MP2/6-31G(d) ΔG kJ/mol*
Cone ben[a] axial	**0.0**	**1.1**	**0.0**	**11.0**
Cone ben eq	1.0	0.0	24.0	32.9
chair C_1 Sym	**25.1**	**2.6**	**12.6**	**0.0**
1,2 alt [Hip][b]	24.0	10.1	23.9	19.9
Partial Cone	26.7	13.6	39.7	36.5
1,3-Chair	42.0	27.2	47.7	42.8
Boat ben axial	**51.1**	**26.7**	**42.9**	**28.4**
chair C_i Sym	**70.9**	**45.3**	**68.6**	**52.8**
1,3 alt Saddle	79.6	62.0	73.9	66.2
1,2 alt [Hoop][c]	85.6	67.8	96.3	88.5

[a] ben = benzene as the pendent R-group
[b] [Hip] = phenolic hydrogens in plane
[c] [Hoop] = phenolic hydrogens out of plane

Cone

Chair C_i Symmetry
Chair C_1 Symmetry

Boat

Saddle

1,2 alt
1 H oop

Partial
Cone

1,2 alt
all H's in plane

1,2 alt
2 H's oop
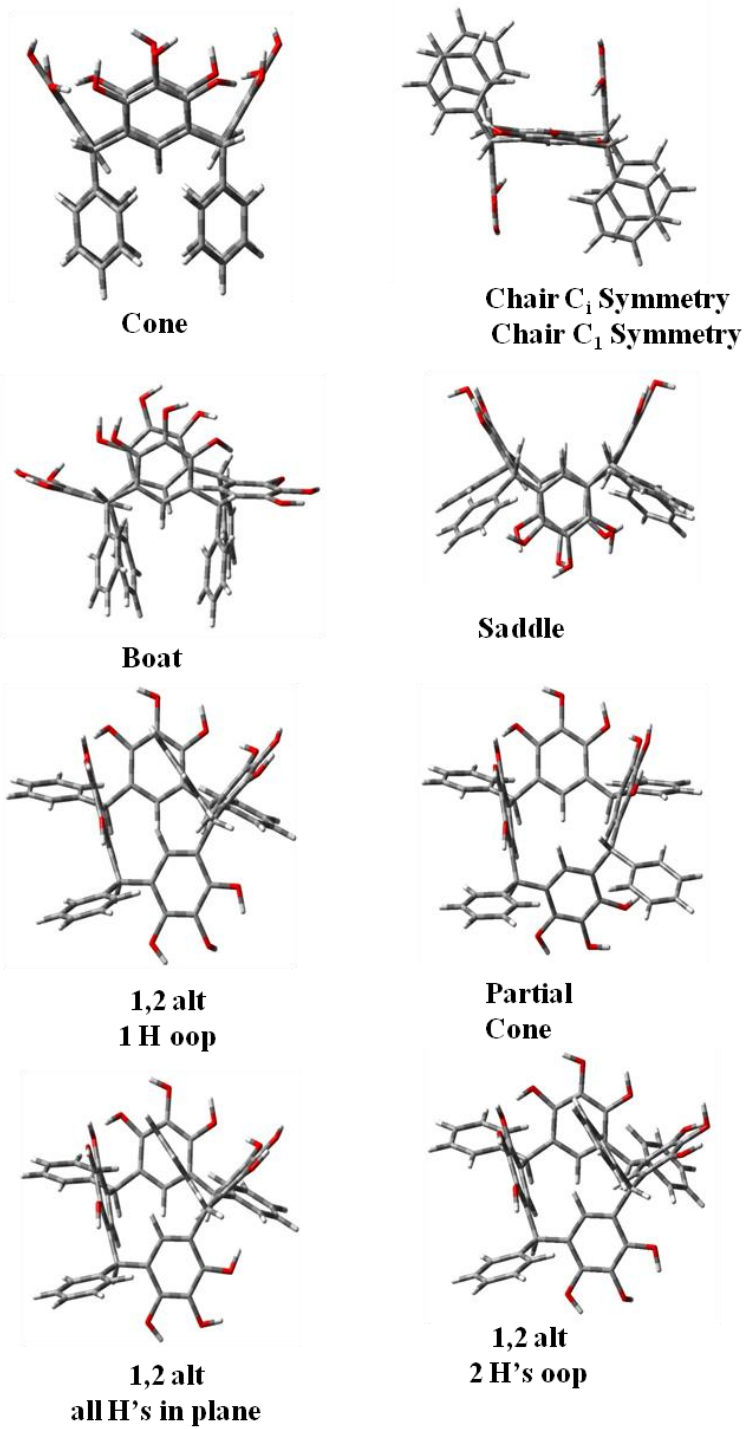
Figure 2.6: Predicted optimized structures, which were then used to find the global minimum. O: red, C: grey, and H: white.

Solvent can also play an important role in the preferred stereostructure of *C*-phenylpyrogallol[4]arene. We[93] are currently looking at how interaction with solvent, through solvent reaction field calculations or the introduction of explicit solvent molecules, affects the relative stabilities of all of the possible conformations. The reaction field calulations employ the polarizable continuum model (PCM) in which overlapping spheres are used to create the solute cavity.[95,96,97] These studies indicate that the solvent role in stabilizing the *rctt* chair stereostructure is much larger than originally anticipated (**Table 2.3**). In the presence of solvent, the most stable stereostructure is the *rctt* chair, even at the B3LYP/6-31G(d) level of theory. Note also that for the first time the C_i chair is more stable than the C_1 chair, in agreement with XRD experimental data.

Table 2.3: Enthalpies and free energies using the polarizable continuum model (PCM B3LYP/6-31G(d)) to test solvent effects.

	DMSO		*Methanol*		*Acetonitrile*	
Conformer	ΔH (kJ/mol)	ΔG (kJ/mol)	ΔH (kJ/mol)	ΔG (kJ/mol)	ΔH (kJ/mol)	ΔG (kJ/mol)
Cone	**0.0**	**0.0**	**0.0**	**0.0**	**0.0**	**0.0**
Chair, C_1	**15.5**	**-8.0**	**4.1**	**-19.4**	**14.7**	**-8.9**
Partial Cone	22.3	8.1	9.5	-4.6	26.5	12.3
Boat	**26.3**	**0.8**	**15.1**	**-10.4**	**27.8**	**2.3**
Chair, C_i	**7.2**	**-20.1**	**-2.1**	**-29.4**	**11.5**	**-15.8**

2.3 Experimental Studies: Synthesis and characterization of selected *C*-arylpyrogallol[4]arenes

With the intention of gaining a broader understanding of aryl-substituted pyrogallol[4]arenes, a crystallographic database was created. My aim was to synthesize a variety of *C*-arylpyrogallol[4]arenes and to fully characterize them through NMR, and more importantly, single crystal x-ray diffraction (XRD). All NMR spectra were taken in d^6-DMSO. Using the experimental data obtained from these studies will help to reinforce and explain the computational results that suggest that *C*-arylpyrogallol[4]arenes do not follow the thermodynamic trends of the other members in the calix[4]arene family.

2.3.1   Synthesis and characterization of *C*-phenylpyrogallol[4]arene 2.1

Synthesis of *C*-phenylpyrogallol[4]arene (PgPh) **2.1** was readily achieved following previous methods (**Scheme 2.1**).[98,99] See **Section 2.7** for the complete experimental details of all syntheses.
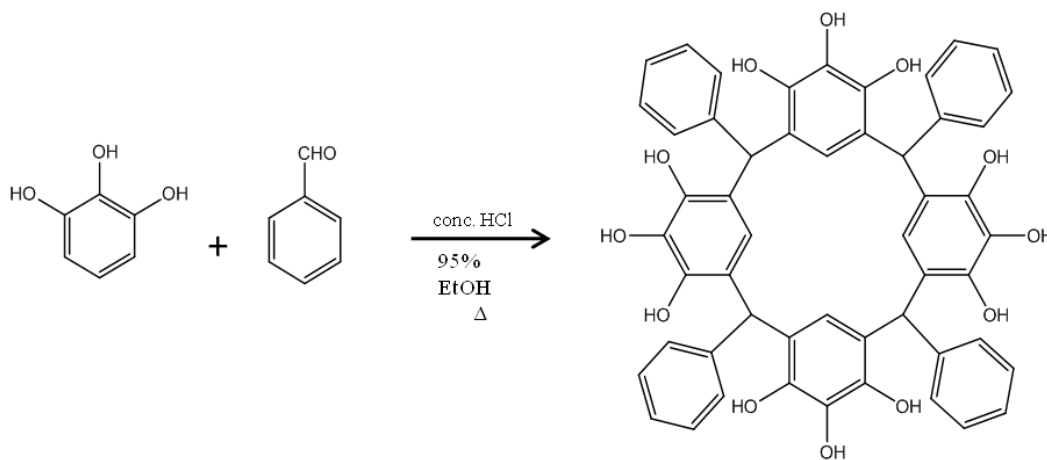
Scheme 2.1: The synthetic route for *C*-phenylpyrogallol[4]arene.

To my knowledge, when this work was started no ^{1}H NMR spectrum of **2.1** was reported in the literature. Thus, initially a spectrum was obtained with bulk *C*-phenylpyrogallol[4]arene using a Bruker AXR300 to identify key characteristic peaks. See **Appendix A** for all of the ^{1}H NMR spectra. Two (2) singlets at 7.636 ppm and 7.464 ppm in a 2:1 ratio indicate the presence of all three phenolic protons. Taken together with the singlet at 5.579 ppm associated with the methine proton, synthesis of *C*-phenylpyrogallol[4]arene **2.1** is confirmed. However, the presence of several other characteristic peaks, similar to the above-mentioned peaks, indicates that multiple stereoisomers exist in solution.

Isolation of stereostructures through selective crystallography was utilized to assign specifc peaks to specific stereostructures. Crystals of *C*-phenylpyrogallol[4]arene • (DMSO)$_6$ in the chair conformation **2.1a** were redissolved in d^6-DMSO in order to run the ^{1}H NMR (**Figure 2.7**). With respect to the key characteristic peaks, the methine proton is now located at 5.668 ppm and the aromatic protons from the phenyl R-groups (Ph-H) now give a multiplet with an AA'BB'C splitting pattern at 6.838 ppm. The aryl protons (Ar-H) of the axial and equatorial pyrogallols produced two different singlets at 5.179 ppm and 6.002 ppm, with each peak integrating to 0.5 hydrogen atoms. Even more telling are the peaks from the phenolic protons. Normally the OH moieties of pyrogallol will afford two singlets with a 2:1 ratio at 7.465 ppm and 7.764 ppm, respectively. Thus, the presence of another set of peaks with similar chemical shifts, 7.575 ppm and 7.895 ppm, is curious. One possible explanation for the second set of peaks is long-range J^5 coupling between a phenolic and an aryl proton on a given pyrogallol. The peak splitting is too large to be associated with J^5 coupling, however, since J^5 coupling results in peak

differences of 1-2 Hz. Thus, it was concluded that the two sets of peaks are a direct result of the unique chemical environments of the phenolic protons of the axial vs. equatorial pyrogallols in the chair conformer. The splitting pattern for the Ph-H protons is also consistent with this conclusion.
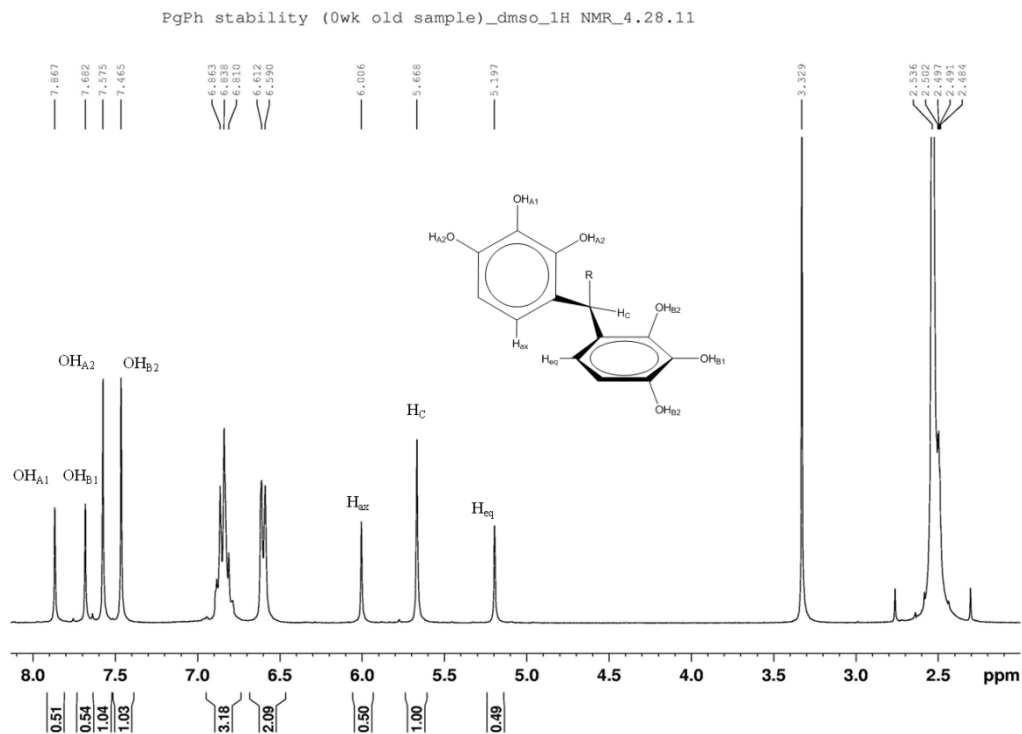
Figure 2.7: ^{1}H NMR spectra of **2.1a** indicating the key characteristic peaks often associated with *C*-arylpyrogallol[4]arenes.
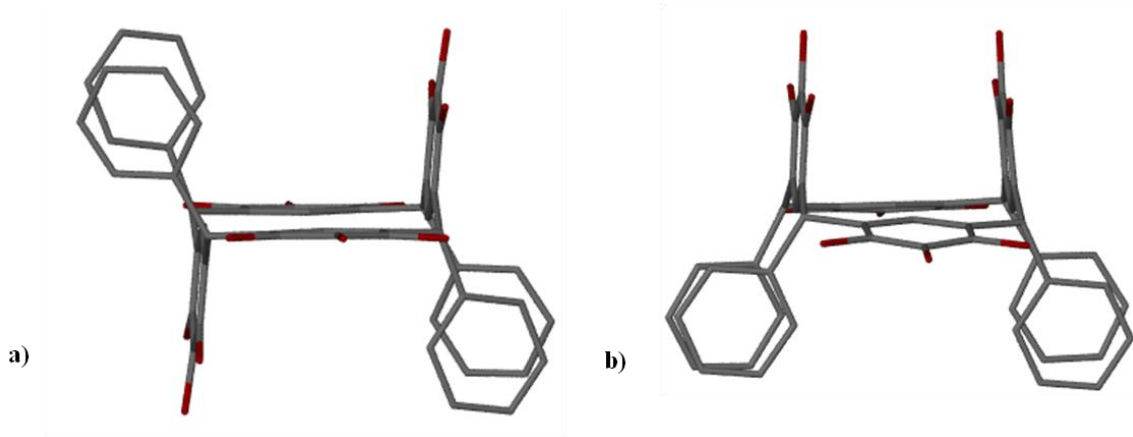
Figure 2.8: Crystallographic images of a) the predominate *C*-phenylpyrogallol[4]arene in the *rctt* chair stereostructure **2.1a** yielded from a variety of solvents and b) *C*-phenylpyrogallol[4]arene in the *rccc* boat stereostructure **2.1b** isolated from methanol. O: red, C: grey, and H: white.

Mattay and co-workers[100] have shown for resorcin[4]arenes that aprotic solvents tend to favor the cone conformation, whereas protic solvents result in the boat conformation. With this in mind, single crystals of *C*-phenylpyrogallol[4]arene were obtained through slow evaporation in various solvents. This work has demonstrated that separation of a desired stereostructure of *C*-phenylpyrogallol[4]arene can be controlled by varying the solvent system. Solvents such as DMF, DMSO, pyridine, and a 3:1 ratio of methanol (MeOH):acetonitrile (ACN) result in the selective crystallization of the chair conformation (**Figure 2.8**). See **Section 2.7** for complete crystallographic data. However, testing the effect of methanol on stereostructure led to a new stereoisomer, the *rccc* boat or flattened cone, of *C*-phenylpyrogallol[4]arene (compound **2.1b, Figure 2.8**). The *rccc* boat stereostructure has been isolated previously for a variety of resorcin[4]arene macrocycles, including perphosphorylated resorcin[4]arenes with alkyl R-groups,[101]

resorcin[4]arenes with aryl R-groups,[102] and tetranitroresorcin[4]arene with alkyl R-groups.[103] This stereostructure, however, has never before been reported for *C*-arylpyrogallol[4]arenes. To overcome the higher solubility of the boat vs. the chair conformer, fractional separation in MeOH was performed. Analysis of the solid-state structure **2.1b** yields two unique π-π distances between the aryl R-groups of 4.873 Å and 5.056 Å. The O–H···O hydrogen bonds between macrocycle and solvent range from 2.587 Å - 2.871 Å (O-to-O distance).

Solvent also has a role in determining the geometrical structures of *C*-arylpyrogallol[4]arenes in the solid state, especially with respect to the arrangement of the phenolic protons. As an example, oxygenated aprotic solvents such as dimethyl sulfoxide (DMSO) and dimethylformamide (DMF) are capable of forming O–H···O(solvent) hydrogen bonds with the pyrogallol moieties, causing one or more phenolic protons to flip out of the plane of the pyrogallol. These interactions affect the relative stability (**Table 2.1**) of a conformer by altering the number and types of intra- and intermolecular hydrogen bonds.

Analyzing the different intra- and intermolecular interactions in the *rctt* chair stereoisomers crystallized from both DMSO and a methanol:acetonitrile mixture helps to explain the trends observed in the quantum chemical computational data(**Table 2.3**). The dimethyl sulfoxide solvate of *C*-phenylpyrogallol[4]arene shows six (6) unique hydrogen bonds ranging from 2.646 Å - 2.853 Å,and the *C*-phenylpyrogallol[4]arene methanol:acetonitrile solvate shows three (3) hydrogen bonds ranging from 2.710 - 2.783 Å.The π-π (centroid-to-centroid) distance between the R-groups is 4.754 Å for the DMSO solvate and 4.403 Å for the MeOH solvate. The data suggest that, comparatively,

hydrogen bonding may be more important in stabilizing the chair conformer in DMSO solvate but that π-π stacking may be more important in stabilizing the chair conformer in MeOH solvate. In any case, these attractive interactions help to rationalize the observed change in preferred stereostructure from the gas-phase to PCM computations for *C*-phenylpyrogallol[4]arene.

More direct experimental support for the *rctt* chair as the preferred thermodynamic stereostructure was obtained by refluxing **2.1a** in DMSO for a week. Crystals were then obtained to reveal no change in the stereostructure. In contrast, refluxing *C*-phenylresorcin[4]arene in DMSO leads to interconversion from the chair to the cone conformer.

2.3.2   Synthesis   and   characterization   of   mono-substituted   *C*-phenylpyrogallol[4]arenes[104]

Since the computational and experimental data suggest that a phenyl R-group leads to a different thermodynamic product for pyrogallol[4]arene than for resorcin[4]arene and calix[4]arene, the effect of other aryl R-groups on conformational preference was investigated. See **Table 2.4** for a complete list of the *C*-arylpyrogallol[4]arenes that were synthesized and their resultant conformation. The macrocycles vary with respect to not only the substituent on the phenyl R-group but also the position of the substituent on the phenyl ring. Comparing the characteristics, such as twist angle and intermolecular interactions, of the macrocycles formed from the various mono-substituted benzaldehydes will give insight into the stabilizing influences in the

various stereostructures. X-ray crystallography was used to fully characterize the mono-substituted aryl macrocycles.

Synthesis of *C*-4-methylphenyl-, *C*-4-ethylphenyl-, *C*-3-nitrophenyl-, *C*-4-nitrophenyl-, *C*-3-hydroxyphenyl-, *C*-4-hydroxyphenyl-, *C*-2-methoxyphenyl-, *C*-4-methoxyphenyl-, *C*-4-propoxyphenyl-, and *C*-naphthylpyrogallol[4]arenes (**2.2, 2.3, 2.4, 2.5, 2.6, 2.7, 2.8, 2.9, 2.10, 2.11**) was achieved by a procedure similar to the synthesis of PgPh, but substituting the appropriate benzaldehyde derivative for benzaldehyde (**Section 2.7**). **Scheme 2.2** below illustrates the different mono-substituted phenylpyrogallol[4]arenes synthesized.
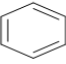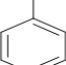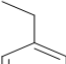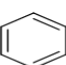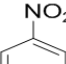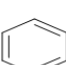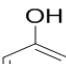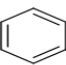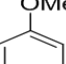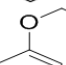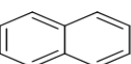
Table 2.4: Complete list of all synthesized *C*-arylpyrogallol[4]arenes, their isolated conformations and the solvent systems. Boxes highlighted in blue are macrocycles that have been isolated as both the chair and boat conformers.

Pendent R Group	Conformation	Solvent System	π-π distance	Twist angle
Phenyl	1,2-Chair	DMSO/3:1MeOH:ACN	4.754	9.21
	Boat	MeOH	4.873	5.73
4-methylphenyl	1,2-Chair	DMSO	4.698	12.89
4-ethylphenyl	1,2 Chair	DMSO	4.908	32.29
3-nitrophenyl	1,2 Chair	DMSO	4.176	15.64
4-nitrophenyl	1,2 Chair	DMSO	4.394	19.81
3-hydroxyphenyl	1,2 Chair	DMSO	4.992	7.42
4-hydroxyphenyl	1,2 Chair	MeOH	4.274	5.42
2-methoxyphenyl	1,2-Chair	DMF/DMSO	4.377	2.34
4-methoxylphenyl	1,2-Chair	DMSO	4.586	6.47
4-propoxyphenyl	1,2-Chair	DMSO	4.680	28.63
	Boat	MeOH	4.543	1.75
2,3-dimethoxyphenyl	1,2-Chair	Pyridine	4.416	9.81
2,4-dimethoxyphenyl	1,2-Chair	DMF : H_2O	4.747(up)	12.92
			4.534 (down)	20.30
3,4-dimethylphenyl	1,2-Chair	DMSO	4.433	3.71
3,5-dihydroxyphenyl	1,2-Chair	MeOH : H_2O	4.268	7.08
3,4,5-trimethoxyphenyl	1,2-Chair	DMSO	4.651	1.80
	Partial Cone	MeOH:1,4-butadiene	N/A	N/A

2.3.2.1 Analysis of *C*-4-methylphenylpyrogallol[4]arene 2.2 and *C*-4-ethylphenylpyrogallol[4]arene 2.3

^{1}H NMR and single crystal x-ray diffraction (XRD) were used in the structural determination of **2.2** and **2.3**. In both cases the ^{1}H NMR revealed a tetrameric macrocycle, as indicated by the singlet produced by the methine proton at 5.617 ppm (**2.2**) or 5.587 ppm (**2.3**). Aside from the characteristic methyl singlet for *C*-4-methylpyrogallol[4]arene (Pg(4-MePh)) versus the ethyl triplet and quartet splitting patterns for *C*-4-ethylphenylpyrogallol[4]arene (Pg(4-EtPh)), there is little difference between the **2.2** and **2.3** ^{1}H NMR spectra. Single crystals of both **2.2** and **2.3** were obtained by slow evaporation in DMSO (**Figure 2.9a and b**). When comparing Pg(4-MePh) and Pg(4-EtPh) to PgPh, a unique trend appears. As the number of carbons at the *para-* position increases, the twist angle increases to relieve the steric congestion caused by the change in functional group. In *C*-phenylpyrogallol[4]arene the twist angle between the pendent R-groups is 9.21°; it is 12.89° and 32.29° in **2.2** and **2.3,** respectively. Also, because of the increase in steric congestion, when comparing **2.2** to **2.3** the π–π (R-group centroid-to-centroid) distance increases from 4.698 Å to 4.908 Å (**Figure 2.9c and d**). Both compounds exhibit similar hydrogen bonding between the solvent and the pyrogallol subunits. In compound **2.2,** two (2) distinct solvent-to-macrocycle O–H···O hydrogen bonds with an O···O distance of 2.761 Å and 2.893 Å are observed. The solid state structure of compound **2.3** three (3) distinct solvent-to-macrocycle O–H···O hydrogen bonds with an O···O distances ranging from 2.70 Å - 2.76 Å.
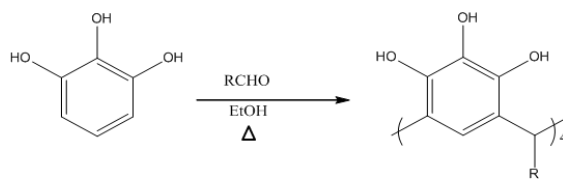
Product ID	R-Group		% yield	Conformation	Capsule formation
2.1	Phenyl		80.6	Chair & Boat	Yes
2.2	4-methylphenyl		73	Chair	No
2.3	4-ethylphenyl		71	Chair	No
2.4	3-nitrophenyl		68	Chair	No
2.5	4-nitrophenyl		91	Chair	No
2.6	3-hydroxyphenyl		89	Chair	No
2.7	4-hydroxypphenyl		73	Chair	Yes
2.8	2-methoxyphenyl		86	Boat	No
2.9	4-methoxyphenyl		83	Chair	No
2.10	4-propoxyphenyl		70	Chair & boat	Yes
2.11	Naphthyl		72	Not crystalline	Yes

Scheme 2.2: General reaction scheme and conformations of the mono-substituted *C*-arylpyrogallol[4]arene reaction products.
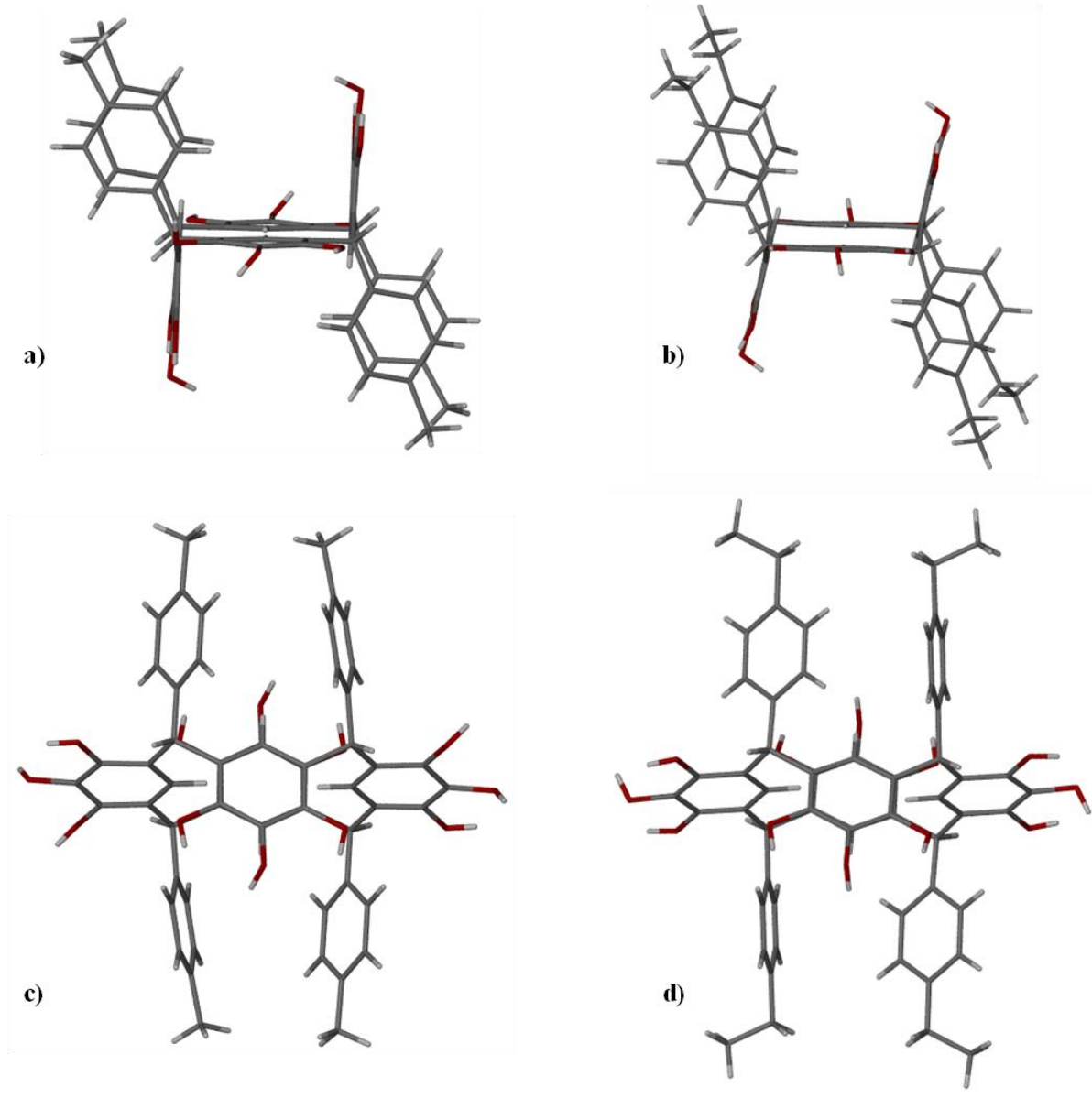
Figure 2.9: Crystallographic views of a) *C*-4-methyphenylpyrogallol[4]arene and b) *C*-4-ethylphenylpyrogallol[4]arene with c) and d) showing side views of the corresponding macrocycles to illustrate the twist angle difference incurred from the additional steric congestion. O: red, C: grey, and H: white.

2.3.2.2 Analysis of *C*-3-nitrophenylpyrogallol[4]arene 2.4 and *C*-4-nitrophenylpyrogallol[4]arene 2.5

XRD was used in conjunction with ^{1}H NMR for the complete characterization of **2.4** and **2.5**. Single crystals of both **2.4** and **2.5** were obtained by slow evaporation of 100 mg of compound dissolved in DMSO (**Figure 2.10**). The methine peak in the ^{1}H NMR spectra of **2.4** and **2.5** in d^6-DMSO confirms that the addition of a nitro group does not hinder the overall condensation reaction. Unlike **2.1** the reaction times were noticeably longer for **2.4** and **2.5**. Unique to both spectra is the large difference in the chemical shifts associated with the aryl protons: a singlet at 4.521 ppm (4.564 ppm) and a singlet at 5.914 ppm (5.875 ppm) for **2.4** (**2.5**). The aromatic region of **2.4** exhibits standard splitting for a *meta*-substituted benzene (singlet (H_A), doublet (H_B), triplet (H_C), doublet (H_D)) (**Figure 2.11**). The AA'BB' splitting pattern observed in the aromatic region of **2.5** is standard for a *para*-substituted benzene. The ^{1}H NMR spectra of both **2.4** and **2.5** reveal no evidence of a stereoisomer other than the *rctt* chair in solution, unlike that of **2.1**. While the differences between the two crystal structures are not drastic, differences do exist. At 4.176 Å and 15.64°, the π–π distance between neighboring R-groups and twist angle are smaller for compound **2.4**, than their values for compound **2.5,** 4.394 Å and 19.81°.
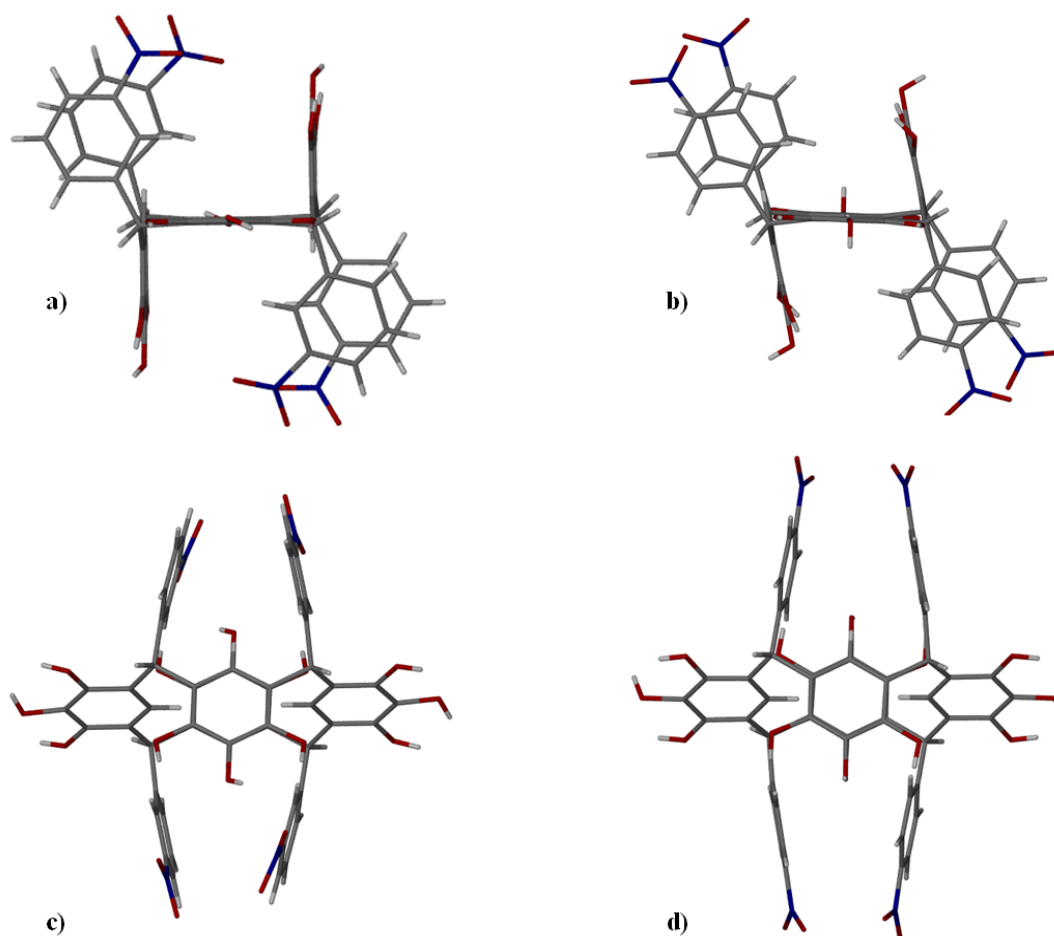
Figure 2.10: Crystallographic views of a) *C*-3-nitrophenylpyrogallol[4]arene **2.4** and b) *C*-4-nitrophenylpyrogallol[4]arene **2.5** with c) and d) showing side views of the corresponding macrocycles to illustrate the twist angle difference incurred from the additional steric congestion. O: red, C: grey, N: blue, and H: white.
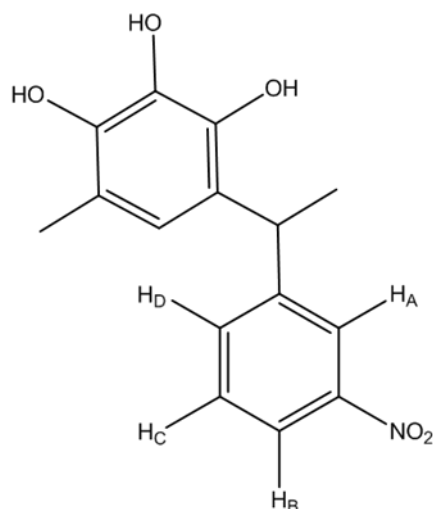
Figure 2.11: Schematic illustration of an example of the nomenclature used in NMR peak determination for *meta*-substituted aryls. For *para*-substituted aryls the substituent and H_B will be interchanged.

2.3.2.3 Analysis of *C*-3-hydroxyphenylpyrogallol[4]arene 2.6 and *C*-4-hydroxyphenylpyrogallol[4]arene 2.7

Hydroxy functionalization at different positions on the phenyl ring of the pendent R-groups was of interest because it could allow for further functionalization to be carried out. *Meta*- and *para*-hydroxybenzaldehdye were used in forming compounds **2.6** and **2.7,** respectively, to also test the effect of different hydrogen donor positions on the intermolecular hydrogen-bonding network and the overall stability. Similar to *C*-3-nitrophenylpyrogallol[4]arene the ^{1}H NMR of **2.6** yields a *meta* splitting pattern with a singlet from H_A at 6.077 ppm, a doublet from H_B at 6.055 ppm, a triplet from H_C at 6.672 ppm, and a doublet from H_D at 6.247 ppm (See **Figure 2.11** for naming scheme.) However, the chemical shift difference between the two aryl protons (Ar-H) on the

equatorial and axial pyrogallols is considerably smaller at 0.500 ppm than the chemical shift difference of 1.393 ppm for **2.4**. A similar result with respect to the Ar-H protons was observed for **2.7** vs. **2.4**. The ^{1}H NMR spectrum for **2.7** also shows two (2) aryl-H singlets, with 0.5 integration, at 5.936 ppm and 5.532 ppm (as a result of the different chemical environments) and a methine singlet at 5.562 ppm. Due to the *para*-substitution of the phenyl ring (R-group) of **2.7**, the Ph-H protons give a typical AA'BB' pattern, and peak integration accounts for all four (4) phenyl protons.

Single crystals of **2.6** were obtained through slow evaporation in DMSO. However, due to the increased solubility of **2.7** in methanol, single crystals for this compound were obtained in methanol. Analysis of **2.6** in the solid state reveals a C–H···π host-guest interaction distance between DMSO (guest) and an axial pyrogallol subunit within the macrocycle (host) with an H···π distance of 2.744 Å (**Figure 2.12**). Solvent-to-macrocycle O–H···O hydrogen bonding resulted in O-to-O distances of 2.536 Å, 2.560 Å, 2.665 Å, and 2.702 Å. The macrocycle-to-macrocycle O-to-O hydrogen bonding distance of 2.678 Å between neighboring pendent R-groups results in one-dimensional growth. In keeping with measuring π-π distances in comparison with twist angle in order to determine if there exists a positive correlation between them, the π–π distance of 4.992 Å is combined with a twist angle of 7.42° for **2.6**. Along with the unique host-guest interactions, a bi-layer packing motif is observed with two encapsulated DMSO molecules incarcerated between two macrocycles and a solvent channel for free DMSO (**Figure 2.13**).
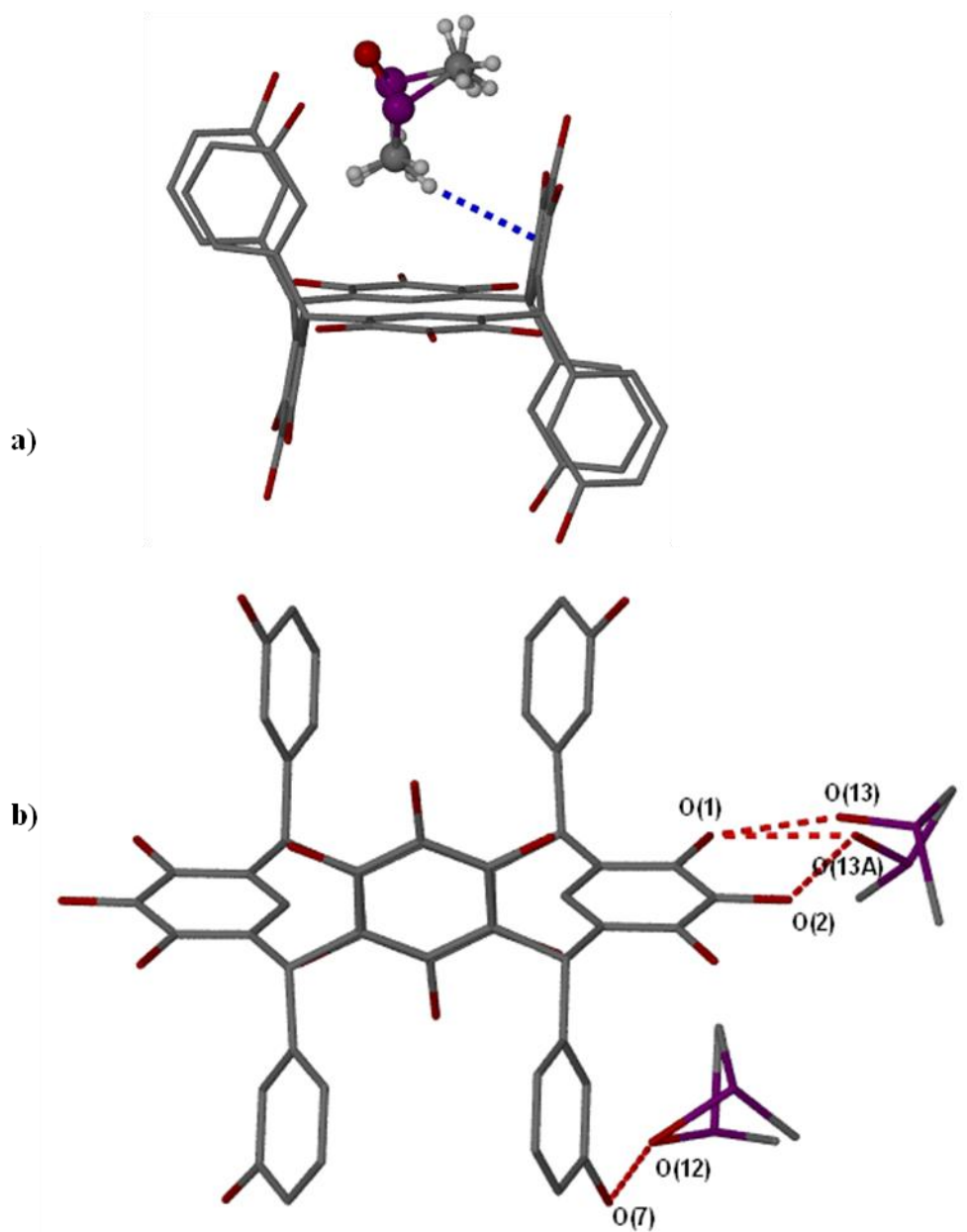
Figure 2.12: a) Crystallographic image of **2.6** with a single C–H⋯π host-guest interaction present in the solid state. b) Intermolecular hydrogen bonding between macrocycle and DMSO solvent molecules. O: red, C: grey, and S: purple. Hydrogen atoms are omitted for clarity.
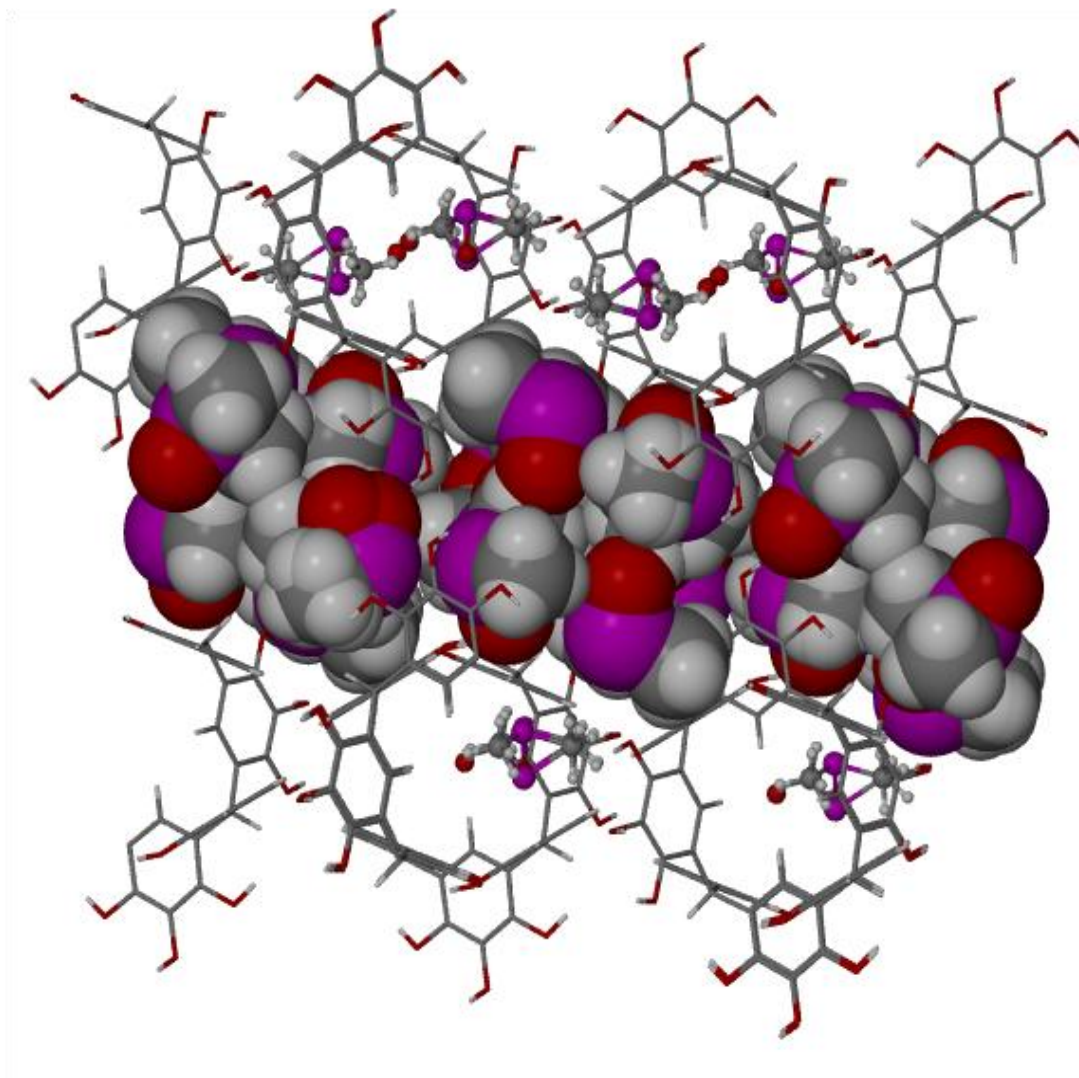
Figure 2.13: Crystallographic packing diagram of **2.6** illustrating both the bi-layer packing order as well as the free solvent channel as compared to the encapsulated DMSO molecules (1:1 DMSO:macrocycle). O: red, C: grey, H: white, and S: purple. Solvent channel DMSO molecules shown as space filled.

Because slow evaporation techniques were utilized to produce single crystals, atmospheric water appeared in the solid-state structure of **2.7**. Intermolecular interactions occur between the atmospheric H_2O molecules and the macrocycle. The O–H···O hydrogen bonds exhibit acceptable O-to-O distances between 2.663 Å - 2.943 Å. In this structure H_2O shows a propensity for linking the axial and equatorial pyrogallol subunits within a given macrocycle, as illustrated by the two (2) hydrogen bonds of 2.897 Å and 2.943 Å in length (O···O). Crystallization in methanol also allows for C–H···π interactions between methanol and R-groups or equatorial pyrogallol subunits (**Figure 2.14**). Also of interest are two (2) distinct macrocycle-to-macrocycle intermolecular hydrogen-bonding interactions. In one hydrogen-bonding motif, neighboring pendent R-groups interact via the OH moieties, generating growth along the a-axis (**Figure 2.15a**). The other hydrogen-bonding motif results in staggered hydrogen bonds between the phenolic groups of adjacent equatorial and axial pyrogallols, generating growth along the b-axis (**Figure 2.15b**).
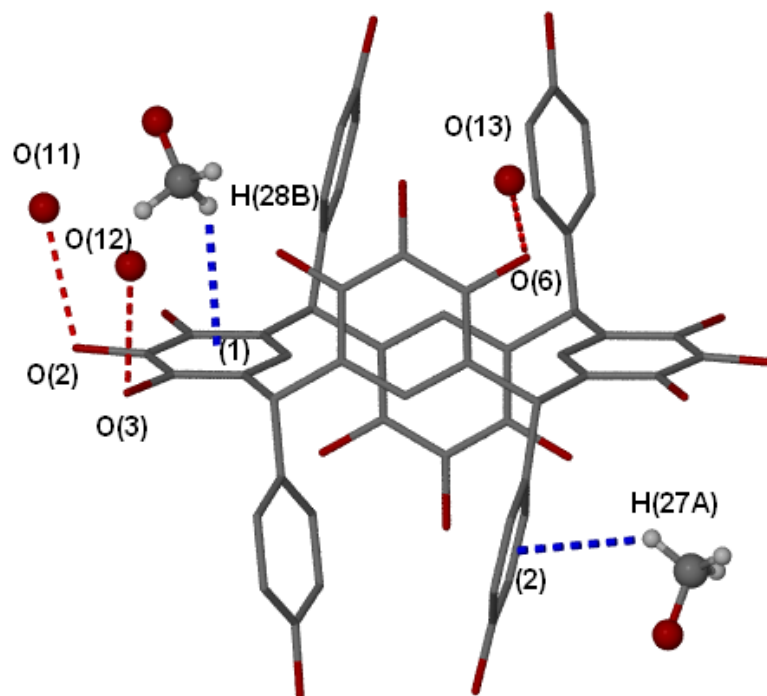
Figure 2.14: Crystallographic image of **2.7** illustrating both the O–H···O hydrogen-bonding network (dashed red) between the H$_2$O and phenolic groups of the pyrogallol as well as the C–H···π interactions between the MeOH and macrocycle (dashed blue). O: red, C: grey, and H: white.

.
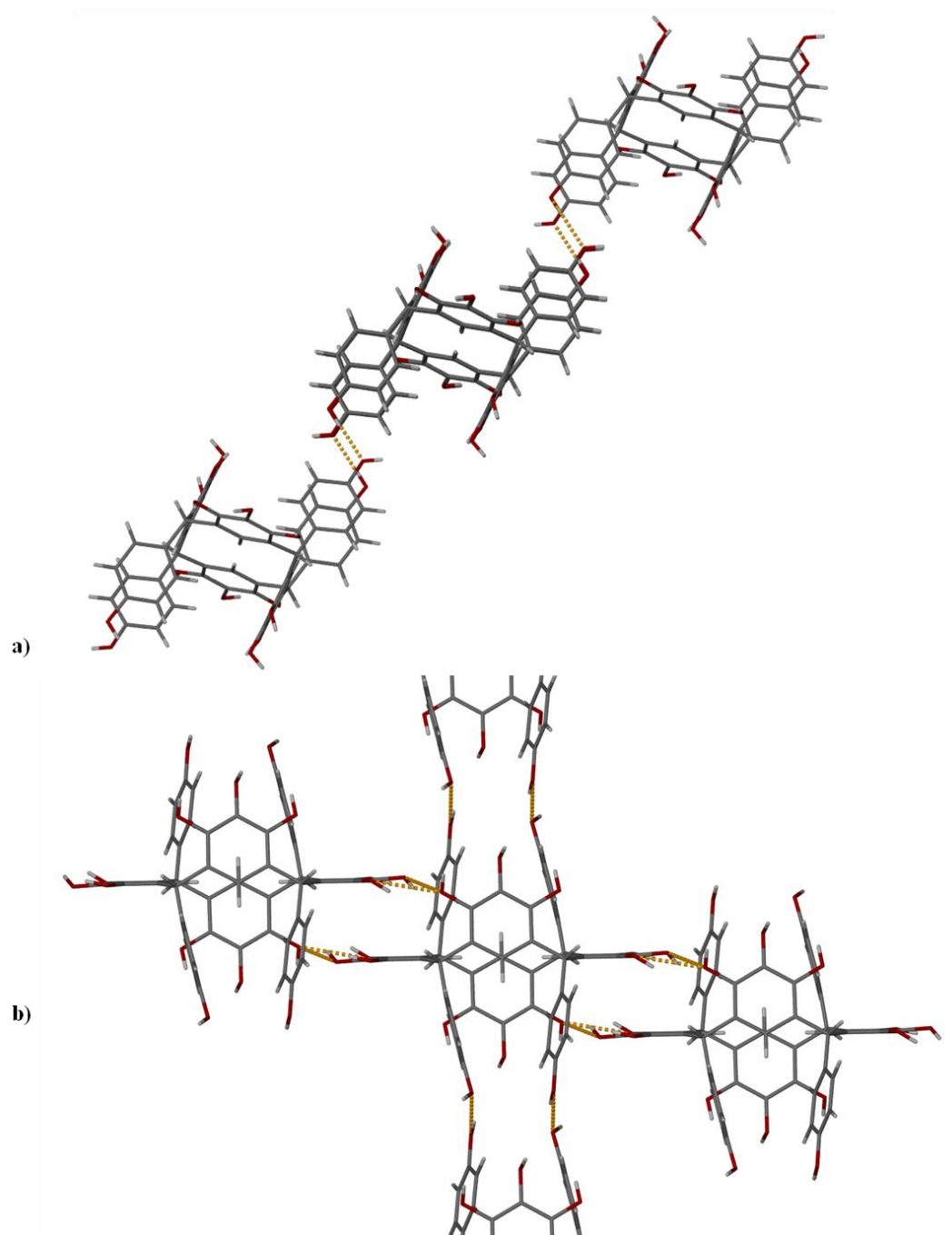
Figure 2.15: a) Crystallographic image of **2.7** with macrocycle-to-macrocycle hydrogen bonding along the vertical axis (dashed gold). b) Horizontal staggered macrocycle-to-macrocycle hydrogen bonding (dashed gold). O: red, C: grey, and H: white.

2.3.2.4 Analysis of *C*-2-methoxyphenylpyrogallol[4]arene 2.8 and *C*-4-methoxyphenylpyrogallol[4]arene 2.9

To examine the correlation between stereostructure and added bulk on the pendant R-groups, methoxybenzaldehydes were employed as starting materials for the acid-catalyzed condensation reaction (**Scheme 2.2**). *C*-2-methoxyphenyl-pyrogallol[4]arene **2.8** and *C*-4-methoxyphenylpyrogallol[4]arene **2.9** were also examined to probe whether the symmetry of the pendent R-groups affects formation of dimeric nanocapsules (see **Chapter 3**). ^{1}H NMR was utilized, taking advantage of the unique splitting patterns associated with the pyrogallol subunits, to confirm complete synthesis of both compounds **2.8** and **2.9**. As with *C*-phenylpyrogallol[4]arene **2.1**, however, the complex ^{1}H NMR spectrum of **2.8** is indicative of the presence of several stereoisomers in solution. Further purification was attempted through various crystallizations, but subsequent XRD analyses surprisingly revealed only the *rccc* boat stereostructure, the second example of this type of stereostructure isolated for *C*-arylpyrogallol[4]arenes.

The ^{1}H NMR of **2.9** not only shows the typical splitting pattern of a *para*-substituted phenyl ring, AA'BB', but also indicates formation of the *rctt* chair stereostructure. The characteristic singlet of the methine proton is observed at 5.567 ppm, and the Ar-H protons (axial and equatorial) are split over two (2) positions at 5.936 ppm and 5.534 ppm.

Single crystals of **2.8** and **2.9** were obtained by slow evaporation in DMF and DMSO, respectively (**Figure 2.16**). The *rccc* boat stereostructure of *C*-2-

methoxyphenylpyrogallol[4]arene **2.8** has a π–π (centroid-to-centroid) distance of 4.377 Å. The boat conformers, so aptly named flattened cones, both exhibit a greater than 90° angle between the axial and equatorial pyrogallol subunits. For example, in **2.8** this angle is 109.3° or 19.3° past perpendicular. Like the other boat conformer isolated in this research, the twist angle between pendent R-groups in **2.8** is minimal, 2.3°. Also found for **2.8** are two distinct solvent-to-macrocycle O–H···O hydrogen bonds, with O-to-O distances of 2.731 Å and 2.822 Å. Although the stereostructure of compound **2.9** is the *rctt* chair, **2.9** exhibits similar characteristics to **2.8**, such as a small twist angle of 6.4° and two (2) distinct solvent-to-macrocycle O–H···O hydrogen bonds, with O-to-O distances of 2.657 Å and 2.731 Å. However, **2.9** does have a larger π–π distance of 4.586 Å versus 4.337 Å. Also note the essentially perpendicular angle between the axial and equatorial pyrogallol subunits.
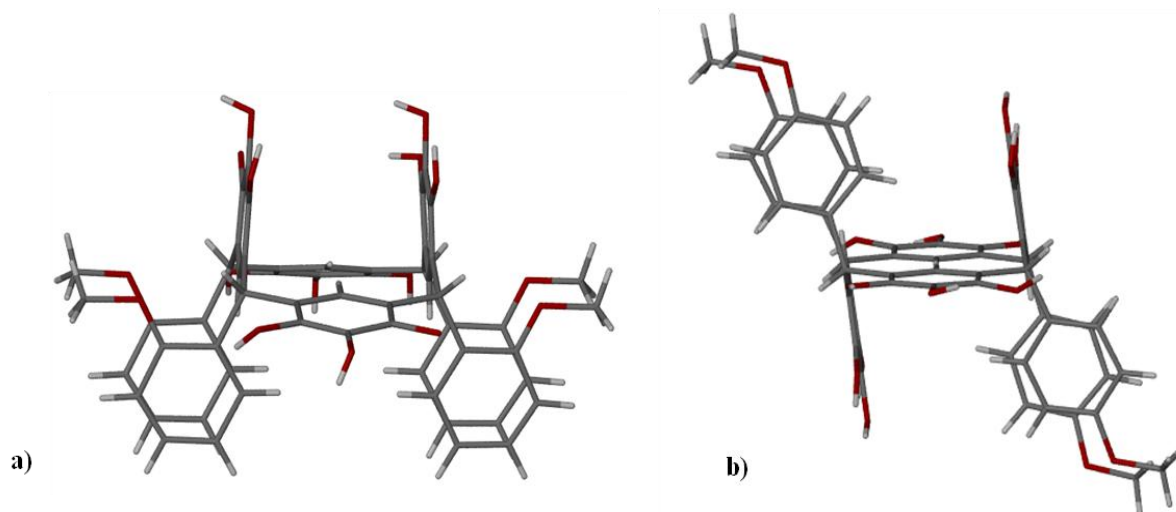
Figure 2.16: Crystallographic images of a) the *rccc* boat stereostructure of *C*-2-methoxyphenylpyrogallol[4]arene **2.8** and b) the *rctt* chair stereostructure of *C*-4-methoxyphenylpyrogallol[4]arene **2.9** . O: red, C: grey, and H: white.

2.3.2.5 Analysis of *C*-4-propoxyphenylpyrogallol[4]arene 2.10

In an attempt to make *C*-arylpyrogallol[4]arenes more soluble, alkylation of 4-hydroxybenzaldehyde was achieved by the addition of K_2CO_3 in a two-fold excess followed by the addition of stoichiometric amounts of iodopropane to form *C*-4-propoxyphenylpyrogallol[4]arene **2.10**. Crystallization of **2.10** in DMSO afforded the *rctt* chair stereostructure, **2.10a**, whereas crystallization of bulk **2.10** in MeOH yielded the third *rccc* boat stereostructure, **2.10b** (**Figure 2.17**). Presumably, the greater solubility of the minor product (the boat conformer) allows for separation from the less soluble major product. As with the other two *rccc* boat stereostructures, the degree of bend between the axial and equatorial pyrogallol units of **2.10b** is further past perpendicular than that of *rctt* chair stereostructures (**Figure 2.17**). In **2.10a** the bend angle is 93.06° as compared to 112.78° in **2.10b**. This increase in angle could contribute to the lower overall stability of the boat conformer with respect to the chair conformer, as the larger angle pushes the pendent R-groups closer to each other.

Examination of the two (2) crystal structures of **2.10** indicates a difference between the R-group aryl-aryl distances. The π–π centroid distances for the chair **2.10a** and boat **2.10b** are 3.84 Å and 4.54 Å, respectively, thus increasing the overall stability of the chair as compared to the boat conformer. Another factor stabilizing the chair with respect to the boat is the more favorable dipole-dipole interactions for the former, as measured by the dipole moments. (*Ab initio* electronic structure calculations yield a dipole moment of eight (8) D for the C_2 *rccc* boat form as compared to zero (0) D for the C_i *rctt* chair.) Upon further scrutiny of the two (2) crystal structures, neither C–H···π nor
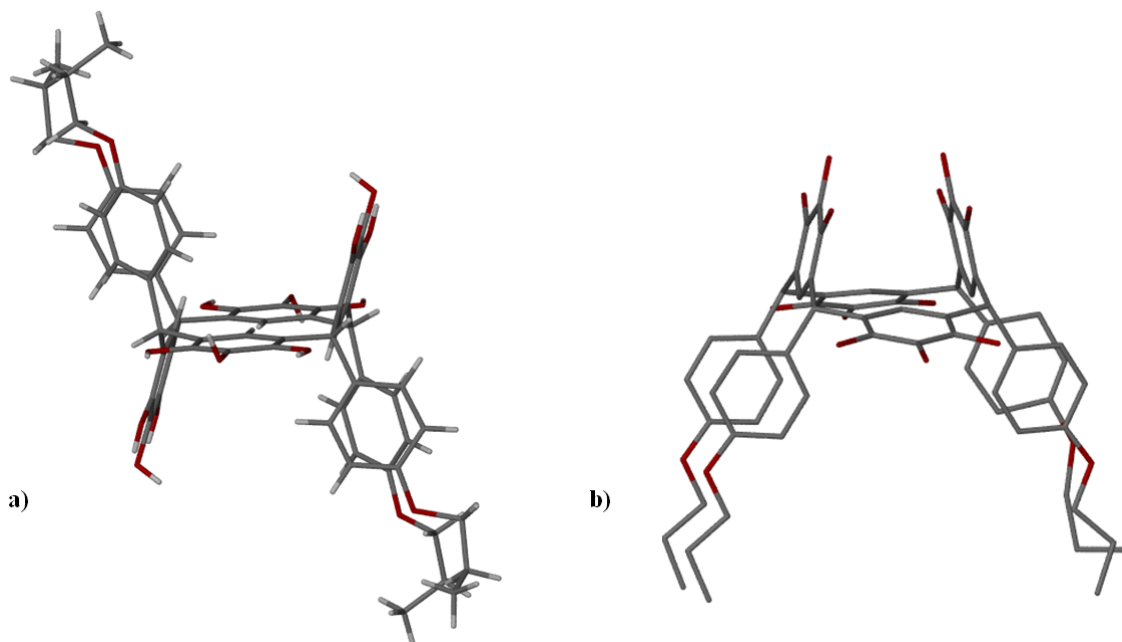
Figure 2.17: Crystallographic images of a) the *rctt* chair stereostructure of *C*-propoxy-phenylpyrogallol[4]arene **2.10a** and b) the *rccc* boat stereostructure of *C*-propoxyphenyl-pyrogallol[4]arene **2.10b**. Hydrogen atoms were calculated for a) and not located in b). O: red, C: grey, and H: white.

C–H···O interactions appear to contribute to the larger thermodynamic stability of the chair arrangement (**Figure 2.17**). Although phenyl C–H bonds point directly towards OH groups in the chair structure, the distance between the two moieties is too large for the intramolecular interactions to play a significant role in differentiating between the stabilities of the conformers (**Figure 2.17a**).

2.3.3 Synthesis and characterization of di-substituted *C*-phenylpyrogallol[4]arenes

Synthesis of *C*-2,3-dimethoxyphenyl-, *C*-2,4-dimethoxyphenyl-, *C*-3,4-dimethylphenyl-, and *C*-3,5-dihydroxyphenylpyrogallol[4]arenes (**2.12, 2.13, 2.14, 2.15**) was achieved by a similar procedure to the synthesis of **2.1** (**Scheme 2.2**). Di-substituted arylpyrogallol[4]arenes were studied to determine whether size limitations exist that would prohibit macrocycle formation or affect stereostructure or capsule formation.

2.3.3.1 Analysis of *C*-2,3-dimethoxyphenylpyrogallol[4]arene 2.12 and *C*-2,4-dimethoxyphenylpyrogallol[4]arene 2.13

From the analysis of the ^{1}H NMR spectrum of *C*-2,3-dimethoxyphenylpyrogallol[4]arene **2.12** from bulk material, it was concluded that two stereoisomers were present in solution. The two (2) sets of structural peaks include two (2) methine singlets at 5.978 ppm and 6.037 ppm, two (2) sets of aryl singlets, and two (2) sets of methoxy singlets. Although the regions of the aryl singlets (5.0 − 6.5 ppm) and methoxy singlets (3.0-4.0 ppm) can be assigned, specific values for the individual stereostructures cannot.

At this point, only the *rctt* chair stereostructure has been isolated for *C*-2,3-dimethoxyphenylpyrogallol[4]arene and *C*-2,4-dimethoxyphenylpyrogallol[4]arene **2.13**. Despite the similarity in functionality and conformation, **2.12** and **2.13** exhibit different structural properties, solvent interactions and packing patterns.

Because of its inherent lack of solubility resulting from both the aromatic pendent R-groups and the chair conformer, thus far *C*-2,3-dimethoxyphenylpyrogallol[4]arene

2.12 has dissolved in only DMSO, DMF and pyridine, with only pyridine affording suitable single crystals. It was originally thought that the addition of bulky substituents would increase the twist angle to decrease electrostatic repulsions; however, the resulting solid-state structure indicates only a 9.81° twist angle, which is significantly smaller than the twist angles found for some of the mono-substituted species. The π–π distance of 4.416 Å is correspondingly small. With most solvates of pyrogallol[4]arenes showing several types of intermolecular solvent-to-macrocycle hydrogen bonding, it was not unexpected to see four (4) distinct O–H···N hydrogen bonds, with O-to-N distances ranging from 2.711 Å - 3.067 Å (**Figure 2.18b**). In the structures discussed previously, most of the intermolecular interactions are limited to conventional hydrogen bonding. However, as the functionalization of the pendent R-groups increases, the number of C–H···O and C–H···π interactions increases as well. For **2.12**, a C–H···O (solvent-to-macrocycle) intermolecular interaction with a distance of 2.318 Å creates stabilizing forces in the solid state. Also contributing to the stabilization are the intramolecular C–H···O interactions between adjacent methoxy substituents on the same R-group and between methoxy substituents on neighboring R-groups (**Figure 2.18a**). The H···O distances for these interactions range from 2.393 Å to 3.034 Å. The packing pattern forms a bi-layer, which precludes intermolecular interactions between macrocycles across the solvent channel.
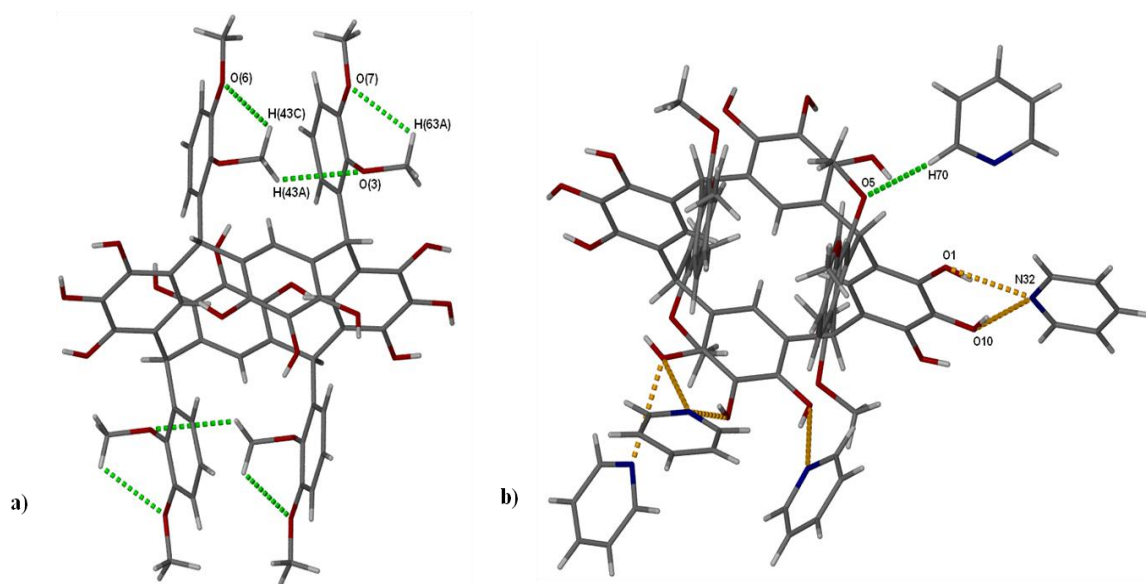
Figure 2.18: Crystallographic images of **2.12** showing a) C–H⋯O intramolecular interactions (lime green) and b) both C–H⋯O (dashed lime green) and O–H⋯N (dashed gold) intermolecular interactions. O: red, C: grey, and N: blue. Hydrogen atoms are shown in white

Similarly, compound **2.13** is soluble in DMSO, DMF and pyridine but only DMF produced suitable single crystals for x-ray diffraction. Analysis of the solid-state structure indicates that for the first time the equatorial pyrogallols are twisted 12.90° out of plane, to accommodate a single DMF molecule between the pendent R-groups and the axial pyrogallol (**Figure 2.19**). This twisting causes the macrocycle to be asymmetrical and thus results in two different twist angles and π-π distances as well as an increased number of distinct solvent-to-macrocycle hydrogen bonds. It is now necessary to distinguish between the two sets of pendent R-groups, which will be labeled *up* or *down* based on their orientation in **Figure 2.19**. Before the solid-state analysis of **2.13**, a direct correlation between twist angle and π-π distance was observed. In this compound, the

larger π–π (down) distance of 4.747 Å is combined with the smaller twist angle of 12.92°, and the smaller π–π (up) distance of 4.534 Å is combined with the larger twist angle of 20.30°.

This host-guest complex is stabilized by a C–H···π interaction with a H···π distance of 2.938 Å, created by the methyl group from the DMF molecule interacting with an axial pyrogallol. DMF molecules also contribute to the stability of the solid-state structure through eight (8) distinct hydrogen bonds (O–H···O) with O-to-O distances ranging from 2.631 Å - 2.801 Å. Once again, atmospheric water appears in the solid-state structure and is modeled as partial water clusters involved in four (4) hydrogen bonds with O···O distances between 2.693 Å - 2.816 Å. It is worth noting that, like **2.7,** a single H_2O molecule links an axial and equatorial pyrogallol subunit via O–H···O hydrogen bonds.
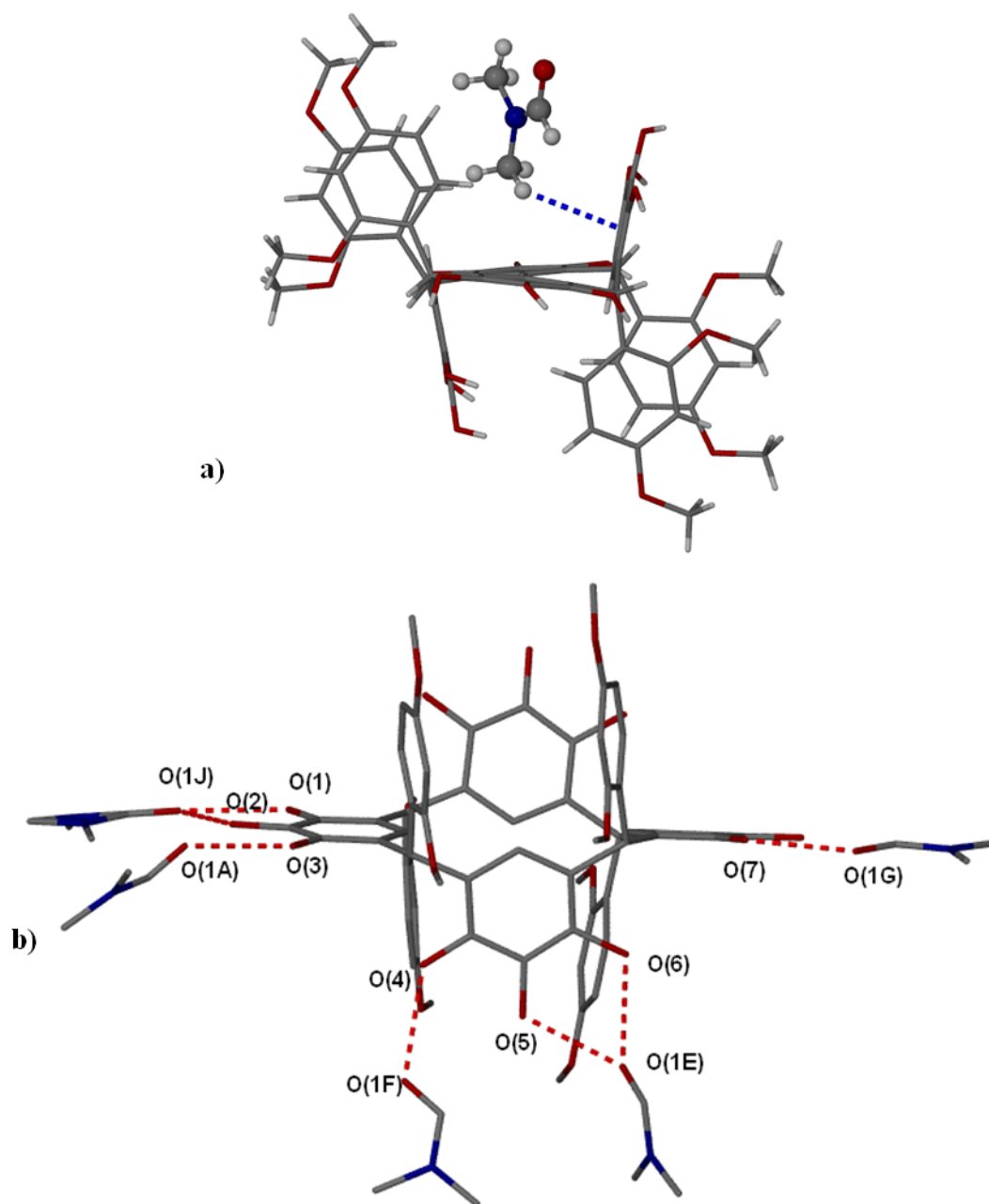
Figure 2.19: a) Crystallographic image of **2.13** showing the *rctt* chair stereoisomer and the C–H⋯π host-guest interaction (dashed blue). b) Crystallographic image of **2.13** showing the intermolecular macrocycle-to-solvent O–H⋯O hydrogen bonds (dashed gold). Hydrogen atoms in b) omitted for clarity. O: red, C: grey, N: blue, and H: white.

2.3.3.2 Analysis of *C*-3,4-dimethylphenylpyrogallol[4]arene 2.14

Single crystals of the *rctt* chair stereostructure of *C*-3,4-dimethylphenylpyrogallol[4]arene, **2.14** were obtained by recrystallization of the bulk material in DMSO. Analysis of **2.14** in the solid state reveals a structure with a π–π distance of 4.433 Å and a twist angle of 3.74°, making this twist angle the smallest observed for all the studied di-substituted *C*-arylpyrogallol[4]arenes (**Figure 2.20**). The axial and equatorial pyrogallol subunits contribute a total of eight (8) distinct intermolecular O–H⋯O(solvent) hydrogen bonds, with O-to-O distances ranging from 2.570 Å - 3.038 Å.

a) b)
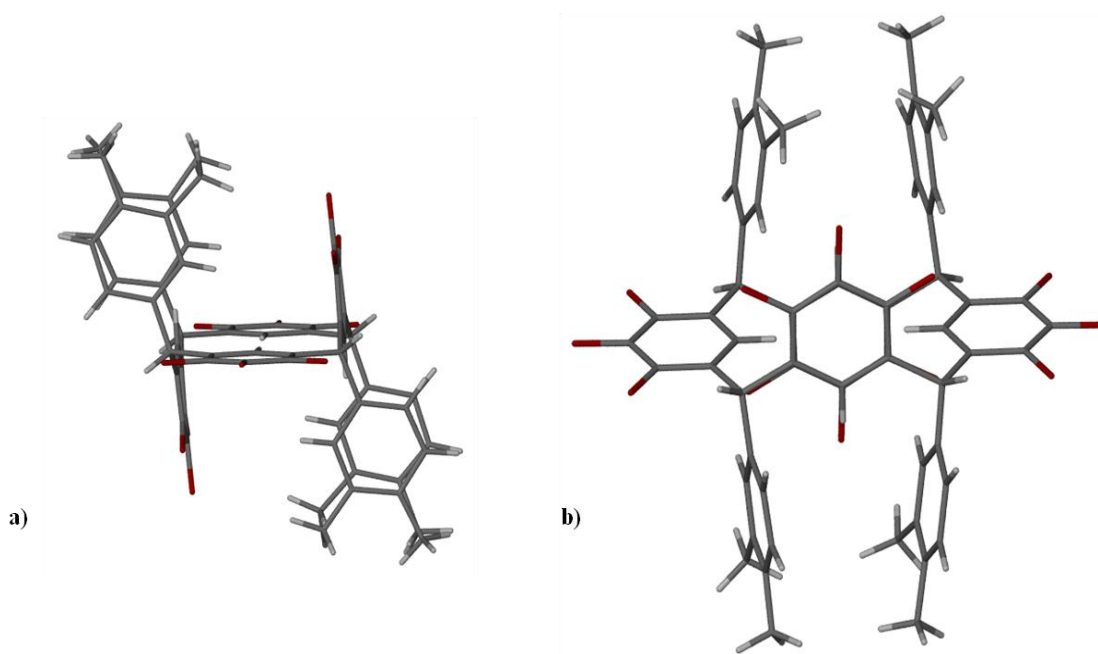
Figure 2.20: Two (2) crystallographic views of *C*-3,4-dimethylphenylpyrogallol[4]arene **2.14** illustrating the π-π distances and twist angles. O: red, C: grey, and H: white.

2.3.3.3 Analysis of *C*-3,5-dihydroxyphenylpyrogallol[4]arene 2.15

Due to the addition of a second hydroxyl group, *C*-3,5-dihydroxyphenylpyrogallol[4]arene, compound **2.15**, was easily dissolved in MeOH. This is in stark contrast to the previously discussed di-substituted arenes, which dissolved in only aprotic polar solvents such as DMF, DMSO, and pyridine. While suitable single crystals of the *rctt* chair stereostructure were obtained from slow evaporation of the methanol solution, analysis of the solid-state data revealed water rather than MeOH solvent molecules interacting with **2.15**. The six (6) water molecules help to stabilize the structure through eleven (11) O–H⋯O hydrogen bonds between the solvent and macrocycle; the O⋯O distances range from 2.612 Å - 3.040 Å. The solid-state structure of **2.15** forms a bi-layer packing pattern (**Figure 2.21**); however, as opposed to **2.12**, the use of water rather than pyridine as a solvent allows for a narrower solvent layer, which encourages macrocycle-to-macrocycle hydrogen bonding. Thus, two (2) different macrocycle-to-macrocycle O–H⋯O hydrogen bonding motifs are observed for **2.15** (**Figure 2.22**). The first motif involves two (2) equatorial pyrogallol subunits interacting across the solvent layer, producing a hydrogen bond with an O⋯O distance of 2.701 Å. In the second motif, the hydrogen bonds occur between pendent R-groups on neighboring macrocycles. The O-to-O distance of these hydrogen bonds is 2.719 Å.

For comparison with the other structures, the measured π–π distance is 4.268 Å and the twist angle is 7.08°. The complete set of data for the mono- and di-substituted R-groups demonstrates that the twist angle is only one contributing factor to the observed π–π distance. The functional group, position of the substituent on the pendent R-group,

and degree of bend between the axial and equatorial pyrogallols are also contributing factors.
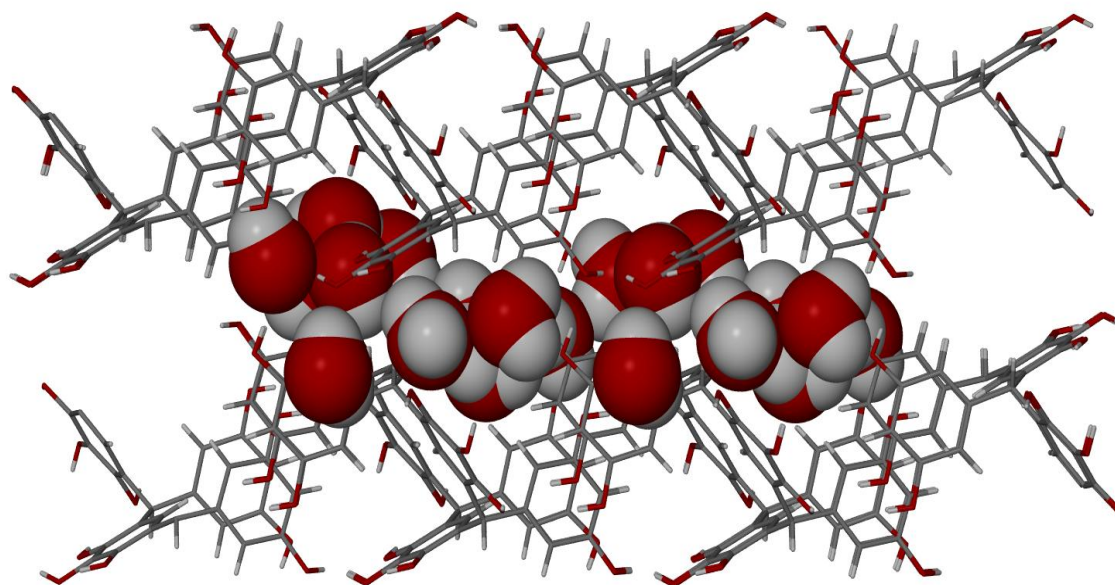
Figure 2.21: Crystallographic image of the bi-layer packing pattern for **2.15** that results from multiple solvent-to-macrocycle and macrocycle-to-macrocycle interactions. Solvent H_2O molecules shown as space filled. O: red, C: grey, and H: white.
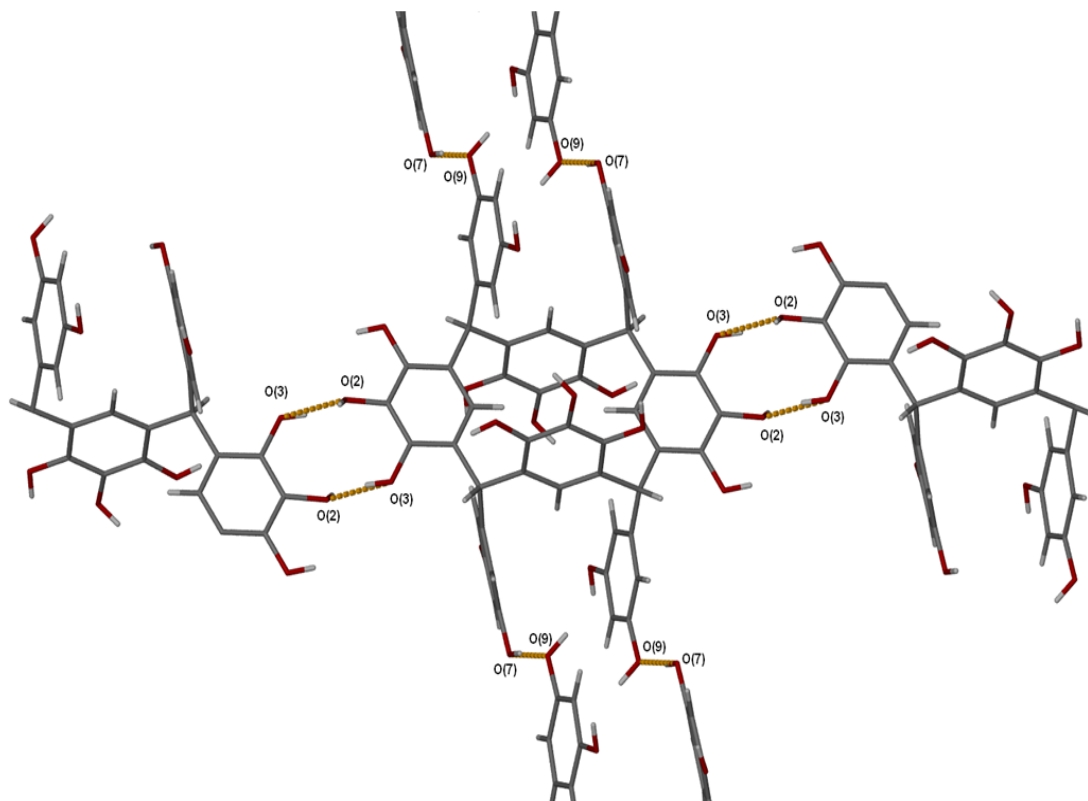
Figure 2.22: Crystallographic image of **2.15** showing two (2) discrete macrocycle-to-macrocycle hydrogen bonding motifs. O: red, C: grey, and H: white.

2.3.4 Tri- substituted *C*-arylpyrogallol[4]arenes

As discussed in previous sections several attempts were made to push the limits of size with regard to the pendent R-groups. Various trimethoxybenzaldehydes were reacted with pyrogallol but none prevented macrocycle formation. Compounds *C*-2,3,4-trimethoxyphenylpyrogallol[4]arene, **2.16**, *C*-2,4,5-trimethoxyphenylpyrogallol[4]arene, **2.17**, and *C*-3,4,5-trimethoxyphenyl-pyrogallol[4]arene were all synthesized but only *C*-3,4,5-trimethoxyphenylpyrogallol[4]arene **2.18** afforded easy characterization through [1]H

NMR and single crystal XRD. After careful analysis of the NMR spectrum of **2.18**, the presence of at least two (2) different stereostructures in solution was established. The spectrum contains four (4) sets of two (2) peaks resulting in the aryl protons split over two (2) positions because of different arene conformations. Since the *rccc* cone stereoisomer produces a singlet from the methine protons in conjunction with a singlet from the four equivalent pyrogallol aryl protons, the *rccc* cone cannot be one of the conformers in solution. Recall that both the *rccc* boat and *rctt* chair stereoisomers produce a singlet from the methine protons in conjunction with two (2) singlets from the non-equivalent aryl protons on the axial and equatorial pyrogallols. Therefore, it can be deduced that the two stereostructures present in solution are the *rctt* chair and *rccc* boat. It should be noted that there are several sets of minor peaks in the spectrum of **2.18** that could not be assigned, but that could, and in fact do, indicate the presence of other conformers in solution, as will be discussed in **Section 3.3**.

Single crystals of **2.18** suitable for XRD were produced in a manner similar to that reported for the previous compounds (**Figure 2.23**). Investigations of the solid-state structure revealed a *rctt* chair stereostructure with a π–π (centroid-to-centroid) distance of 4.651 Å. Of more interest is the small twist angle of 1.8°, which seems to disagree with the previous notion that the bulkier the pendent R-group the larger the twist angle. However, the increased functionality also increases the potential intra- and intermolecular interactions, which can in fact aid in decreasing the twist angle while at the same time continuing to stabilize the macrocycle. As expected then, compound **2.18**, being the most functionalized, has the greatest number of both intra- and intermolecular interactions.
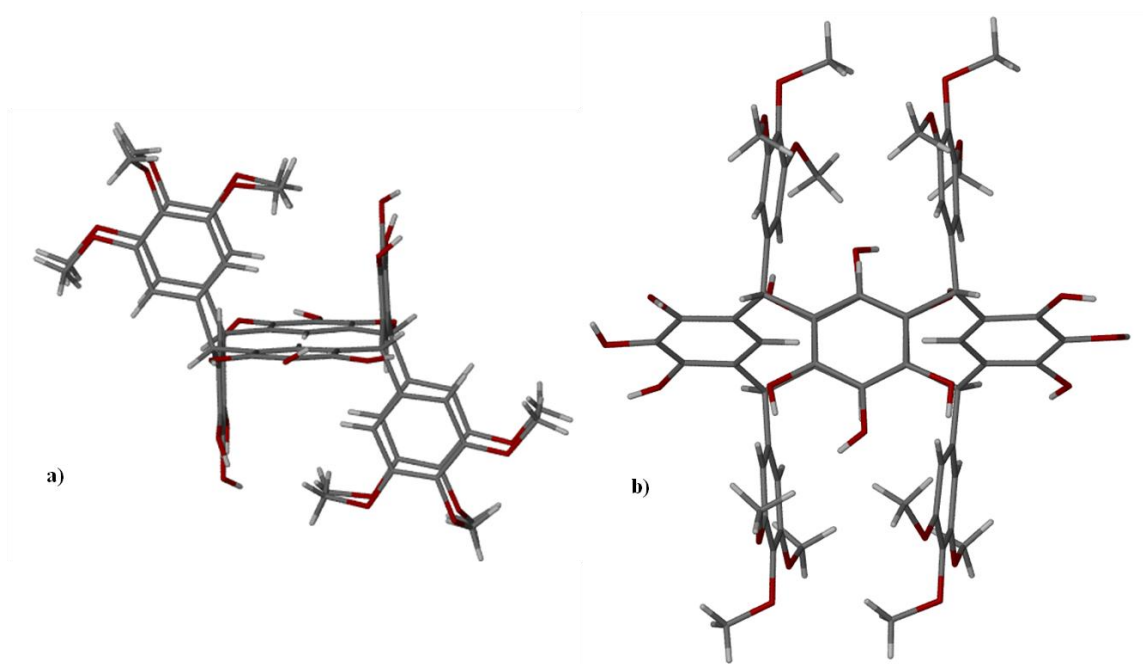
Figure 2.23: Crystallographic image of **2.18** showing both a) the standard chair view along the a-axis and b) the side view, used to study the twist angle of the pendent R-groups. O: red, C: grey, and H: white.

Along with seven (7) unique O–H···O hydrogen bonds between the macrocycle and DMSO, for which the O-to-O distances range from 2.637 Å – 2.757 Å (**Figure 2.24**), **2.18** contains five (5) different C–H···O interactions with H-to-O distances of 2.476 Å - 2.785 Å (**Figure 2.25**).
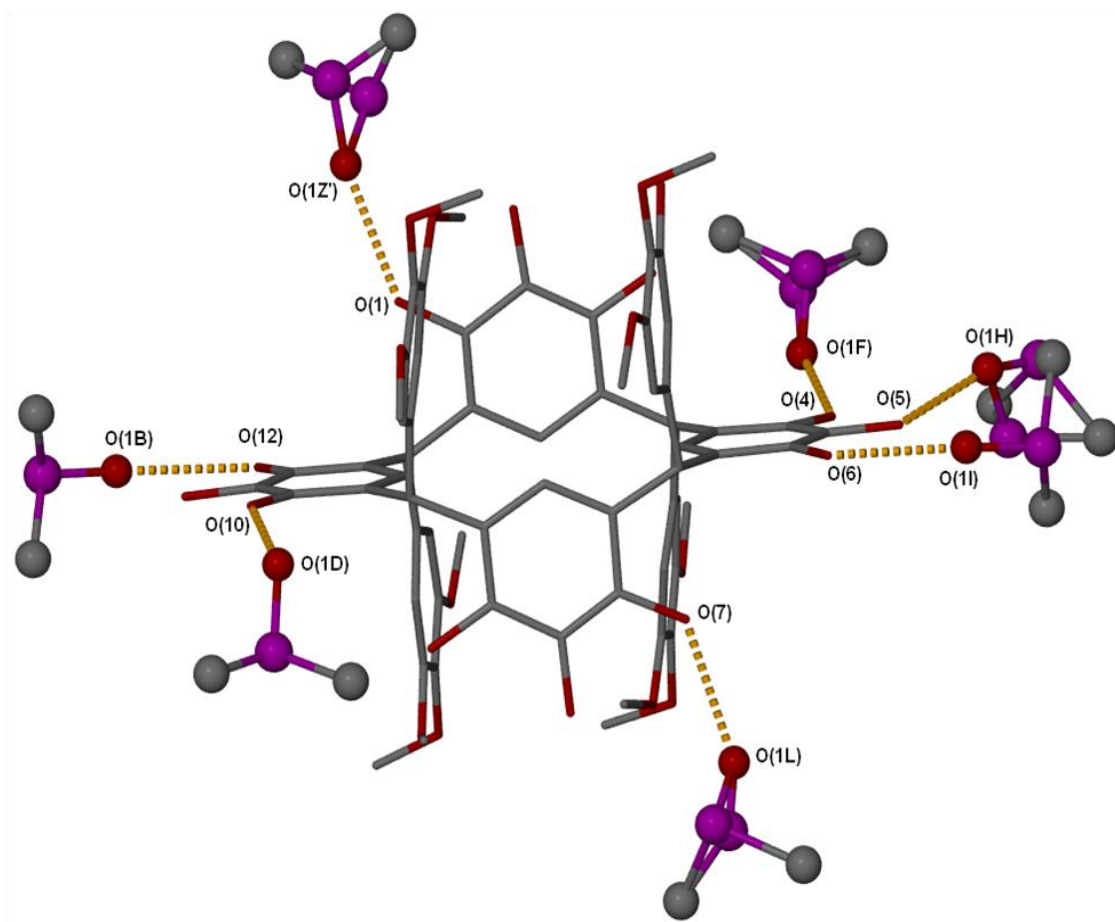
Figure 2.24: Crystallographic image of **2.18** illustrating the various DMSO-to-macrocycle O–H···O hydrogen bonds (dashed gold). O: red, C: grey, and S: purple. Hydrogen atoms omitted for clarity.
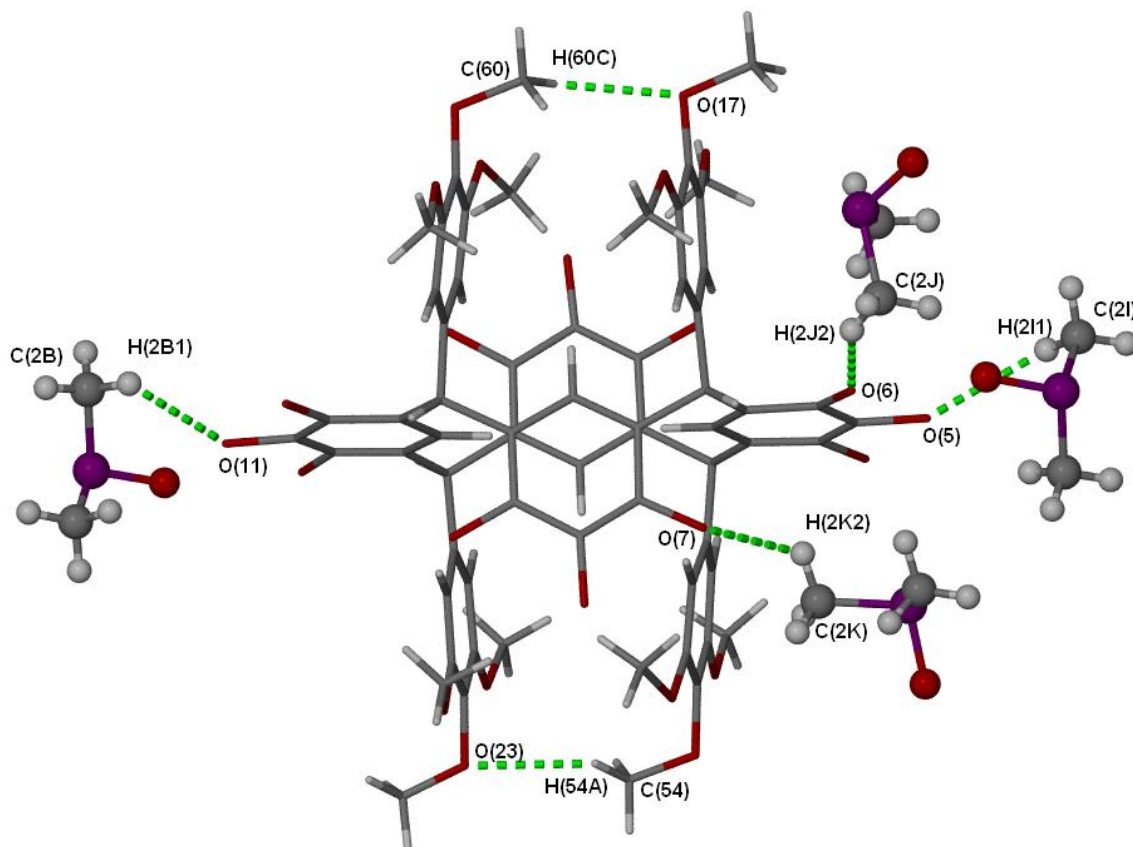
Figure 2.25: Crystallographic image of **2.18** illustrating the various C–H···O interactions (dashed green). O: red, C: grey, and S: purple. Hydrogen atoms on the pyrogallol subunits omitted for clarity.

2.4 Inherent instability and decomposition of pyrogallol[4]arenes

The tendency of resorcin[4]arenes and pyrogallol[4]arenes to form dimeric, hexameric, and tubular assemblies has been reported in countless journals over the last ten (10) years. However, despite the large amount of research done synthesizing larger supramolecular structures, properties such as ease of formation, dynamics, stability and mesomorphic behavior have attracted considerably less attention.[105-108] As with other

organic compounds, resorcin[4]arenes and pyrogallol[4]arenes are considered to be sufficiently stable in solution that decomposition below melting point temperatures is rare. Our interest in crystallizing *C*-pyrogallol[4]arenes in methanol has shown, however, that these arenes can in fact decompose at temperatures below their melting points. This phenomenon is not observed for the corresponding resorcin[4]arenes and does not discriminate between alkyl and aryl pendent R-groups.

It was thought that if *C*-phenylpyrogallol[4]arene **2.1** could be crystallized in methanol, incorporation of this solvent in the crystal lattice would allow close enough packing for a channeled structure to form and thus allow for further applications in gas sorption. Upon further investigation, crystallization over a span of one (1) month led to the new, previously unreported structure **2.19** (**Figure 2.26**). Documented accounts of similar stability studies using *C*-ethylpyrogallol[4]arene by E Kalenius *et al*.[109] indicate that a structural transformation occurs in a two-step process, with each step corresponding to a loss of either propene or ketene. This trasformation takes place in both protic polar methanol and aprotic polar acetonitrile. Although **2.19** was obtained in methanol, there was no such loss of either a propene or ketene, but rather the addition of a solvent molecule to the macrocycle.
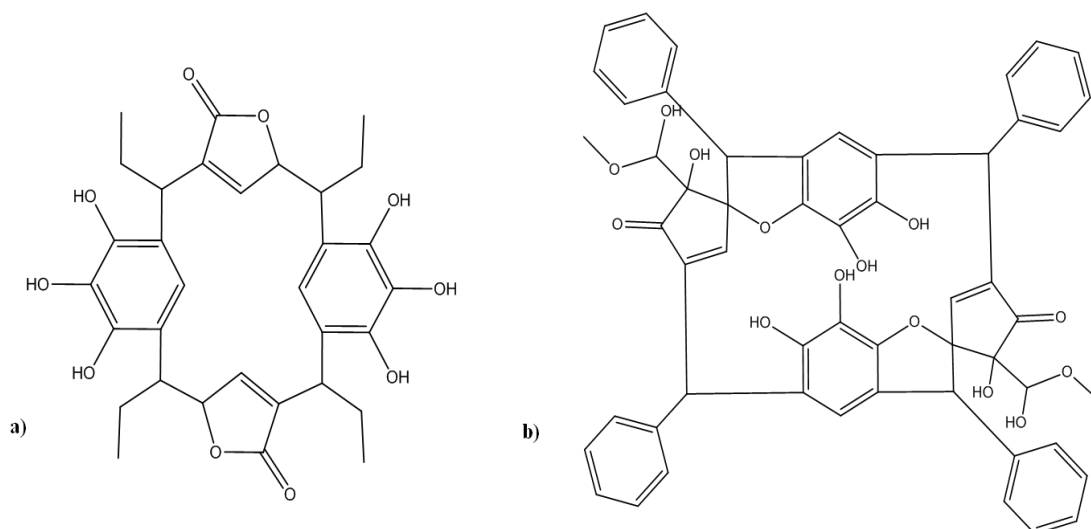
Figure 2.26: Schematic representation of a) pyrogallolarene bis-lactone and b) **2.19**, termed a spiropyrogallol[4]arene.

Although more work is needed to understand the mechanism by which **2.19** is obtained, analysis of the solid-state structure reveals interesting properties, especially with respect to molecular recognition. Analysis of the crystals of spiropyrogallol[4]arene **2.19** (**Figure 2.27**), named for the *spiro* connectivity between the cyclic subunits in the structure, reveals a monoclinic cell with the chiral space group of P2(1)/n. The short distance of 1.337 Å for the C(10)–C(11) bond indicates that it is a double bond. The O(7)–C(14) and C(12)–O(4) bonds have similar lengths of 1.199 Å and 1.212 Å, respectively, typical of carbonyl bonds. The crystals of spiropyrogallol[4]arene have an intricate lattice composed of channels along both the a-axis and the b-axis.
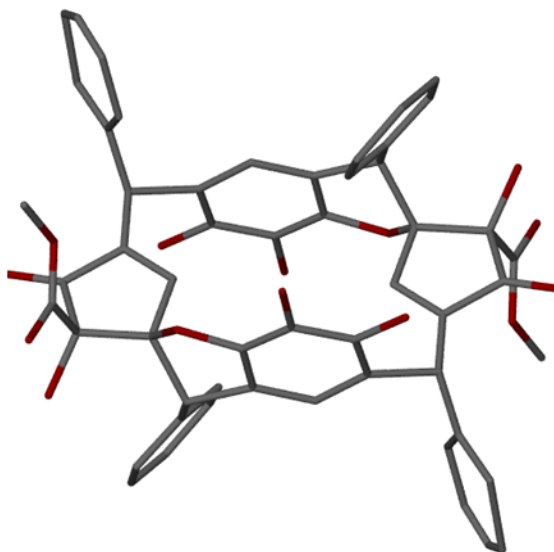
Figure 2.27: Cyrstallographic view along the c-axis of **2.19.** O: red, C: grey. Hydrogen atoms omitted for clarity.

Methanol solvent molecules along the a-axis of the crystalline lattice are disordered over two positions (bifurcated) (**Figure 2.28a**). In contrast, the channel along the b-axis contains only ordered solvent molecules, illustrative of the different sizes of the channels (**Figure 2.28b**). The segregation of solvent molecules by the channels provides an excellent example of molecular recognition.

The presence of the staggered intercalating layers led to consideration of possible CO_2 gas sorption properties for these crystals. Upon further investigation **2.19** showed no measurable sorption of CO_2, which was later rationalized by channel collapse under vacuum.
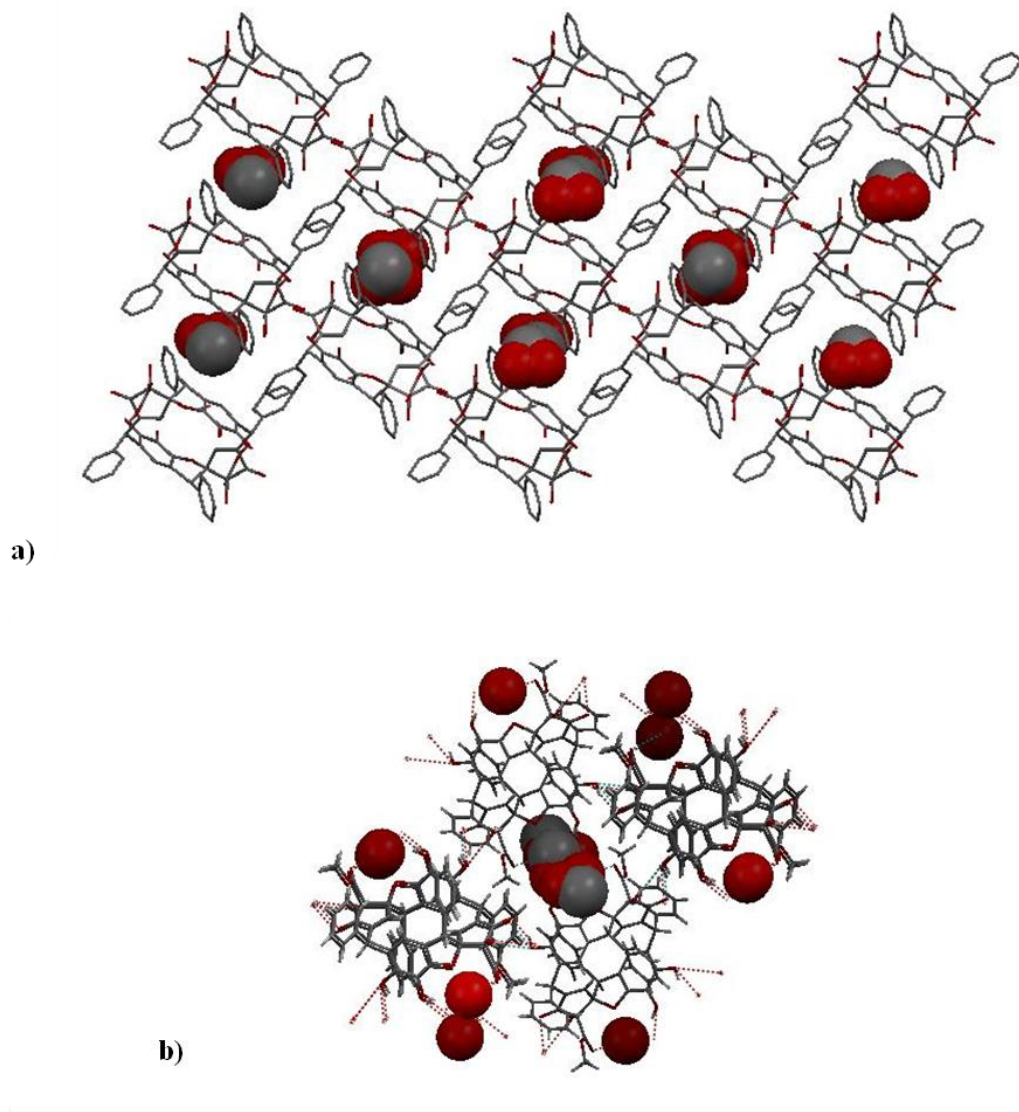
Figure 2.28: a) Partial packing diagram of **2.19** viewed down the a-axis of the monoclinic cell illustrating the bifurcated MeOH. b) View of the b-axis channel showing ordered solvent. O: red, C: grey, and S: purple. Hydrogen atoms omitted for clarity.

2.4 Conclusions

The work in all three phases (solid, solution and gas) points to the *rctt* chair and *rccc* boat arrangements as the products of the acid-catalyzed condensation reactions between substituted benzaldehydes and pyrogallol. This research provided the first three examples of *C*-arylpyrogallol[4]arenes in the *rccc* boat stereostructure. We have shown through computation and experiment that the chair conformation may be thermodynamically preferred in all three phases for aryl-substituted pyrogallol[4]arenes. This result differs from the preferred *rccc* cone stereostructure for alkyl- and aryl-substituted resorcin[4]arenes and alkyl-substituted pyrogallol[4]arenes. Intra- and intermolecular interactions, R-group substitution, packing effects and solvent effects all appear to contribute to the overall stereostructure of these macrocycles in the solid state.

2.5 Future Studies

Currently, a wider range of *C*-arylpyrogallol[4]arenes are being synthesized to examine not only the conformational preferences but also the size limitations of the pendent R-group. For example, pyridinecarboxaldehyde has been used in the condensation reaction with little success. It is thought that larger amounts of acid may be needed to protonate the nitrogen on the pyridine before cyclization can occur. The reaction with pyrazenecarboxaldehyde could prove interesting as various color changes occur at different reaction times. Further chemistry should be performed on the pendent R-groups to synthesize compounds that cannot be purchased and otherwise would be impossible to study.

2.7 Experimental Data

C-phenylpyrogallol[4]arene 2.1

Benzaldehyde (2.083 mL, 18.8 mmol) and pyrogallol (2.38 g, 18.8 mmol) were added to 40 mL ethanol. The solution was allowed to stir at room temperature for 30 min. 2 mL conc. HCl was then added. The mixture was allowed to reflux for 24 hr. The solution was then filtered using a cold methanol wash yielding 3.27g white precipitate to produce of 80.6% yield.

^{1}H NMR (300 MHz, DMSO-d_6, shifts relative to DMSO): δ = 7.89 (1 H Ar-OH, *s*), 7.70 (1 H Ar-OH', *s)*, 7.575 (2 H Ar-OH, *s*), 7.465 (2 H Ar-OH', *s*), 6.838 (5 H, Ph-H *m*), 6.011 (1 H Ar-H, *s*), 5.668 (1 H, RC-H, *s*), 5.185 (1 H, Ar-H', *s*)

Crystallographic data C-phenylpyrogallol[4]arene : $C_{72}H_{100}O_{22}S_{10}$, M = 1091.28 g/mol, ρ = 0.8892g/cm^3, a = 11.6125(2), b = 11.8904(2), c = 16.1797(3), α = 80.962(1), β = 74.912(1), γ = 71.909(1), U = 2043.31(6) Å^3, triclinic, space group P-1 Z = 1, λ(Mo) = 71073 Å, T=173 K, 12549 reflections, 8205 unique R_1= 0.1109, wR_2= 0.3908 (all data), R_{int}= 0.0258 GOF= 1.492 CCDC 752684.

C-4-methylphenylpyrogallol[4]arene 2.2

The same procedure used for compound **2.1** was applied, substituting the appropriate aldehydes. (3.02 g, 0.024 mol) pyrogallol, (2.85 g, 0.024 mol) 4-methylbenzaldehyde, 50 mL EtOH, 2 mL of conc. HCl. (73% yield)

^{1}H NMR (300 MHz, DMSO-d$_6$, shifts relative to DMSO): δ = 8.189 (1 H, Ar-OH, *s*), 7.987 (2 H, Ar-OH', *s*), 7.952 (2 H, Ar-OH, *s*), 7.914 (1 H, Ar-OH', *s*), 7.748 (2 H,Ph-H, *d*), 6.822 (2 H, Ph-H, *d*), 5.875 (1 H, Ar-H, *s*), 5.748 (1 H, RC-H, *s*), 4.564 (1 H, Ar-H', *s*).

Crystal data for *C*-4-methylphenylpyrogallol[4]arene: C$_{36}$H$_{48}$O$_{10}$S$_4$, *M* = 768.98, colorless prism, 0.10 x 0.09 x 0.04 mm^3, triclinic, space group *P*-1 (No. 2), *a* = 11.4986(15), *b* = 12.1427(15), *c* = 15.1495(19) Å, *α* = 66.781(2), *β* = 89.342(2), *γ* = 79.598(2)°, *V* = 1907.8(4) Å^3, *Z* = 2, *D*$_c$ = 1.339 g/cm^3, *F*$_{000}$ = 816, Bruker Apex II CCD diffractometer, synchrotron radiation, λ = 0.77490 Å, *T* = 100(2)K, 2*θ*$_{max}$ = 67.3°, 27355 reflections collected, 11353 unique (R$_{int}$ = 0.0338). Final *GooF* = 1.023, *R1* = 0.0460, *wR2* = 0.1209, *R* indices based on 8677 reflections with I >2sigma(I) (refinement on *F*^{2}), 461 parameters, 0 restraints. Lp and absorption corrections applied, *μ* = 0.304 mm^{-1}.

C-4-ethylphenylpyrogallol[4]arene **2.3**

The same procedure used for compound **2.1** was applied, substituting the appropriate aldehydes. (3.12 g, 0.025 mol) pyrogallol, (3.31 g, 0.025 mol) 4-ethylbenzaldehyde, 50 mL EtOH, 2 mL conc. HCl. (71% yield)

^{1}H NMR (300 MHz, DMSO-d$_6$, shifts relative to DMSO): δ = 7.50 (3 H, Ar-H, *m*) (broadend by duterium exchange), 6.667 (2 H, Ph-H, *d*), 6.48 (2 H, Ph-H, *d*), 5.949 (1 H, Ar-H, *s*), 5.577 (1 H, RC-H, *s*), 5.350 (1 H, Ar-H', *s*), 2.440 (2 H, CH$_2$, *q*), 1.032 (3 H, CH$_3$, *t*)

Crystal data for *C*-4-ethylphenylpyrogallol[4]arene: $C_{40}H_{58}O_{11}S_5$, M = 875.16, colorless Prism, 0.20 x 0.15 x 0.04 mm^3, triclinic, space group *P*-1 (No. 2), a = 11.937(3), b = 12.044(3), c = 15.595(6) Å, α = 85.651(3), β = 89.857(4), γ = 83.007(2)°, V = 2219.0(11) Å^3, Z = 2, D_c = 1.310 g/cm^3, F_{000} = 932, Bruker APEXII CCD area detector, MoKα radiation, λ = 0.71073 Å, T = 173(2)K, $2\theta_{max}$ = 52.8°, 24239 reflections collected, 9027 unique (R$_{int}$ = 0.0553). Final *GooF* = 1.061, *R1* = 0.0748, *wR2* = 0.1896, *R* indices based on 5536 reflections with I >2sigma(I) (refinement on F^2), 509 parameters, 20 restraints. Lp and absorption corrections applied, μ = 0.317 mm^{-1}.

C-3-nitrophenylpyrogallol[4]arene 2.4

The same procedure used for compound **2.1** was applied, substituting the appropriate aldehydes. (3.08 g, 0.024 mol) pyrogallol, (3.69 g, 0.024 mol) 3-nitrobenzaldehyde, 50 mL EtOH, 2 mL conc. HCl. (68% yield)

^{1}H NMR (300 MHz, DMSO-d$_6$, shifts relative to DMSO): δ = 7.809 (1 H, Ar-OH, *s*), 7.578 (1 H, Ar-OH', *s*), 7.525 (2 H, Ar-OH, *s*), 7.388 (2 H, Ar-OH', *s*), 6.744 (2 H, Ph-H, *d*), 6.470 (2 H, Ph-H, *d*), 5.947 (1 H, Ar-H, *s*), 5.603 (1 H, RC-H, *s*), 5.202 (1 H, Ar-H', *s*), 2.134 (3 H, CH$_3$, *s*).

Crystal data for *C*-3-nitrophenylpyrogallol[4]arene: $C_{34}H_{44}N_2O_{15}S_4$, M = 848.95, 0.35 x 0.20 x 0.10 mm^3, triclinic, space group *P*-1 (No. 0), V = 1973.8(3) Å^3, Z = 2, D_c = 1.428 g/cm^3, F_{000} = 892, Bruker APEXII CCD area detector, MoKα radiation, λ = 0.71073 Å, T = 173(2)K, $2\theta_{max}$ = 55.1°, 23063 reflections collected, 8898 unique (R$_{int}$ = 0.0237).

Final *GooF* = 1.047, *R1* = 0.0404, *wR2* = 0.0959, *R* indices based on 7039 reflections

with I >2sigma(I) (refinement on F^2), 536 parameters, 0 restraints. Lp and absorption

corrections applied, μ = 0.311 mm^{-1}.

C-4-nitrophenylpyrogallol[4]arene 2.5

The same procedure used for compound **2.1** was applied, substituting the appropriate

aldehyde. (3.00 g, 0.024 mol) pyrogallol, (3.59 g, 0.024 mol) 4-nitrobenzaldehyde, 50

mL EtOH, 2 mL conc. HCl. (91% yield)

^{1}H NMR (300 MHz, DMSO-d$_6$, shifts relative to DMSO): δ = 8.189 (1 H, Ar-OH, *s*),

7.987 (2 H, Ar-OH', *s*), 7.952 (2 H, Ar-OH, *s*), 7.914 (1 H, Ar-OH', *s*), 7.748 (2 H

,Ph-H, *d*), 6.822 (2 H, Ph-H, *d*), 5.875 (1 H, Ar-H, *s*), 5.748 (1 H, RC-H, *s*), 4.564 (1

H, Ar-H', *s*).

Crystal data for *C-4-nitrophenylpyrogallol[4]arene:* $C_{40}H_{49.20}N_2O_{14.50}S_{4.50}$, *M* =

934.28, Colorless Prism, 0.20 x 0.20 x 0.10 mm^3, triclinic, space group *P*-1 (No. 2), *a* =

10.368(5), *b* = 15.122(8), *c* = 16.483(8) Å, α = 99.067(6), β = 102.188(6), γ =

105.751(6)°, *V* = 2367(2) Å^3, *Z* = 2, D_c = 1.311 g/cm^3, F_{000} = 982, Bruker APEXII CCD

area detector, MoKα radiation, λ = 0.71073 Å, *T* = 173(2)K, $2\theta_{max}$ = 52.8°, 25531

reflections collected, 9612 unique (R_{int} = 0.1122). Final *GooF* = 1.100, *R1* = 0.1211, *wR2*

= 0.3264, *R* indices based on 3851 reflections with I >2sigma(I) (refinement on F^2), 566

parameters, 23 restraints. Lp and absorption corrections applied, μ = 0.287 mm^{-1}.

C-3-hydroxyphenylpyrogallol[4]arene **2.6**

The same procedure used for compound **2.1** was applied, substituting the appropriate aldehyde. (3.04 g, 0.024 mol) pyrogallol, (2.92 g, 0.024 mol) 3-hydroxybenzaldehyde, 50 mL EtOH, 2 mL conc. HCl. (89% yield)

^{1}H NMR (300 MHz, DMSO-d$_6$, shifts relative to DMSO): δ = 8.684 (1 H, Ph-OH, *s*), 7.813 (1 H Ar-OH, *s*), 7.715 (1 H Ar-OH', *s*), 7.566 (2 H Ar-OH, *s*), 7.441 (2 H Ar-OH', *s*), 6.672 (1 H, Ph-H, *t*), 6.249 (1 H, Ph-H, *d*), 6.077 (1 H, Ph-H, s), 6.055 (1 H, Ph-H, *d*), 5.971 (1 H, Ar-H, *s*), 5.620 (1 H, RC-H, *s*), 5.471 (1 H, Ar-H', *s*).

Crystal data for *C-3-hydroxyphenylpyrogallol[4]arene*: C$_{35.80}$H$_{49.40}$O$_{13}$S$_{4.80}$, *M* = 841.64, prism colorless, 0.10 × 0.10 × 0.05 mm^3, monoclinic, space group *C2/c* (No. 15), *a* = 19.3732(14), *b* = 13.8349(10), *c* = 31.099(2) Å, *β* = 102.417(2)°, *V* = 8140.4(10) Å^3, *Z* = 8, *D*$_c$ = 1.373 g/cm^3, *F*$_{000}$ = 3560, Bruker Apex II CCD diffractometer, synchrotron radiation, λ = 0.77490 Å, *T* = 100(2)K, $2\theta_{max}$ = 55.0°, 29970 reflections collected, 7182 unique (R$_{int}$ = 0.0680). Final *GooF* = 1.027, *R1* = 0.1023, *wR2* = 0.2760, *R* indices based on 5215 reflections with I >2sigma(I) (refinement on *F*^{2}), 573 parameters, 0 restraints. Lp and absorption corrections applied, *μ* = 0.420 mm^{-1}.

C-4-hydroxyphenylpyrogallol[4]arene **2.7**

The same procedure used for compound **2.1** was applied, substituting the appropriate aldehyde. (3.01 g, 0.024 mol) pyrogallol, (2.91 g, 0.024 mol) 4-hydroxybenzaldehyde, 50 mL EtOH, 2 mL conc. HCl. (73% yield)

^{1}H NMR (300 MHz, DMSO-d_6, shifts relative to DMSO): δ = 8.710 (1 H, Ph-OH, *s*), 7.785 (1 H Ar-OH, *s*), 7.695 (1 H Ar-OH', *s*), 7.493 (2 H Ar-OH, *s*), 7.321 (2 H Ar-OH', *s*), 6.407 (2 H, Ph-H, *d*), 6.322 (2 H, Ph-H, *d*), 5.936 (1 H, Ar-H, *s*), 5.562 (1 H, RC-H, *s*), 5.532 (1 H, Ar-H', *s*).

Crystal data for *C*-4-hydroxyphenylpyrogallol[4]arene: $C_{54}H_{60}O_{24}$, M = 1093.06, prism colorless, $0.02 \times 0.15 \times 0.25$ mm^3, monoclinic, space group P-1 (No.2), a = 10.7317(14), b = 11.2238(71), c = 12.0991(77) Å, α= 116.391(7) ° β = 96.8817(9)° γ= 98.803(9), V = 1260.71(10) Å^3, Z = 1, D_c = 1.4395 g/cm^3, F_{000} = 3560, Bruker Apex II CCD diffractometer, synchrotron radiation, λ = 0.77490 Å, T = 100(2)K, $2\theta_{max}$ = 55.0°, 27970 reflections collected, 7262 unique (R_{int} = 0.0680). Final *GooF* = 1.027, *R1* = 0.0893, *wR2* = 0.2370, *R* indices based on 5515 reflections with I >2sigma(I) (refinement on F^2), 573 parameters, 0 restraints. Lp and absorption corrections applied, μ = 0.420 mm^{-1}.

C-2-methoxyphenylpyrogallol[4]arene **2.8**

The same procedure used for compound **2.1** was applied, substituting the appropriate aldehyde. (3.10 g, 0.025 mol) pyrogallol, (3.35 g, 0.025 mol) 2-methoxybenzaldehyde, 50 mL EtOH, 2 mL conc. HCl. (86% yield)

^{1}H NMR (300 MHz, DMSO-d$_6$, shifts relative to DMSO): δ = 7.646 (1 H Ar-OH, *s*), 7.5782 (1 H Ar-OH', *s*), 7.356 (2 H Ar-OH, *s*), 7.232 (2 H Ar-OH', *s*), 6.561 (2 H, Ph-H, *d*), 6.553 (2 H, Ph-H, *d*), 6.102 (1 H, Ar-H, *s*), 5.943 (1 H, RC-H, *s*), 5.414 (1 H, Ar-H', *s*), 3.314 (3 H, OCH$_3$, *s*)

Crystal data for work *C*-2-methoxyphenylpyrogallol[4]arene: C$_{35.50}$H$_{23.50}$N$_{2.50}$O$_{10}$, *M* = 645.07, .15 × .1 × .25 mm^3, monoclinic, space group *P*2$_1$/*n* (No. 14), *a* = 17.818(3), *b* = 21.151(3), *c* = 17.821(3) Å, *β* = 93.413(2)°, *V* = 6704.1(17) Å^3, *Z* = 8, *D*$_c$ = 1.278 g/cm^3, *F*$_{000}$ = 2672, MoKα radiation, λ = 0.71073 Å, *T* = 296(2)K, 2*θ*$_{max}$ = 45.3°, 52414 reflections collected, 8887 unique (R$_{int}$ = 0.1258). Final *GooF* = 1.560, *R1* = 0.1634, *wR2* = 0.4323, *R* indices based on 3447 reflections with I >2sigma(I) (refinement on *F*^{2}), 400 parameters, 0 restraints. Lp and absorption corrections applied, *μ* = 0.095 mm^{-1}.

C-4-methoxyphenylpyrogallol[4]arene **2.9**

The same procedure used for compound **2.1** was applied, substituting the appropriate aldehyde. (3.10 g, 0.025 mol) pyrogallol, (3.35 g, 0.025 mol) 4-methoxybenzaldehyde, 50 mL EtOH, 2 mL conc. HCl. (83% yield)

^{1}H NMR (300 MHz, DMSO-d$_6$, shifts relative to DMSO): δ = 8.675 (1 H, RCHO, *s*),

7.775 (1 H Ar-OH, *s*), 7.685 (1 H Ar-OH', *s*), 7.484 (2 H Ar-OH, *s*), 7.313 (2 H Ar-OH', *s*), 6.413 (2 H, Ph-H, *d*), 6.317 (2 H, Ph-H, *d*), 5.936 (1 H, Ar-H, *s*), 5.567 (1 H, RC-H, *s*), 5.534 (1 H, Ar-H', *s*), 3.368 (3 H, OCH$_3$, *s*)

Crystal data for *C*-4-methoxyphenylpyrogallol[4]arene: C$_{36}$H$_{52}$O$_{14}$S$_4$, *M* = 837.02, 0.50 x 0.10 x 0.05 mm^3, monoclinic, space group *P*2$_1$/*c* (No. 14), *a* = 16.162(5), *b* = 11.599(3), *c* = 22.169(6) Å, *α* = 94.001(3)°, *V* = 4146(2) Å^3, *Z* = 4, *D*$_c$ = 1.341 g/cm^3, *F*$_{000}$ = 1776, MoKα radiation, λ = 0.71073 Å, *T* = 173(2)K, 2θ$_{max}$ = 52.8º, 44071 reflections collected, 8469 unique (R$_{int}$ = 0.0362). Final *GooF* = 1.058, *R1* = 0.0977, *wR2* = 0.2720, *R* indices based on 6191 reflections with I >2sigma(I) (refinement on *F*^{2}), 487 parameters, 0 restraints. Lp and absorption corrections applied, μ = 0.292 mm^{-1}.

C-4-propoxyphenylpyrogallol[4]arene 2.10

4-hydroxybenzaldehyde (1 g, .818 mmol) in acetone followed by addition of K$_2$CO$_3$ in a 2 fold excess and the addition of stoichiometric amounts of iodopropane resulted in the synthesis of 4-propoxybenzaldehyde. Pyrogallol (2 g, 1.585 mmol) was then added to a solution of ethanol and 4-propoxybenzaldehyde (2.60 g, 1.585 mmol) followed by the addition of 2 mL conc. HCl. (76% yield)

rctt chair stereoisomer: ^{1}H NMR (300 MHz, DMSO-d$_6$, shifts relative to DMSO): δ = 7.825 (1 H Ar-OH, *s*), 7.690 (1 H Ar-OH', *s*), 7.536 (2 H Ar-OH, *s*), 7.381 (2 H Ar-OH', *s*), 6.506 (2 H, Ph-H, *d*), 6.451 (2 H, Ph-H, *d*), 5.950 (1 H, Ar-H, *s*), 5.594 (1 H, RC-H, *s*), 5.370 (1 H, Ar-H', *s*), 3.756 (2 H, CH$_2$, *t*), 1.689 (2 H, CH$_2$, *m*), 1.027 (3 H,

CH$_3$, *t*)

rccc boat stereoisomer: ^{1}H NMR (300 MHz, DMSO-d$_6$, shifts relative to DMSO): δ = 7.785 (1 H Ar-OH, *s*), 7.607 (2 H Ar-OH, *s*), 6.676 (2 H, Ph-H, *d*), 6.585 (2 H, Ph-H, *d*), 5.734 (1 H, RC-H, *s*), 5.432 (1 H, Ar-H, *s*), 5.427 (1 H, Ar-H', *s*), 4.497 (2 H, CH$_2$, *t*), 2.496 (2 H, CH$_2$, *m*), 2.305 (3 H, CH$_3$, *t*)

C-naphthylpyrogallol[4]arene **2.11**

^{1}H NMR was attempted several different times; however identification of individual peaks proved difficult due to resolution. It was proposed that there were several stereoisomers present in solution based on several characteristics peaks (methine proton and aryl protons) being duplicated. Purification of any individual conformers has yet to be accomplished.

C-2,3-dimethoxyphenylpyrogallol[4]arenes **2.12**

The same procedure used for compound **2.1** was applied, substituting the appropriate aldehyde. (3.10 g, 0.025 mol) pyrogallol, (3.35 g, 0.025 mol) 2,3-dimethoxybenzaldehyde, 50 mL EtOH, 2 mL conc. HCl. (87% yield)

^{1}H NMR of the bulk material gave two different conformers:

rctt chair stereoisomer: ^{1}H NMR (300 MHz, DMSO-d$_6$, shifts relative to DMSO): δ = Peak broadening above 7.213 made it difficult to identify the Ar-OH peaks due to

duterium exchange. 6.530 (1 H, Ph-H, *t*), 6.103 (1 H Ar-H, *s*), 6.057 (1 H, Ph-H, *d*), 5.978 (1 H, RC-H, *s*), 5.105 (1 H, Ar-H', *s*), 3.688 (3 H, OCH$_3$, *s*), 3.146 (3 H, OCH$_3$, *s*).

Boat *rccc* stereoisomer: ^{1}H NMR (300 MHz, DMSO-d$_6$, shifts relative to DMSO): δ = Peak broadening above 7.213 made it difficult to identify the Ar-OH peaks due to duterium exchange. 6.674 (1 H, Ph-H, *t*), 6.345 (1 H Ar-H, *s*), 6.3.101 (1 H, Ph-H, *d*), 6.037 (1 H, RC-H, *s*), 5.225 (1 H, Ar-H', *s*), 3.717 (3 H, OCH$_3$, *s*), 2.978 (3 H, OCH$_3$, *s*).

Crystal data for *C*-2,3-dimethoxyphenylpyrogallol[4]arenes: C$_{55}$H$_{53}$N$_5$O$_{10}$, *M* = 944.02, triclinic, space group *P*-1 (No. 2), *a* = 13.5457(13), *b* = 13.9334(14), *c* = 14.4940(14) Å, α = 70.521(2), β= 75.140(2), γ= 76.110(2)°, *V* = 2456.6(4) Å^3, *Z* = 2, *D*$_c$ = 1.276 g/cm^3, *F*$_{000}$ = 996, Bruker APEXII CCD area detector, MoKα radiation, λ = 0.71073 Å, *T* = 173(2)K, 2θ$_{max}$ = 54.2º, 17476 reflections collected, 10559 unique (R$_{int}$ = 0.0927). Final *GooF* = 1.020, *R1* = 0.1238, *wR2* = 0.2439, *R* indices based on 3984 reflections with I >2sigma(I) (refinement on *F*^{2}), 635 parameters, 0 restraints. Lp and absorption corrections applied, μ = 0.089 mm^{-1}.

C-2,4-dimethoxyphenylpyrogallol[4]arenes **2.13**

The same procedure used for compound **2.1** was applied, substituting the appropriate aldehyde. (3.10 g, 0.025 mol) pyrogallol, (3.35 g, 0.025 mol) 2,4-dimethoxybenzaldehyde, 50 mL EtOH, 2 mL conc. HCl. (76% yield)

^{1}H NMR (300 MHz, DMSO-d_6, shifts relative to DMSO): δ = 7.678 (1 H, Ar-OH, *s*), 7.498 (1 H, Ar-OH', *s*), 7.293 (2 H, Ar-OH, *s*), 7.113 (2 H, Ar-OH', *s*) 6.452 (1 H, Ph-H, *s*), 6.275 (1 H, Ph-H, *d*), 6.141 (1 H, Ph-H, *d*), 6.014 (1 H Ar-H, *s*), 5.806 (1 H, RC-H, *s*), 5.381 (1 H, Ar-H', *s*), 3.734 (3 H, OCH$_3$, *s*), 3.337 (3 H, OCH$_3$, *s*).

C-3,4-dimethylphenylpyrogallol[4]arenes **2.14**

The same procedure used for compound **2.1** was applied, substituting the appropriate aldehyde. (3.10 g, 0.025 mol) pyrogallol, (3.35 g, 0.025 mol) 3,4-dimethybenzaldehyde, 50 mL EtOH, 2 mL conc. HCl. (86% yield)

Crystal data for *C-3,4-dimethylphenylpyrogallol[4]arenes*: $C_{40}H_{22}O_{11}S_9$, M = 967.12, $\times$ $\times$ mm^3, triclinic, space group *P*-1 (No. 2), a = 11.100(3), b = 13.987(4), c = 16.541(5) Å, α = 68.020(3), β = 73.332(4), γ = 74.713(4)°, V = 2245.9(12) Å^3, Z = 2, D_c = 1.430 g/cm^3, F_{000} = 988, MoKα radiation, λ = 0.71073 Å, T = 173(2)K, $2\theta_{max}$ = 53.1°, 24489 reflections collected, 9244 unique (R$_{int}$ = 0.0418). Final *GooF* = 2.401, *R1* = 0.2410, *wR2* = 0.5884, *R* indices based on 4929 reflections with I >2sigma(I) (refinement on F^2), 425 parameters, 0 restraints. Lp and absorption corrections applied, μ = 0.500 mm^{-1}.

C-3,5-dihydroxyphenylpyrogallol[4]arenes **2.15**

The same procedure used for compound **2.1** was applied, substituting the appropriate aldehyde. (3.10 g, 0.025 mol) pyrogallol, (3.35 g, 0.025 mol) 3,5-dihydroxybenzaldehyde, 25 mL EtOH, 25 mL H_2O, 2 mL conc. HCl. (81% yield)

Crystal data for *C-3,5-dihydroxyphenylpyrogallol[4]arenes:* $M = C_{52}H_{64}O_{32}$, 0.15 x 0.25 x 0.5 mm^3, triclinic, space group *P*-1 (No. 2), $V = 1340.69$ Å^3, $a = 10.5238(11)$, $b = 111.9116(12)$, $c = 12.4644(12)$ Å, $\alpha = 112.709(1)$, $\beta = 104.576(1)$, $\gamma = 980595(41°$ $Z = 1$, $D_c = 1.4874$ g/cm^3, $F_{000} =$, Bruker APEXII CCD area detector, MoKα radiation, $\lambda = 0.71073$ Å, $T = $ K, $2\theta_{max} = 52.7°$, 14567 reflections collected, 5429 unique ($R_{int} = 0.0221$). Final *GooF* = 1.024, *R1* = 0.0507, *wR2* = 0.1419, *R* indices based on 4456 reflections with I >2sigma(I) (refinement on F^2), 425 parameters, 18 restraints. Lp and absorption corrections applied, μ = mm^{-1}.

C-3,4,5-trimethoxyphenylpyrogallol[4]arenes **2.18:**

The same procedure used for compound **2.1** was applied, substituting the appropriate aldehyde. (3.10 g, 0.025 mol) pyrogallol, (3.35 g, 0.025 mol) 3,4,5-trimethybenzaldehyde, 50 mL EtOH, 2 mL conc. HCl. (86% yield)

^{1}H NMR (300 MHz, DMSO-d$_6$, shifts relative to DMSO): δ = 8.102 (1 H, Ar-OH, *s*), 7.802 (1 H, Ar-OH', *s*), 7.681 (2 H, Ar-OH, *s*), 7.655 (2 H, Ar-OH', *s*) 7.521 (1 H, Ph-H, *s*), 7.231 (1 H, Ph-H, *s*), 5.948 (1 H Ar-H, *s*), 5.541 (1 H, RC-H, *s*), 5.360 (1 H,

Ar-H', *s*), 3.441 (6 H, OCH$_3$, *s*), 3.384 (3 H, OCH$_3$, *s*).

Crystal data for *C*-3,4,5-trimethoxyphenylpyrogallol[4]arenes: C$_{44}$H$_{68}$O$_{19}$S$_6$, *M* = 1093.34, .10 × .25 × .05 mm^3, triclinic, space group *P*1 (No. 1), *a* = 13.4347(14), *b* = 14.8480(16), *c* = 15.9732(17) Å, α = 116.670(2), β = 107.283(2), γ = 90.998(2)°, *V* = 2676.0(5) Å^3, *Z* = 2, *D*$_c$ = 1.357 g/cm^3, *F*$_{000}$ = 1160, MoKα radiation, λ = 0.71073 Å, *T* = 173(2)K, 2θ_{max} = 54.1°, 18679 reflections collected, 15896 unique (R$_{int}$ = 0.0219). Final *GooF* = 1.322, *R1* = 0.0665, *wR2* = 0.1764, *R* indices based on 11581 reflections with I >2sigma(I) (refinement on *F*^{2}), 1320 parameters, 35 restraints. Lp and absorption corrections applied, μ = 0.326 mm^{-1}. Absolute structure parameter = 0.41(10)

3 Formations of Metal-Organic Nanocapsules (MONCs) Through Conformational Flipping

3.1 Influences in the design of dimeric nanocapsule formation

Currently, several research groups are pushing the limits of supramolecular chemistry in an attempt to expand our knowledge of the effect of factors such as size, kinetic control, and solubility on nanocapsule formation.[110-111] These factors, if balanced, can give rise to a simple synthetic procedure with limitless possibilities. Directed synthesis of these nanocapsules depends on a better understanding of self-assembly. In addition to its dependence on complementarity of shape, size, and chemical functionalitites, self-assembly also depends on the spontaneous construction of defined structural noncovalent arrays from smaller engineered building blocks.[112,113]

Two types of these noncovalent arrays are *carcerands* (*carceplexes* when containing a guest) and *hemicarcerands* (*hemicarceplexes* when containing a guest) (**Figure 3.1**). A carcerand is defined as a closed molecular container or capsule without portals of significant size through which a guest can either enter or leave. Guest molecules within a carcerand are therefore permanently trapped within the internal volume unless bond breakage of the host occurs.[6] A hemicarcerand is then defined as a closed molecular container from which a guest can enter and exit with a measurable activation barrier.

Cram *et al*.[114] reported the first true carceplex, synthetically achieved by coupling two bowl-shaped cavitands in DMF in the presence of Cs_2CO_3 (**Figure 3.1c**).

It was then that Cram, in his Nobel Prize address stated "The first question to be answered was: what guest compound would be trapped inside during the shell closure? The answer was that the [carceplex] contained essentially every kind of component of the medium present during ring closure."[6]
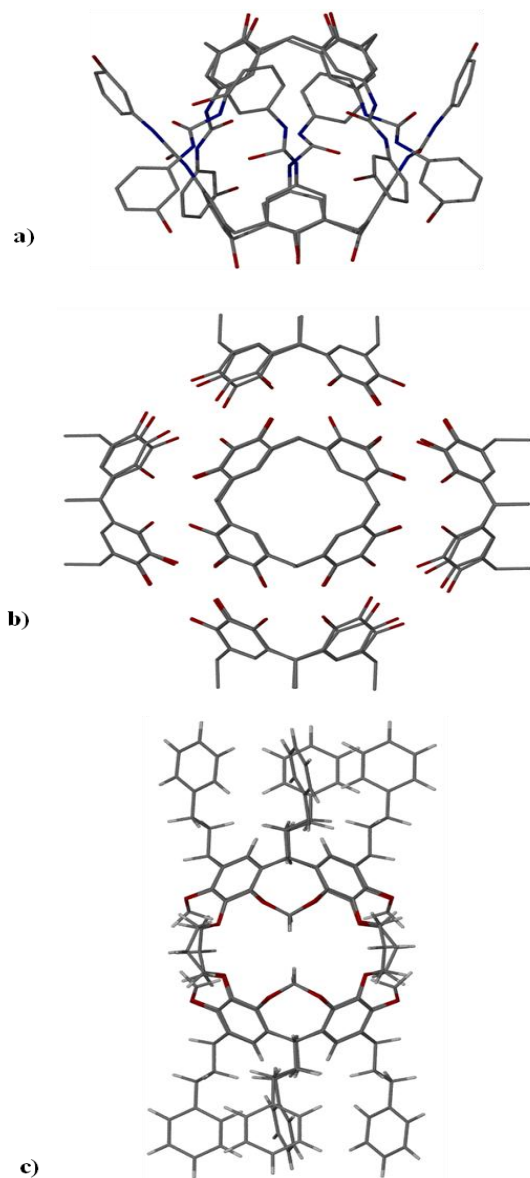
Figure 3.1: Crystallographic examples of different carcerands using various calix[4]arenes as building blocks. O: red, C: grey, H: white.

This is not a trivial observation. For the desired guest to become encapsulated, it must be present before carcerand closure and compete favorably with other possible guests. To illustrate this point, we look at the encapsulation of pyrazine by carcerands. Pyrazine has one of the largest known template ratios; that is, the number of favorable host-pyrazine interactions[115] (C–H···π, C–H···N, and π···π) allows displacement of competing guest molecules that possess fewer favorable interactions. Like most carceplexes, Cram's first generation of carceplexes were extremely insoluble. This insolubility was overcome by increasing the length of the alkly chains on the pendent R-groups or acetyl bridges. However, in the latter approach the longer and more flexible acetyl bridges allowed for passage of small guest species into or out of the container.

Formation of carcerands is not limited to combining symmetric cavitands. Reinhoudt *et al.*[116] have synthesized asymmetric carcerands combining resorcin[4]arenes and calix[4]arenes. The narrow and deep cavity of calix[4]arenes versus the wider and more shallow cavity of resorcin[4]arenes yielded an egg-shaped, highly unsymmetrical cavity. In their study of guest behavior in this carcerand, Reinhoudt *et al.*[117] measured a rotational barrier in the range of 53-73 kJ/mol for dimethylacetamide. Because of the hindered rotation, the guest becomes kinetically locked and two orientational isomers are observed, termed *carceroisomerism* (**Figure 3.2**) and (**Figure 3.3**).
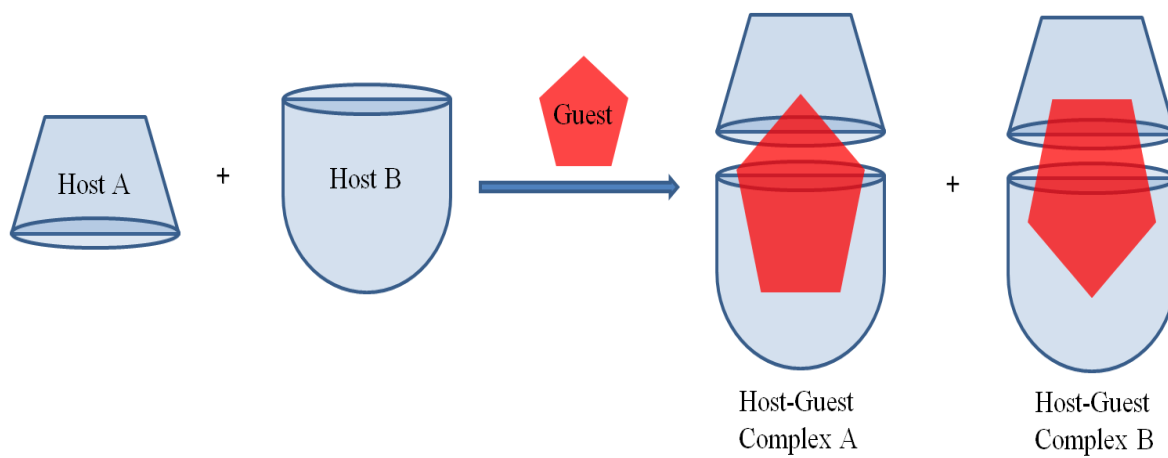
Figure 3.2: Graphical representation of carceroisomerism.

a) b)
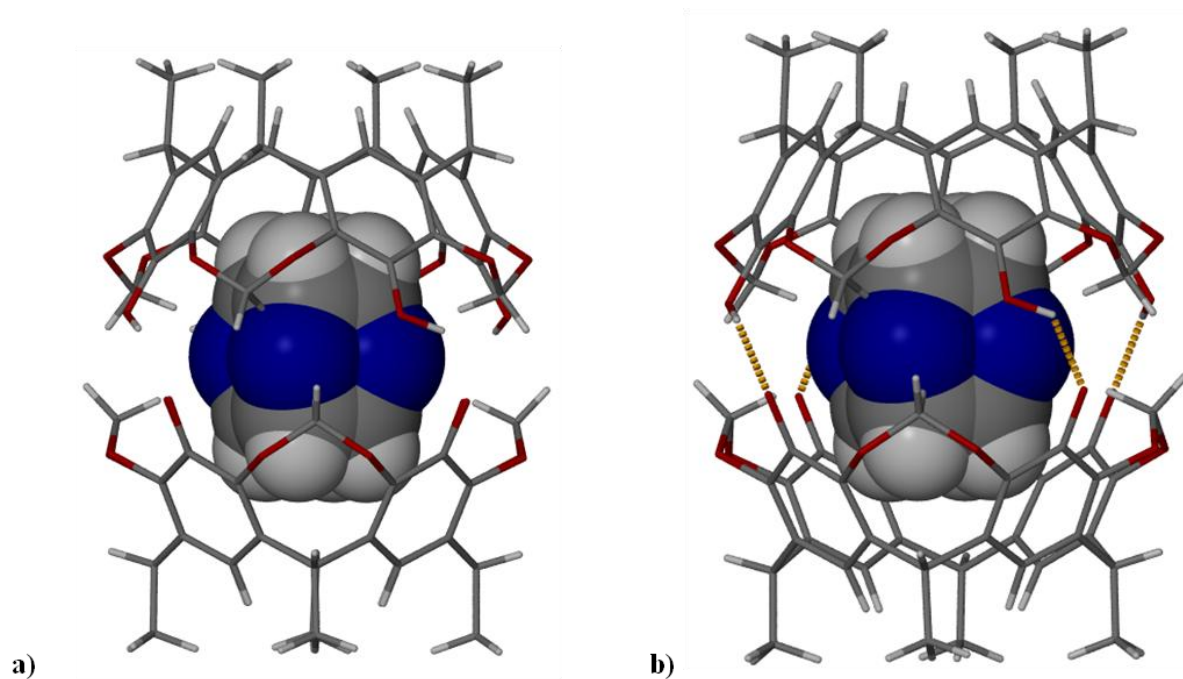
Figure 3.3: Crystallographic images showing carceroisomerism a) without hydrogen bonding, and b) with hydrogen bonding (gold dashed) [118] O: red, C: grey, N: blue, H: white.

The propensity of the calix[4]arene family to complex with metals has pushed the chemistry of these arenes into the realm of metal-organic frameworks (MOFs) and metal-organic nanocapsules (MONCs). Dalcanale *et al.*[119] have shown encapsulation of the anionic guest $CF_2SO_3^-$ in the Pt-seamed carcerand produced from reaction of tetracyanocavitand deriviatives and the square-planar complex $Pt(dppp)(SO_3CF_3)_2$. A Co-seamed hemicarcerand has been synthesized by Harrison *et al.*,[120] taking advantage of cobalt's preference for octahedral coordination (**Figure 3.4**).
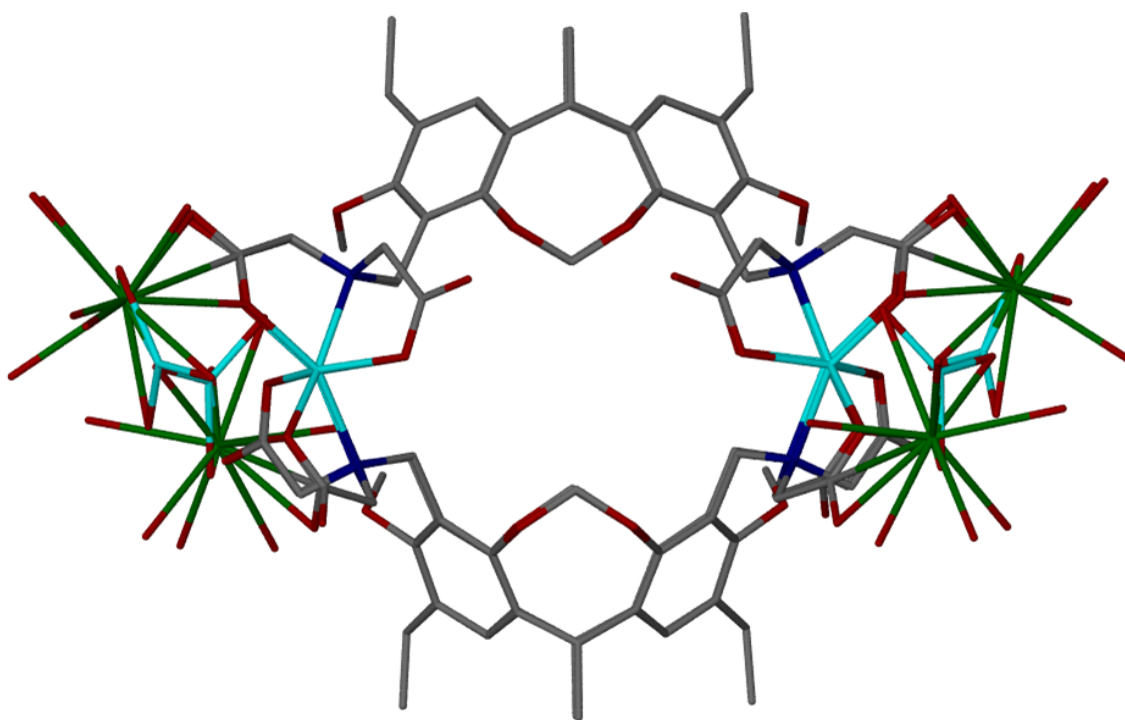
Figure 3.4: Crystallographic image of a dimeric MONC consisting of four cobalt(II) ions having a distorted octahedral geometry. Co: teal, Ba: green, O: red, C: grey, N: blue. Hydrogen atoms omitted for clarity.[120]

It was not until the work of Gavuzzo *et al.*[121] that any information was made available on the possible mechanism of carcerand formation. They demonstrated through XRD that carcerand formation could occur via an *anti* intermediate in which

two (2) *rccc* cone stereostructures are linked together through a covalent bond. As rotation about this single bond proceeds the two sructures bind together in a "zipper-like" fashion (**Figure 3.5**). This work not only addressed the self-assembly process but also illustrated the importance of the inherent shape of the macrocycle to allow the free rotation.
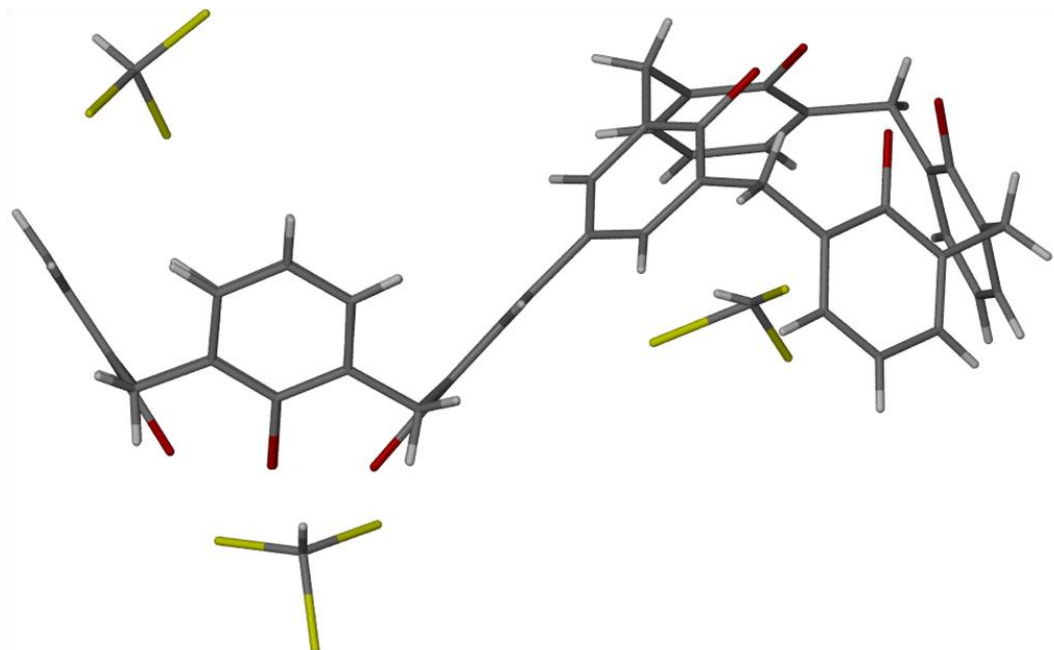
Figure 3.5: Crystallographic image of an isolated intermediate using two (2) calix[4]arene moieties in the *rccc* cone stereostructure.

To extend the breadth of pyrogallol[4]arenes that produce carcerands, the research reported in this chapter tests the potential for nanocapsule formation from macrocycles in the *rctt* chair arrangement. It might seem counterintuitive to utilize a macrocycle that shows none of the previously recognized key features for self-assembly. However, Castellano *et al.*[122] showed conformational control of tetraurea calix[4]arene via intermolecular hydrogen bonding (**Figure 3.6**), which suggested the possibility of

inducing a conformational change during self-assembly of metal-seamed pyrogallol[4]arene nanocapsules.
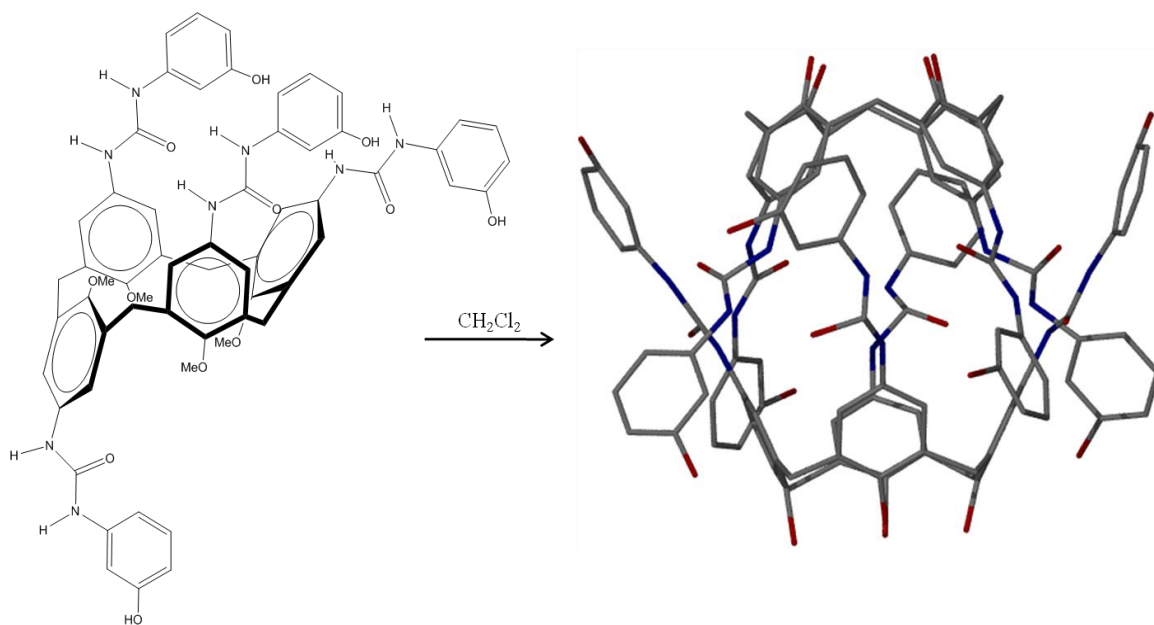
Figure 3.6: Schematic representation of bis(phenylcarbamoylamino))calix[4]arene in the *rcct* partial cone conformation flipping to the *rccc* cone conformer to form a stable dimer of two (2) *rccc* cone conformers, overcoming the interconversion barrier between stereoisomers.

3.2 Synthesis and characterization of dimeric zinc nanocapsules

Two other considerations for the experimental design are the choice of metal and the size of the nanocapsule. As supramolecular structures get larger, the amount of control, with respect to formation of the desired macromolecule, decreases due to the

increase in variables. Dimeric entities were chosen as the desired product to have more control in the study.

Dimeric and hexameric supramolecular entities have been produced using such metals as Cu^{II}, Pt^{II}, Pd^{II}, Co^{II} and Ag^{I}. Because characterization of compounds containing Cu^{II} is not possible through ^1H NMR due to the paramagnetic nature of the metal and Pt^{II}, Pd^{II}, and Ag^{I} metals are expensive, other metals were sought for early testing. Power *et al.*[123] recently reported that Zn^{II} forms metal-seamed dimeric alkylpyrogallol[4]arene nanocapsules, such as [Zn_8(C-propylpyrogallol[4]-arene)$_2$(Pyridine)$_8$⊂(Pyridine)] **3.1**. Using Gaussview to replace the propyl groups in **3.1** with phenyl groups supported the hypothesis that capsule formation was plausible from *C*-arylpyrogallol[4]arenes (**Figure 3.7**). Therefore, this research was begun by testing zinc.
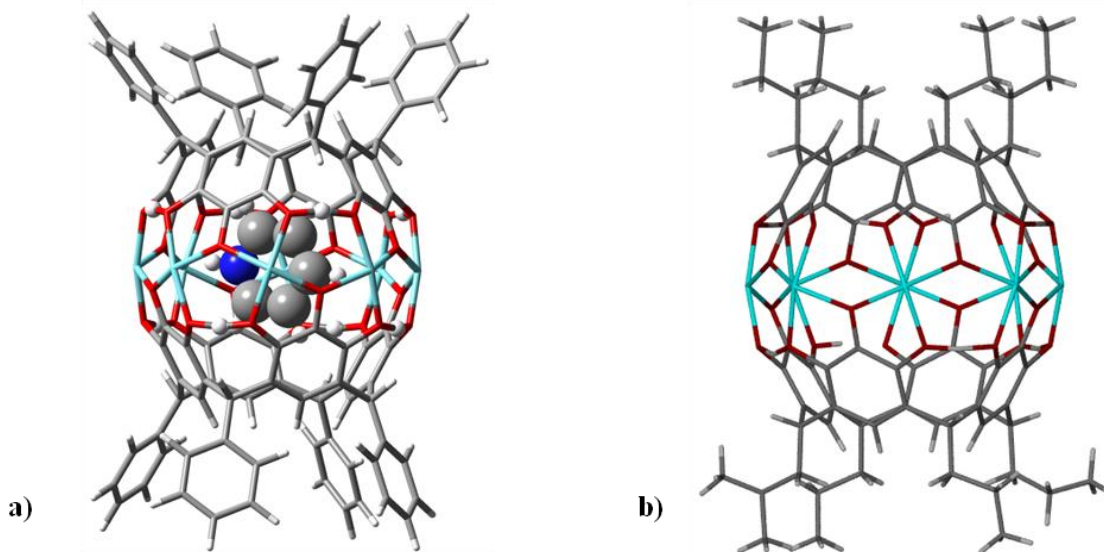
Figure 3.7: a) Predicted structure of **3.2** using Gaussview in comparison to the actual structure of **3.1**.

3.2.1 Synthesis of MONCs formed from *C*-phenylpyrogallol[4]arene

When **2.1** in a solution of 3:1 MeOH:ACN was reacted in a 1:4 ratio with a variety of pentacoordinated zinc(II) complexs ML_3X_2, a dimerization reaction occurs. Here L = equatorial ligand and X = NO_3 (**Figure 3.8**). Collection of the yellow-brown precipitate using a fine fritted filter and washing with cold methanol led to a 57% − 86% yield, depending on the equatorial ligand of $[Zn_8(C$-phenylpyrogallol[4]arene$)_2(L)_8 \subset (L)]$. (It is worth noting that the use of 3-propylpyridine (**Figure 3.8d**) as an equatorial ligand prohibits the formation of a dimeric capsule due to size constraints of the guest.) As crystals of $[Zn_8(C$-phenylpyrogallol[4]arene$)_2(Pyridine)_8 \subset (Pyridine)]$ **3.2** suitable for XRD were difficult to obtain, NMR and MALDI-TOF-MS were used to characterize the product.

Characterization using ^{1}H NMR proved to be not only a viable but also a reliable means of determining capsule formation due to the key characteristic peaks of the intramolecular O–H⋯O hydrogen bonds present in each capsule (**Figure 3.9a**). The ^{1}H NMR spectrum of **3.2** reveals two proton peaks for these intramolecular hydrogen bonds at 17.06 ppm and 17.41 ppm (**Figure 3.9b**), indicative of deshielding by the presence of oxygen-bonded metals. Two separate sets of peaks exist because there are two different hemispheres in the capsule (**Figure 3.9a**). Splitting of these peaks suggests that hydrogen bonding occurs between the phenolic group of the pyrogallol and the guest pyridine. The
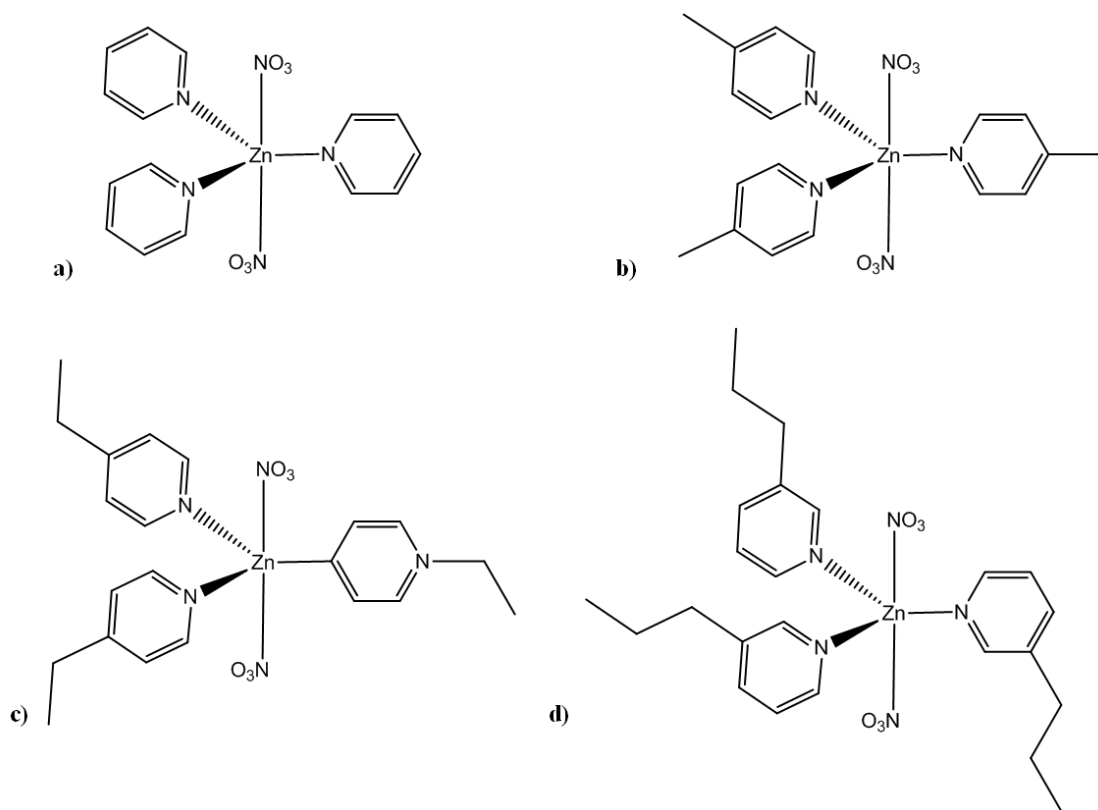
Figure 3.8: Schematic representation of the various Zn^{II} complexes used to form dimeric capsules.

mechanism of formation for **3.2** is not completely understood, but it is known that upon protonation of an equatorial ligand (L of ZnL$_3$X$_2$), ligand displacement occurs. Due to the relatively quick formation of these robust dimeric capsules, one of the three equatorial ligands becomes incarcerated within the host dimeric capsule. The encapsulated pyridine has a unique chemical shift of 6.10 ppm for H$_A$, and overlapping multiplets for H$_B$ and H$_C$ at 5.77 ppm. The difference between free pyridine (8.613 ppm for H$_A$, 7.277 ppm for H$_B$, and 7.655 ppm for H$_C$) and encapsulated pyridine is associated with the shielding provided by the dimeric entity. The pyridine ligands that do not get displaced from the metal center can be detected in the spectra at 8.02 ppm, 7.12 ppm, and 7.54 ppm. A

splitting pattern is not observed for the Zn-bound pyridine protons due to the broadening caused by metal complexation.

Further confirmation of capsule formation is obtained by the analysis of the aryl protons (Ar-H) on the pyrogallols. If, in fact the pyrogallol[4]arenes are now in the cone conformation the ^{1}H NMR pattern for the Ar-H protons should be different from that of the chair. A conformational shift from chair to cone would cause all pyrogallol subunits to be equal, yielding a singlet in the ^{1}H NMR for the aryl protons rather than the splitting over two positions (0.5 H axial and 0.5 H equatorial). The actual ^{1}H NMR spectrum of **3.1** confirms this conformational shift since the singlet at 4.798 ppm (integrating to 1 H) indicates that the Ar-H protons are now all equivalent.

Despite the preference of **2.1** to form the *rctt* chair stereostructure, Zn-seamed metal capsules are obtained. This clearly illustrates that the addition of zinc induces a chair-to-cone conformational change, similar to the interconversion reported by Castellano *et al.*[122]
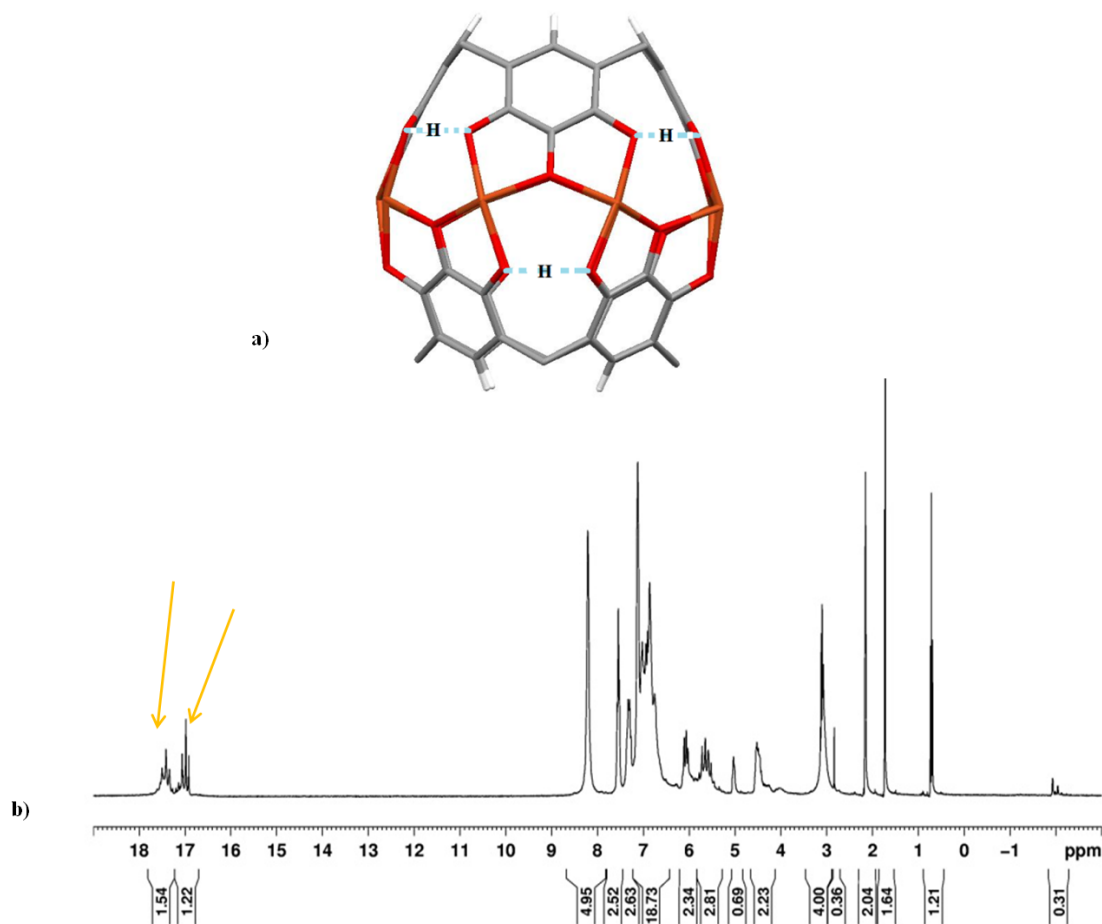
Figure 3.9: a) Crystallographic image of a base unit Zn[II] dimeric capsule showing intramolecular hydrogen bonding. Zn: orange, O: red, C: grey, H: white. Hydrogen bonds shown in light blue. b) ^{1}H NMR data with yellow arrows indicating proton peaks characteristic of the intramolecular hydrogen bonding.

[Zn₈(C-phenylpyrogallol[4]arene)₂(Pyridine)₈⊂(Pyridine)] **3.2:**

C-phenylpyrogallol[4]arene (100 mg, 116 µmol) was added to a flask with [Zn[II](NO₃)₂(Pyridine)₃] (200 mg, 464 µmol) and 5 mL 3:1 methanol:acetonitrile solution. The precipitate was then filtered and dried under vacuum. Yield: 0.130 g,

78%. ^{1}H NMR (300 MHz, DMSO-d$_6$, shifts relative to DMSO): δ = 17.41 (4H, m), 16.97 (4H, m), 8.21 (16H, s), 7.45 (16H, s), 7.31 (8H, s), 7.02 (40H, m), 6.06 (2H, m, ⊂Pyr), 5.71 (2H, m, ⊂Pyr), 5.03 (1H, m, ⊂Pyr), 4.50 (8H, s).

MALDI-TOF MS analysis: Spectra was collected on a Voyager DE-PRO. MALDI sample preparation consisted of co-crystallization of product with dithranol (10 mg/mL in MeOH). All analyses were carried out on a 100 well gold plate. The Voyager DE-PRO was operated in positive ion reflector mode running at 20 kV acceleration, 150 ns delayed extraction, 1000-4000 Da mass range, with low mass filter gate on at 1000 Da. Laser intensity was set to 1708 at 250 shots per acquisition, with the laser randomLy positioned per acquisition.

3.2.2 Synthesis of MONCs formed from substituted *C*-arylpyrogallol[4]arenes

The *C*-arylpyrogallol[4]arenes available from the conformational studies, compounds **2.1-2.18**, were used in an attempt to synthesize Zn-seamed dimeric nanocapsules. Yet upon addition of [Zn^{II}(NO$_3$)$_2$(Pyridine)$_3$] to a solution of 3:1 MeOH:ACN containing a *C*-arylpyrogallol[4]arene, not all arenes afforded a dimeric capsule. Of the eighteen (18) different macrocycles used in the reaction, only **2.1**, **2.7**, **2.10**, **2.11**, and **2.18** yielded the desired product. In fact, none of the di-substituted *C*-arylpyrogallol[4]arenes have thus far produced a dimeric capsule and only one tri-substituted *C*-arylpyrogallol[4]arene **2.18** has produced a capsule. R-group bulk, symmetry, and functionality and solvent are all proposed to be central factors in determining the outcome of capsule formation.

In the first reported synthesis of zinc dimeric capsules from *C*-alkylpyrogallol[4]arenes,[125] methanol was chosen as solvent based on the solubilities of both the macrocycle and the pentacoordinated zinc complex. On the basis of that synthesis, a mixture of methanol and acetonitrile was chosen as the solvent for the *C*-arylpyrogallol[4]arene reactions. Subsequent use of DMSO as a solvent for synthesis yielded additional information on the formation of these dimeric capsules. While *C*-arylpyrogallol[4]arenes exhibit good solubility in DMSO, DMSO proved to hinder capsule formation even for the *C*-arylpyrogallol[4]arenes that previously formed dimeric capsules in MeOH:ACN. There exist two (2) possible explanations for this observation. One possibility is that the DMSO displaces the pyridine equatorial ligands on the ZnL_3X_2 starting complex, which then prevents capsule formation. In order for this to be a viable hypothesis, the binding affinity for DMSO with zinc must be greater than that of pyridine. The other possibility is that explicit DMSO molecules bind strongly to both an axial and equatorial pyrogallol of the macrocycle, prohibiting the conformational flip needed to form the dimeric capsule. Further investigation is required to test these hypotheses.

3.3 Solid-state study of the MONCs formed from *C*-arylpyrogallol[4]arenes

Synthesis of the $[Zn_8(C$-4-propoxyphenylpyrogallol[4]-arene$)_2$(Pyridine$)_8 \subset$(Pyridine$)]$ **3.3** (**Figure 3.10**) was carried out with the bulk material obtained from filtration of the precipitate from the reaction mixture. Subsequent formation of single crystals has allowed for structural investigations of the nanocapsules and thus insight into the mechanism for closure.
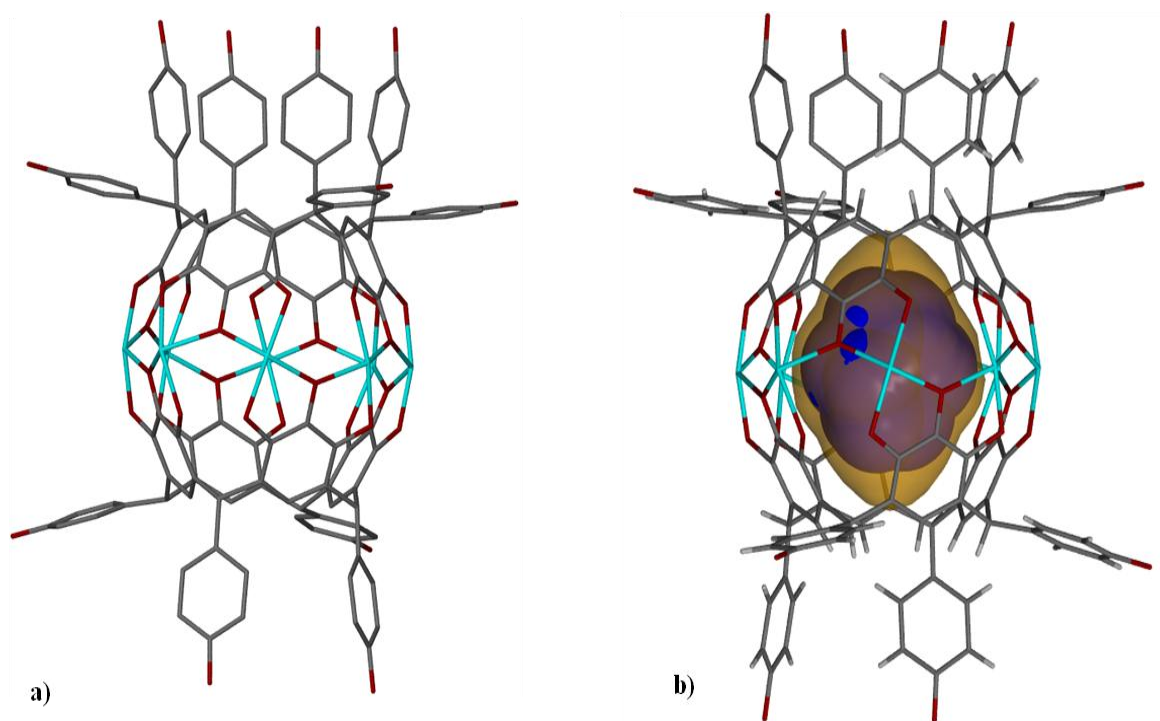
Figure 3.10: a) Crystallographic image of **3.3** showing perceived disorder of the pendent R-groups on only one hemisphere, indicating that the disorder is actually cocyrstallization of multiple conformers of *C*-4-propoxyphenylpyrogallol[4]arene present at the time of capsule formation. b) Crystallographic image of **3.3** showing calculated cavity (orange) and actual pyridine guest (blue). Zn: teal, O: red, C: grey. Hydrogen atoms and carbon atoms on the propoxy tails have been omitted for clarity.

Knowing now that the *rccc* boat stereostructure is present in the bulk material it must also be present in solution upon formation of the MONCs. One question that must be addressed is whether formation of these MONCs occurs only from the *rccc* boat conformation or does the crystallographic evidence support our previous claim that the *rctt* chair stereostrucuture participates in capsule formation.[92]

Analysis of the solid-state structure of **3.3**, paying close attention to the position of the R-groups prior to and after assembly of a capsule, supports our previous claim. If only the *rccc* boat stereostructure participated in capsule formation, the prochirality of the methine carbon and configuration of the pendent R-groups would remain the same. This behavior is in fact observed in the formation of dimeric and hexameric capsules from *rccc* cone alkyl-pyrogallol[4]arenes.[124,125] Surprisingly though, the crystallographic structure indicates an *axial-axial-equatorial-equatorial* (*ax-ax-eq-eq*) geometry of the R-groups on the lower hemisphere (**Figure 3.10**), supporting construction of the dimer from the *rctt* chair. As shown in **Figure 3.10**, the upper hemisphere exhibits what was perceived to be disorder of the pendent R-groups. However, upon further analysis it was concluded that the perceived disorder is actually cocyrstallization of the multiple conformers that participate in capsule formation.

The R-group occupancies in the upper hemisphere were used to determine which conformers contribute to the capsule structure. Analysis of the solid-state structure of 3.3 revealed the following occupancies for the four R-group positions: *ax* (100%); *ax* (73%), *eq* (37%); *ax* (75%), *eq* (25%); *ax* (50%), *eq* (50%). These occupancies indicate that the upper hemisphere is made up of the *rccc* boat stereostructure about 70% of the time and the *rcct* partial cone stereostructure about 30% of the time. Evidence of the latter stereoisomer for a *C*-arylpyrogallol[4]arene once eluded the scientific community. However, refluxing *C*-3,4,5-trimethoxyphenylpyrogallol[4]arene in dilute HCl, 1,4-butadiene, and methanol led to isolation of the *rcct* partial cone stereostructure, thus proving its existence for *C*-arylpyrogallol[4]arenes (**Figure 3.11**).
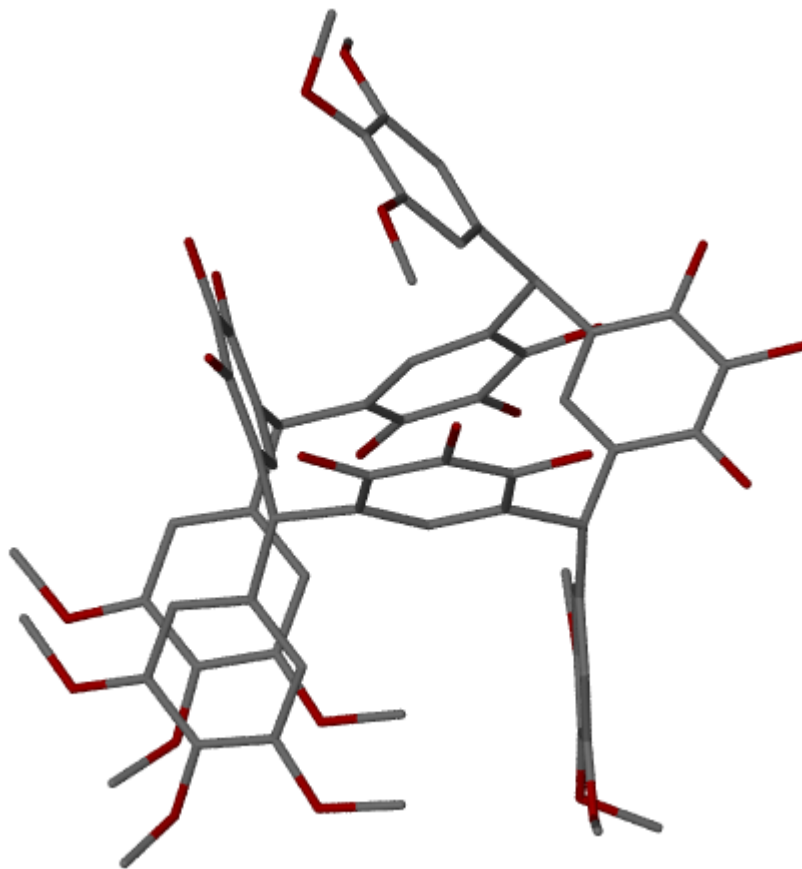
Figure 3.11: Crystallographic image of *C*-3,4,5-trimethoxyphenylpyrogallol[4]arene in the *rcct* partial cone stereostructure. O: red, C: grey. Hydrogen atoms omitted for clarity.

To demonstrate that capsules formed from only the *rctt* chair stereoisomer would result in two symmetric hemispheres, isolated *rccc* cone, as a control, and *rctt* chair stereostructures of *C*-methylpyrogallol[4]arene (PgC_1)[126] were used to synthesize $[Zn_8(C$-methylpyrogallol[4]arene)$_2$(Pyridine)$_8 \subset$(Pyridine)] **3.4** and **3.5**, respectively. Analysis of the solid-state structure of **3.4** revealed two (2) identical hemispheres with the pendent R-groups in the all-*axial* positions. In contrast, the analysis of **3.5** resulted in two (2)

symmetrical hemispheres, both containing the *ax-ax-eq-eq* configuration of the pendent R-groups (**Figure 3.12**).
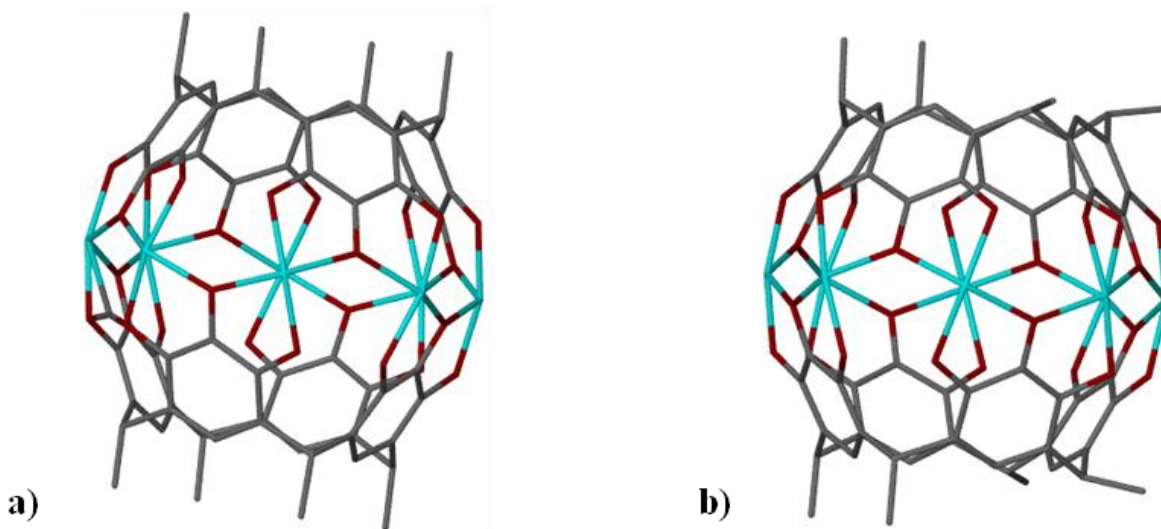
Figure 3.12: a) Crystallographic image of **3.4** noting the all-*axial* pendent R-group configuration. b) Crystallographic image of **3.5** showing the *ax-ax-eq-eq* configuration of the pendent R-groups Zn: teal, O: red, C: grey. Hyrogen atoms have been omitted for clarity.

The simple addition of a phenyl group, acting as the pendent R-group, changes the chemical make-up of a class of calix[4]arenes that was previously thought to be fully understood. In order to study conformational preferences when an alkyl chain separates the aryl R-group from the methine carbon, one, two or three methylene linkers were added between the methine bridge and the phenyl pendent R-group. Single crystals of these macrocycles were obtained in methanol and analyzed in the solid state. Addition of

a single carbon linker results in a return to the acknowledged thermodynamic product for

C-alkylpyrogallol[4]arenes, the *rccc* cone stereostructure (**Figure 3.13a**). To show that

the resulting complexation with a Zn^{II} complex would form a dimeric capsule with the

expected all-*axial* configuration, $[Zn^{II}(NO_3)_2(Pyridine)_3]$ was added to *C*-1-

methylphenylpyrogallol[4]arene. In fact, the all-*axial* configuration of the pendent R-

groups was observed for $[Zn_8(C$-1-methylphenylpyrogallol[4]-

arene$)_2(Pyridine)_8 \subset (Pyridine)]$ **3.6**, (**Figure 3.13b**).

Research on *C*-arylpyrogallol[4]arenes was enticing because of the potential

chemistry that could be carried out of the phenyl R-groups. The addition of a single

carbon linker changes the preferred stereostructure from *rctt* chair to *rccc* cone. This

suggests that chemistry can still be carried out on the phenyl R-group without the added

complications associated with the *rctt* chair stereostructure. So why deal with the *rctt*

chair stereostructure at all? As will be discussed in **Section 3.4,** the required

conformational flip when using *C*-arylpyrogallol[4]arenes causes slower formation of the

dimeric capsules. This could allow for target molecules other than the displaced metal

ligand to become encapsulated.
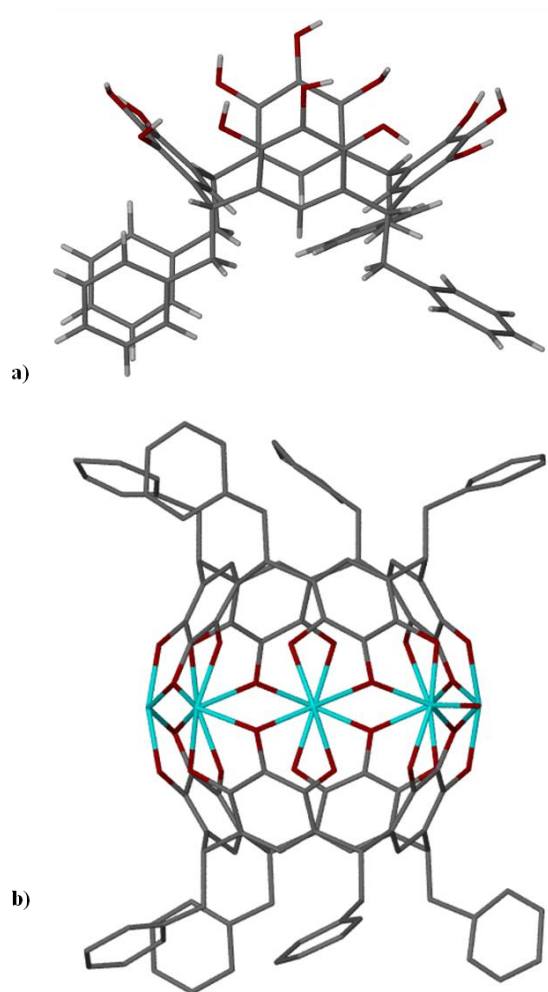
Figure 3.13: Crystallographic images of a) *C*-1-methylphenylpyrogallol[4]arene and b) the dimeric MONC **3.6** with hydrogen atoms omitted for clarity. Zn: teal, O: red, C: grey, H: white.

3.4 Guest characterization and kinetic formation

One problem associated with dimeric MONCs, as it pertains to pharmaceuticals, is the difficulty in achieving desired guest encapsulation. Encapsulation of an equatorial ligand (L) when the Zn-seamed pyrogallol[4]arene nanocapsules are formed hinders

encapsulation of a desired guest. Two options exist to avoid this problem. First, the pharmaceutical agent must be incorporated into the metal complex before the addition to the macrocycle, which limits the acceptable pharmaceutical agents. Second, the rate of closure must be controlled to allow for displacement of ligand (L) by the desired pharmaceutical agent. It was thought that using *C*-arylpyrogallol[4]arenes would encourage slower formation of the dimeric entities, due to the need to force a conformational flip before formation can occur. MALDI-TOF MS analyses were used to test this hypothesis.

When using *C*-phenylpyrogallol[4]arene, **2.1**, in the formation of the dimeric capsule, encapsulation of a displaced pyridine ligand would result in a mass peak of 2298.84 Da and a peak-to-peak difference of 79.1 Da. The data reveal a mass difference between unoccupied and occupied host of 77.85 Da and a total mass peak of 2304.09 Da (**Figure 3.14**). The discrepancy in guest mass is attributed to the fact that no external calibrant was used. Currently there is not a standard mass calibrant that uses dithranol as the matrix. The problem in using a mass calibrant that contains a matrix different from the one used for the analyte is that an initial velocity correction cannot be made. Different initial velocities within one matrix can typically be attributed to areas of different crystallization states, such as a coarsely crystalline droplet rim and a microcrystalline inner part.[127] For mass accuracy, the externally calibrated samples must be in the same matrix as their calibrant. To overcome this issue, production of an external calibrant was attempted. Research suggested that hyperbranched polymers could
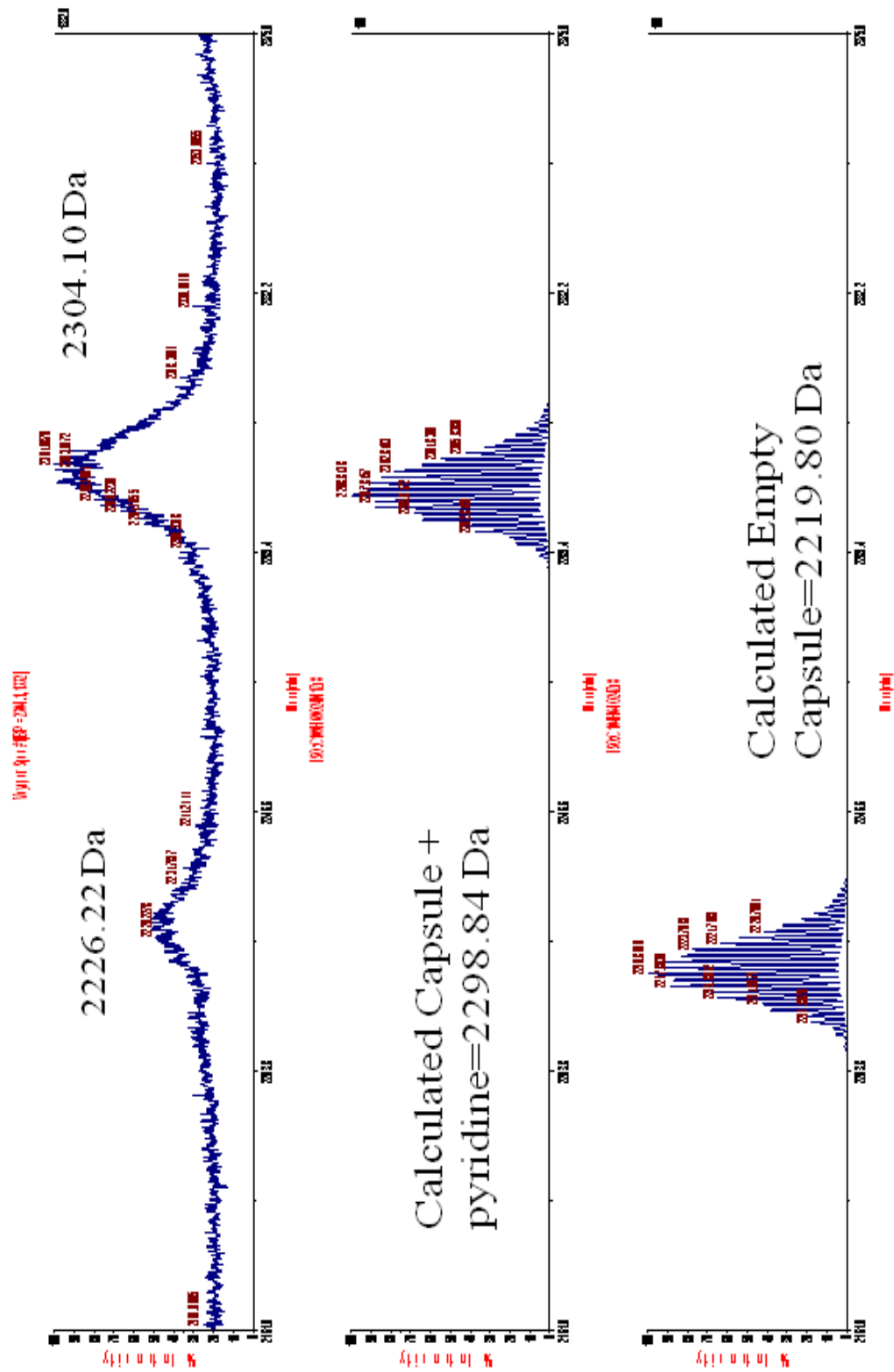
Figure 3.14: MALDI-TOF-MS spectra of the dimeric MONC **3.2**. The x-axis is % intensity while the y-axis is mass (Da).

be easily ionized using dithranol. To test this theory hyperbranched bis-MPA polyester-16-hydroxyl generation 2 (F. W. 1749.79), hyperbranched bis-MPA polyester-16-hydroxyl generation 3 (F. W. 3607.64), and hyperbranched bis-MPA polyester-16-hydroxyl generation 4 (F. W. 7323.32) were combined with dithranol and allowed to cocrystallize , but dithranol did not ionize these polymers. Since an external calibrant could not be generated, mass accuracy for all data has a standard deviation of ± 2 Da, which is sufficient for confirmation of the presence of nanocapsules.

Using *C*-3,4,5-trimethoxyphenylpyrogallol[4]arene, **2.19**, a 3:1 solvent mixture of MeOH:ACN and a zinc(II) metal complex containing 3-methylpyridine rather than pyridine as the equatorial ligand affords [Zn_8(*C*-3,4,5-trimethoxyphenyl-pyrogallol[4]arene)$_2$(3-methylpyridine)$_8 \subset$(3-methylpyridine)], **3.7**. Analysis of the MALDI-TOF-MS spectra revealed two mass peaks at 2947.76 Da and 3022.12 Da, with a resulting mass difference of 74.36 Da (**Figure 3.15**). This mass difference results from encapsulation of a single methanol and a single acetonitrile molecule (total mass of 73.09 Da) rather than a displaced metal center 3-methylpyridine ligand with a mass of 93 Da. Computational studies indicate 3-methypridine is a stable guest inside our host capsule, which leads to the conclusion that the more bulky (3,4,5-trimethoxyphenyl) group hinders capsule closure and allows for displacement of the ligand by solvent.
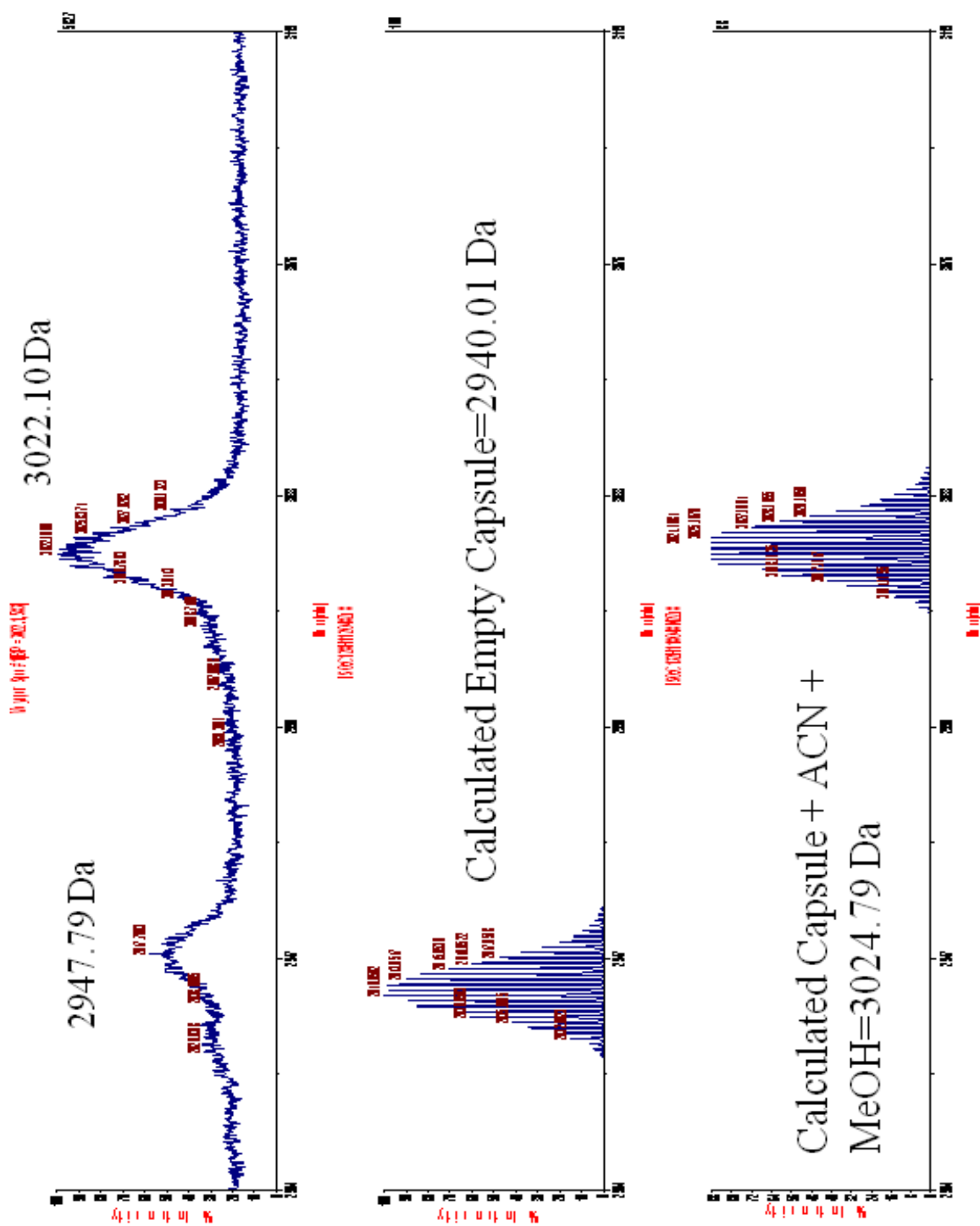
Figure 3.15: MALDI-TOF-MS spectra of the dimeric MONC **3.7**. The x-axis is % intensity while the y-axis is mass (Da).

3.4   Conclusions

In conclusion, metal insertion induces a chair-to-cone conformational change to form zinc-seamed dimeric capsules using compounds **2.1**, **2.7**, **2.10**, **2.11**, and **2.19**. This research has led to better insight into the properties of these complex macrocycles and dimeric nanocapsules. Further studies are needed to understand the intricacies of interconversion and dimeric nanocapsule formation. However, overcoming thermodynamics to induce a conformational change opens the door to new, diverse groups of capsules that allow for easy functionalization. Retention of R-group stereochemistry from the *rctt* chair conformer to the dimer is indicated by the ax-ax-eq-eq geometry of the side chains in the capsule. While the boat conformation of arylpyrogallol[4]arenes could afford capsules from a wider range of metals due to their similarity to the cone conformer, the chair conformers are present in higher yield, require less purification, and allow the possibility of controllable kinetics leading to desired guest inclusion.

3.5   Future Studies

The closure mechanism is not fully understood. Why is it that some *C*-arylpyrogallol[4]arenes are allowed to undergo this conformational change? The research would seem to suggest that it is not only the position of the substituent, but also the functionality that is important. Because these unique dimeric entities are difficult to crystallize, new solvent systems are needed to allow for analysis of the solid state. While not discussed in previous sections, other metals were attempted for complexation. Color

116

changes, indicative of metal complexation, did occur. However, because of the lack of crystalline material, the paramagnetism associated with certain metals, or the insolubility in common volatile organic solvents (methanol, acetonitrile, acetone), characterization of the products was difficult. Further research is needed in this area.

4 The Use of Mixed Macrocycles in New and Diverse Supramolecular Architecture via Solvent Mediation

4.1 Introduction and synthesis of mixed macrocycles

Intermolecular interactions involving solvent continue to play a vital role in many aspects of chemistry. For example, controlled conformational equilibrium,[128-129] isomeric stability,[130] polymorphism,[131-132] and protein folding[133-134] illustrate the importance of solvent in specifically designed systems. In particular, self-assembly exploits solvent polarity, dipole moment, protic/aprotic nature, dielectric constant, and intermolecular interactions with various building blocks. The family of calix[4]arenes has generated consistent attention from the scientific community because of the diversity of their applications,[135-138] notably for the different self-assembled motifs that these building blocks can generate. Previous reports have shown hexameric,[139-143] dimeric,[144-146] bilayer,[147] and nanotubular assemblies,[148-154] in which order results from non-covalent interactions. Recently, a unique approach towards synthesis of these macrocycles has afforded insight into the workings of self-assembly. [155]

Modifying the previously reported synthesis by Niederl *et al.*[156] through the use of two equivalents of both pyrogallol and resorcinol with four equivalents of aldehyde yielded a slurry of possible combinations: 4:0, 3:1, 2:2, 1:3, and 0:4 (resorcinol : pyrogallol), noting that a 2:2 ratio would produce two different isomers (**Scheme 4.1**). Separating the mixture of compounds had proven elusive until recyrstallization in diethyl ether allowed isolation of a 1:3 resorcinol:pyrogallol cyclic

product, leading to a hexameric nanocapsule.[178] However, as described above, different solvent systems can give different architectures. By taking advantage of the properties of different solvents, we have again been able to create order from disorder through solvent mediation, thereby separating individual products from the mixture. Herein we report two new crystal structures of mixed macrocycles. These mixed macrocycles as well as the already published mixed macrocycle were all synthesized with the same protocol; however, recrystallization in different solvent systems led to different superstructures.
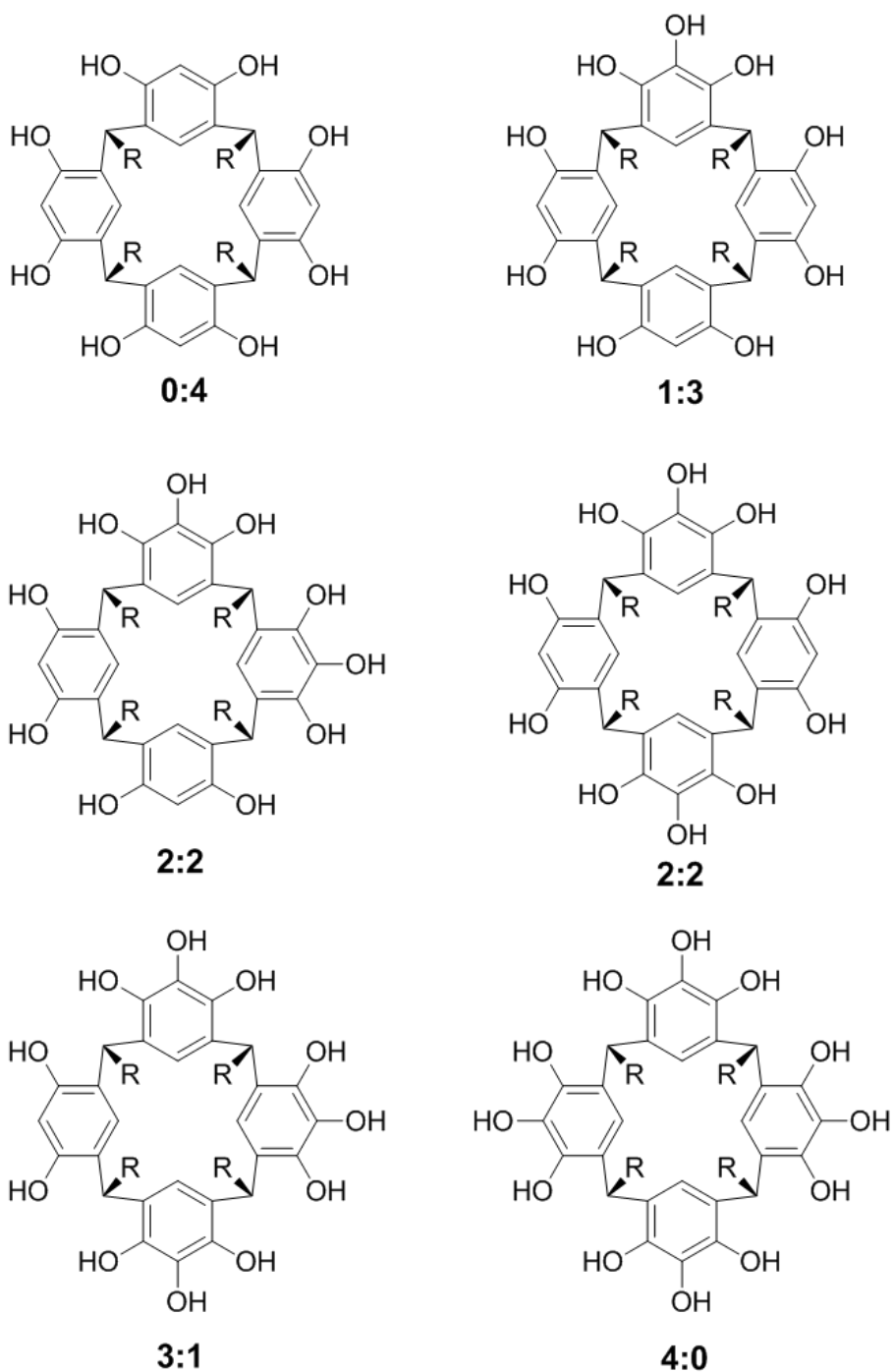
Scheme 4.1: Schematic representation of the different possible product combinations formed from the acid-catalysed condensation reactions with equal equivalents of resorcinol and pyrogallol.

4.2 Synthesis of Organic Nanostrucutres using Mixed Macrocycles

All reagents and solvents were commercially available and used as obtained from the manufacturers without further purification. Mixed macrocycle **4.1** was produced by the addition of 0.040 mol (4.4 g) resorcinol and 0.040 mol (5.0 g) pyrogallol to a 60 mL solution of 95% ethanol and 0.080 mol (8.6 mL) valeraldehyde. 12 mL of 12M HCl was then added and the solution was refluxed for five (5) days under N_2. The volume of the mixture was reduced to half by rotary evaporation and then allowed to cool to room temperature. Crystals of mixed macrocycle **4.1 (Figure 4.1a**) formed after approximately two (2) weeks of slow evaporation.

Mixed macrocycle **4.2** (**Figure 4.1b**) was obtained by similar methods, substituting isovaleraldehyde for valeraldehyde. The resulting precipitate was redissolved in acetone and allowed to slowly evaporate until crystals were produced. We note that the previously reported mixed macrocycle (**Figure 4.1c**) was also obtained through similar methods, again using isovaleraldehyde and was recrystallized in diethyl ether. The single crystal X-ray diffraction data for mixed macrocycles **4.1** and **4.2** were collected on a Bruker Apex II CCD diffractometer at a temperature of 173(2)K using MoKα radiation (.71073 Å).
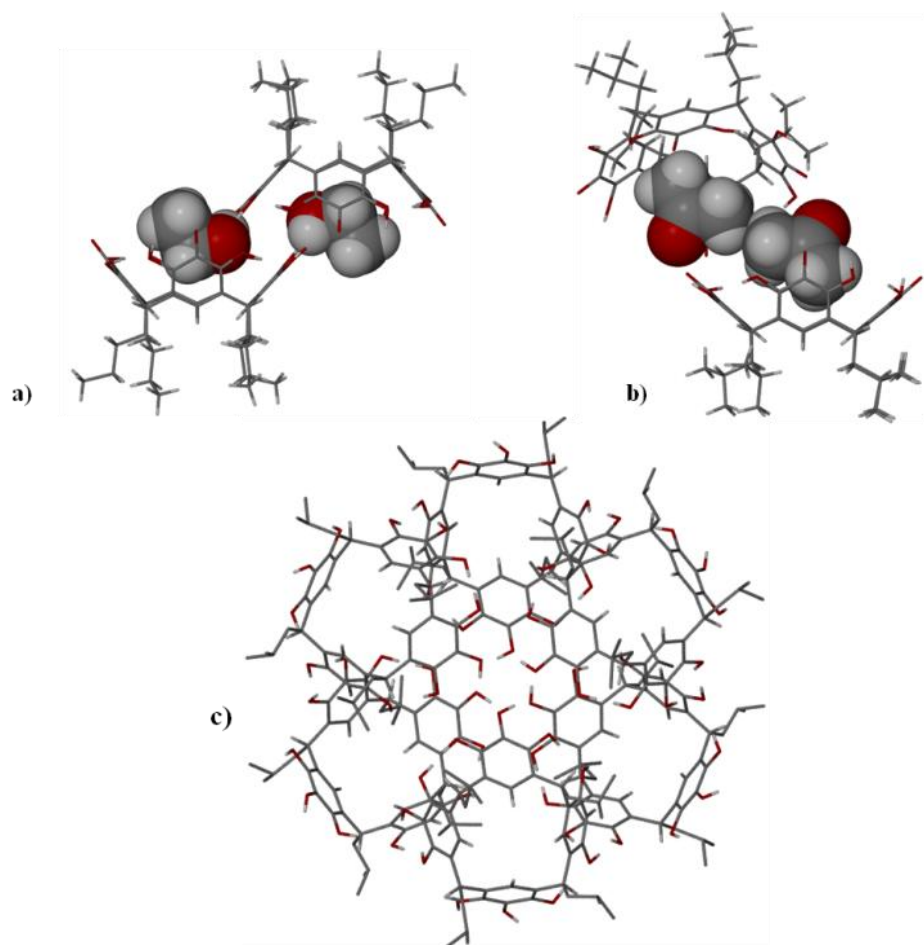
Figure 4.1: a) Crystallographic image of compound **4.1** showing host-guest interactions between the mixed macrocycle and ethanol (space-filled). b) Crystallographic image of compound **4.2** showing host-guest interactions between the mixed macrocycle and acetone (space-filled). c) Crystallographic image of a previously reported mixed macrocycle[178] organized into hexameric orientation for comparison. Hydrogen atoms on alkyl chains and all solvent molecules omitted for clarity. O: red, C: grey, H: white.

4.3 Solid-state investigation of various superstructures using mixed macrocycles as building blocks

This discussion aims to describe two unique superstructures found for similar mixed macrocyclic compounds produced from different solvent systems. Mixed macrocycle **4.1** in ethanol affords an off-set hydrogen-bonded dimer with the inclusion of solvent guest molecules. This dimer exhibits host-guest intermolecular interactions (**Figure 4.2**), but no hydrogen-bonding interactions with adjacent dimers. The thermal parameters of the central oxygen atom were estimated by comparison to adjacent oxygen atoms. Once refined, those calculated thermal parameters were used to solve for the partial occupancies of the central oxygen atoms. The four partial site occupancy factors (SOF) on these atoms range from 0.177 - 0.849 (**Table 4.1**), and add up to 2.293 total oxygen atoms per macrocycle, indicating the presence of both 2:2 and 1:3 ratios of resorcinol:pyrogallol mixed macrocycles.

Table 4.1: Solved partial occupancies of the central oxygen atom of compounds **4.1** and **4.2**.

Compound 1		Compound 2	
Atom Label	**S.O.F.**	**Atom Label**	**S.O.F.**
O(2)	0.711(9)	O(2)	0.713(12)
O(5)	0.177(11)	O(5)	0.673(13)
O(8)	0.556(9)	O(8)	0.308(12)
O(11)	0.849(9)	O(11)	0.636(12)
Total S.O.F	**2.293**	**Total S.O.F**	**2.330**

Also of interest is the unique off-set arrangement of the dimer, which is stabilized through not only hydrogen bonding from upper macrocycle to lower macrocycle but also interactions of host to guest and host to adjacent guest. There are two (2) C–H···π host-to-guest interactions with H-to-centroid distances of 2.70 Å and 2.82 Å and with angles around 160°. Interactions between the upper guest to lower macrocycle and vice versa result in two hydrogen bonds, O(6)–H(6O)···O(13solvent) and, depending on the central oxygen occupancy, O(5)–H(5O)···O(13solvent) with O-to-O distances of 2.65 Å and 2.59 Å, respectively. In addition, host-to-host O(7)–H(7O)···O4' hydrogen bonds of 2.84 Å act as tethers connecting lower and upper hemispheres.

A striking difference between inclusion system **4.1** and most standard calix[4]arene dimers[157-161] is that the top hemisphere is shifted 2.56 Å off center. Equally important is the relatively weak stability of the system as judged by the total

number of intermolecular interactions between the upper and lower macrocycles. There is essentially no interaction between adjacent dimeric systems, and thus each dimer is deemed an independent hydrogen-bonded entity. Within a given hydrogen-bonded dimer the centroid-to-centroid distance is 10.45 Å; between adjacent dimers the centroid-to-centroid distance is 11.20 Å (**Figure 4.2**).
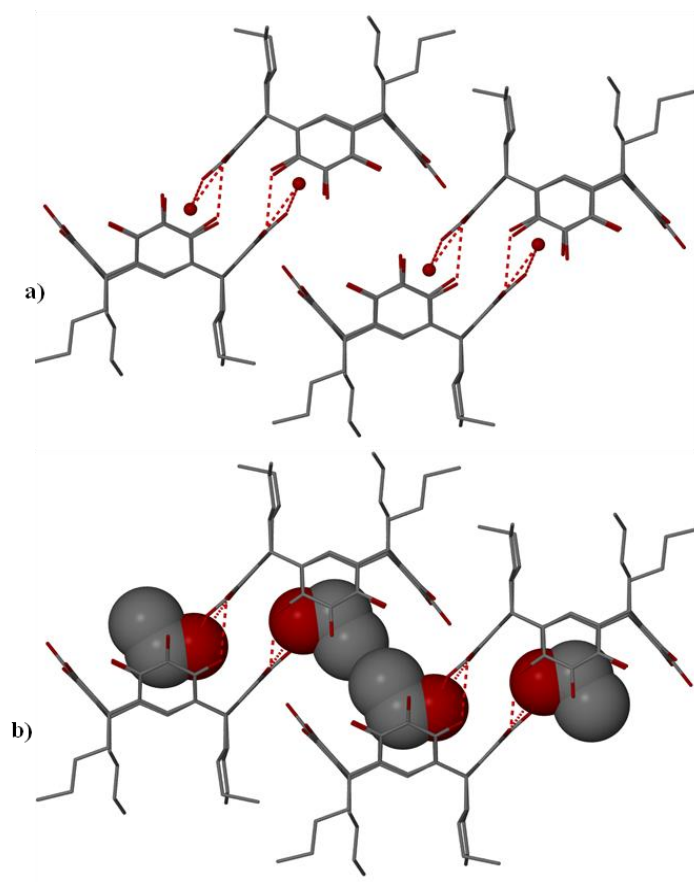
Figure 4.2: Compound **4.1** showing the macrocycle to macrocycle and macrocycle to guest hydrogen-bonding. a) Hydrogen bonds (dashed red); only the oxygen on the guest is shown for clarity b) Solvent guest shown as space-filled. O: red, C: grey. Hydrogen atoms removed for clarity.

Mixed macrocycle **4.2**, an inclusion complex that contains acetone and water, shows an intricate hydrogen-bonding network in the solid-state (**Figure 4.3**). This network is orchestrated by interactions between solvent molecules and individual macrocycles that create spiral tube-like assemblies, rather than individual dimeric entities. The network utilizes adjacent macrocycles to seam the exterior of the tubes. (**Figure 4.4**) As opposed to the nanotubes synthesized by Rissanen *et al.*[162] and Dalgarno *et al.,*[163] in which the hydrogen bonding interactions are accompanied by C–H⋯π and π⋯π interactions between macrocycles, the resulting nanotubes formed by **4.2** are devoid of the latter interactions. The partial occupancies of the four central oxygen atoms were determined in the same manner as previously stated, giving a total of 2.330 central oxygen atoms per macrocycle (**Table 1**), remarkably similar to compound **4.1**. Again this number of central oxygen atoms demonstrates the presence of both 2:2 and 1:3 ratios of resorcinol:pyrogallol mixed macrocycles. Alternating vertical centroid-to-centroid distances of 11.449 Å and 12.968 Å (**Figure 4.3b**) as well as a horizontal centroid-to-centroid distance of 13.526Å (**Figure 4.3a**) are repeated along the infinite channel. The distance along the x-axis of 15.222Å and the distance along the y-axis of 8.948Å (Figure **4.4a**) indicate the size of the internal void, which is large enough for solvent to mediate tube closure. In compound **4.22** there are three (3) C–H⋯π
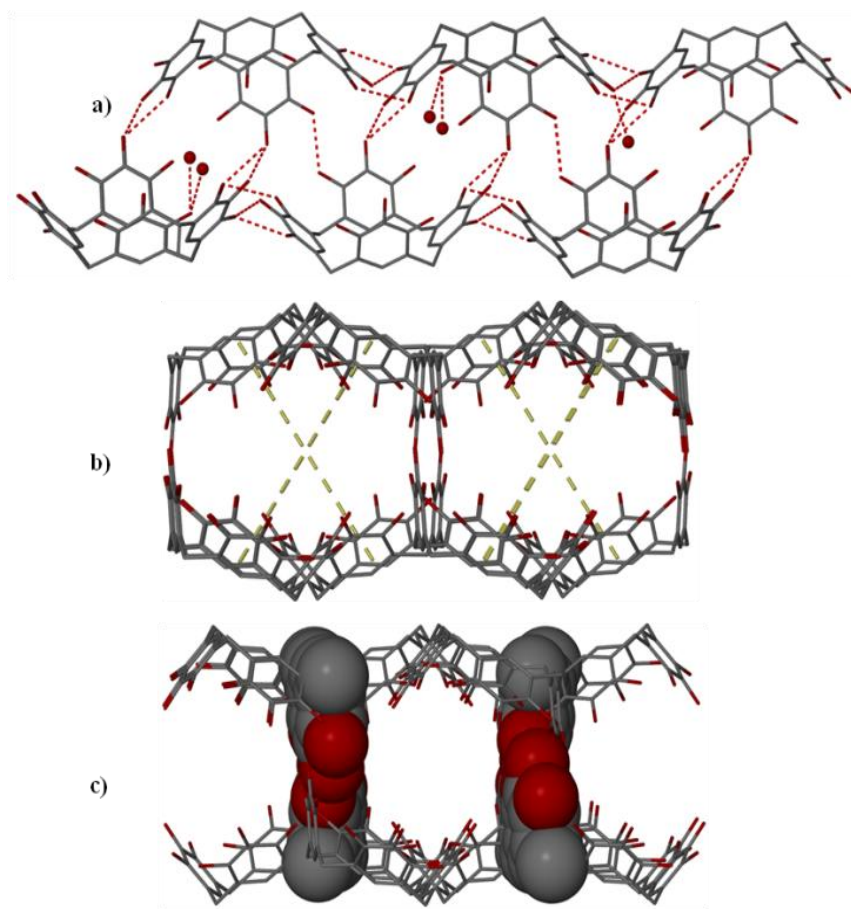
Figure 4.3: a) Hydrogen-bonding network of **4.2** shown as dashed red lines. H_2O and acetone shown as single entities. b) Alternating centroid-centroid distances shown as dashed gold lines. c) Macrocycles from adjacent layers aid in tube closure, shown as space-filled. O: red, C: grey. (Side chains and hydrogen atoms removed for clarity)

interactions with distances of 2.68Å, 2.72Å, and 2.95Å and angles of about 160°. Similar to the hydrogen bonding in compound **4.11**, solvent guest from the lower macrocycle bonds to the upper macrocycle with an O(11)–H(11O)···O(13solvent) distance of 2.71Å. Host-to-host intermolecular hydrogen bonds all fall within an acceptable range of 2.74-3.00Å.
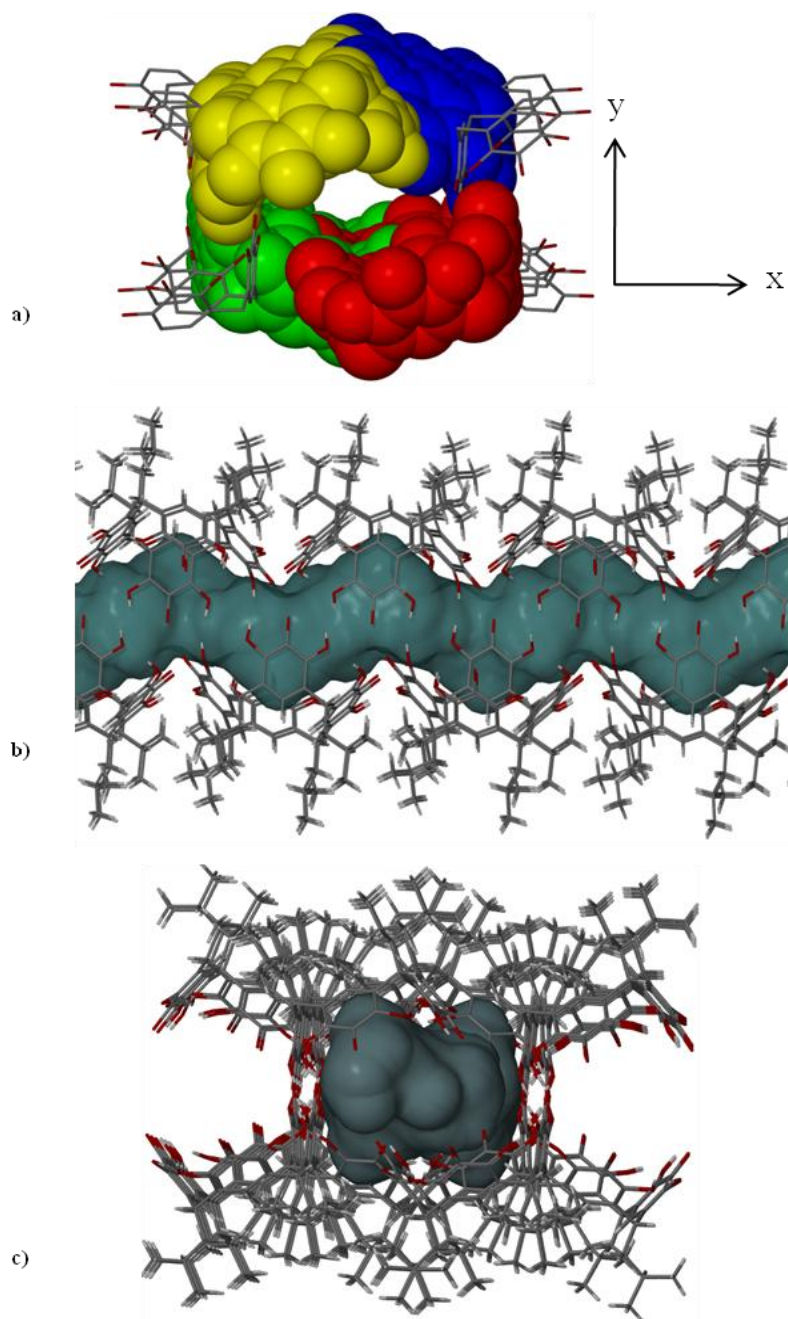
Figure 4.4: a) Tube-like assembly of mixed macrocycle **2** in the presence of H_2O and acetone. Central macrocycles shown as space-filled atoms in various colors to illustrate the spiral effect. Side chains and solvent omitted for clarity. b) Void channel is shown in aqua as calculated by MSroll[164]. c) Side view of b rotated 90°. O: red, C: grey, H: white.

4.4 Conclusions

Nature utilizes both intra- and intermolecular forces to create useful self-assembled entities. To tackle today's problems, scientists endeavor to mimic nature's self-assembly processes and in doing so continue to gain information about such processes. Here, we have shown that while the synthesis of large mixed macrocycles can be accomplished with ease, the self-assembly of these macrocycles into supramolecular entities is a complex process made much more so by the array of functionality presented by such mixed macrocycles. Single crystal XRD was used to calculate the partial occupancies of the central oxygen atoms in the supramolecular entities formed from resorcinol:pyrogallol mixed macrocycles, which indicate the predominance of 2:2 and 1:3 products in the overall mixtures. It was also shown that solvent interactions play an integral role in selective crystallization. We have identified two hydrogen-bonded self-assembled entities, a dimer and a nanotube. These two structures contain pendant R-groups with similar properties leading to the conclusion that packing effects play only a minor role in determining the outcome of the solid-state structure. Further research is still needed to understand the effects that a wider range of solvents would impose.

4.5 Experimental Section

Crystallographic data for Inclusion complex 4.1: $C_{48}H_{68}O_{12.27}$, $M = 776.72$g/mol, $\rho = 1.232$g/cm^3, $a = 10.940(5)$, $b = 12.189(5)$, $c = 17.454(10)$, $\alpha = 78.497(6)$, $\beta = 87.202(7)$, $\gamma = 84.105(4)$, $U = 2268(2)$Å^3, triclinic, space group P -1 Z = 2, λ(Mo) =

.71073 Å, T=173 K, 9178 reflections, 4562 unique R_1= .0766, wR_2= .2696 (all data), GOF= 1.054

Crystallographic data for inclusion complex 4.2: $C_{46.22}H_{65.73}O_{13.72}$, M = 840.80g/mol, ρ = 1.206g/cm^3, a = 39.531(7), b = 10.5545(18), c = 23.913(9), α = 90, β = 111.845(2), γ = 90, U = 9261(3)Å^3, monoclinic, space group C2/c Z = 8, λ(Mo) = .71073 Å, T=173 K, 9470 reflections, 5027 unique R_1= .0834, wR_2= .3028 (all data), GOF= 1.030

Appendix A

C-phenylpyrogallol[4]arene 2.1

PgPh stability (0wk old sample)_dmso_1H NMR_4.28.11

_C_-4-methylpyrogallol[4]arene 2.2

1H NMR Pg(4-Me)Ph

7.809
7.525
7.388

6.744
6.684
6.658
6.615
6.470
6.444

5.947
5.603
5.202

3.449
3.425
3.375

2.987
2.763
2.637
2.585
2.537
2.496
2.305
2.226
2.212
2.134

4.03

2.33
2.13
0.67
1.00
0.44

ppm
8.5 8.0 7.5 7.0 6.5 6.0 5.5 5.0 4.5 4.0 3.5 3.0 2.5 2.0 1.5

132

_C_-4-ethylpyrogallol[4]arene 2.3

1H NMR Pg(4-Et)Ph in d6DMSO

133

_C_-3-nitrophenylpyrogallol[4]arene 2.4

1H NMR Pg(3-NO2)Ph

2.530

3.404

4.521

5.823
5.914

7.128

7.395

7.893
7.923
7.987
8.086

21.76

0.50

1.61

7.59

ppm
2.5
3.0
3.5
4.0
4.5
5.0
5.5
6.0
6.5
7.0
7.5
8.0

_C_-4-nitrophenylpyrogallol[4]arene 2.5

1H NMR Pg(4-NO2)Ph

_C_-3-hydroxyphenylpyrogallol[4]arene 2.6

1H NMR Pg(3-OH)Ph recrystallized in d6-DMSO

2.304
2.435
2.457
2.459
2.460
2.461
2.486
2.491
2.497
2.503
2.536
2.763

3.155
3.169

3.389
3.438

5.459
5.604

5.960
6.068

6.667

7.438
7.564
7.717
7.811

8.708

ppm

2.5
3.0
3.5
4.0
4.5
5.0
5.5
6.0
6.5
7.0
7.5
8.0
8.5
9.0

0.50
0.05
1.42

0.40

0.46
0.96

0.50
1.95
1.03

0.98

0.96
1.00
0.51
0.47

1.01

_C_-4-hydroxyphenylpyrogallol[4]arene 2.7

1H NMR Pg(4-OH)Ph in d6-DMSO

2.304
2.489
2.492
2.498
2.537
2.763
3.444
5.532
5.562
5.936
6.308
6.331
6.393
6.421
7.321
7.493
7.695
7.785
8.710

0.49
1.00
0.48
4.27
0.99
1.01
1.09
1.10

ppm
2.5
3.0
3.5
4.0
4.5
5.0
5.5
6.0
6.5
7.0
7.5
8.0
8.5

***C*-2-methoxyphenylpyrogallol[4]arene 2.8**

1H NMR Pg(2-OMe)Ph isolated rcccc

_C_-4-methoxyphenylpyrogallol[4]arene 2.9

1H NMR Pg4(OMe)Ph

8.675

7.775
7.685
7.484
7.313

6.419
6.391
6.333
6.305

5.936

5.567
5.534

3.368

2.530

ppm

2.0

2.5   7.68

3.0

3.5   2.68

4.0

4.5

5.0

5.5   0.56
       1.00

6.0   0.50

6.5   4.28

7.0

7.5   1.01
       1.03
       0.52
       0.51

8.0

8.5   1.04

_C_-4-propoxylphenylpyrogallol[4]arene 2.10

1H NMR Pg(4-propoxy)Ph in d6-DMSO
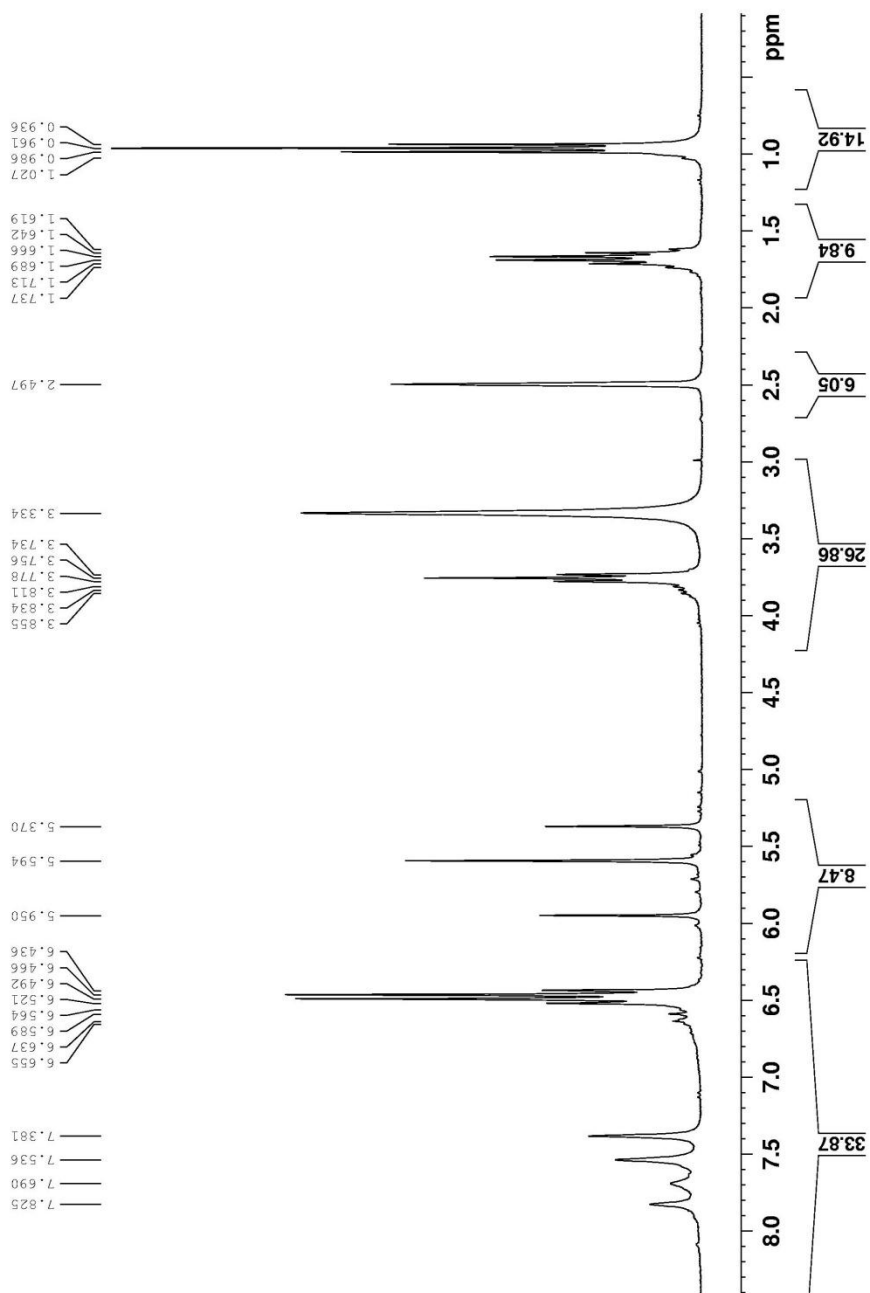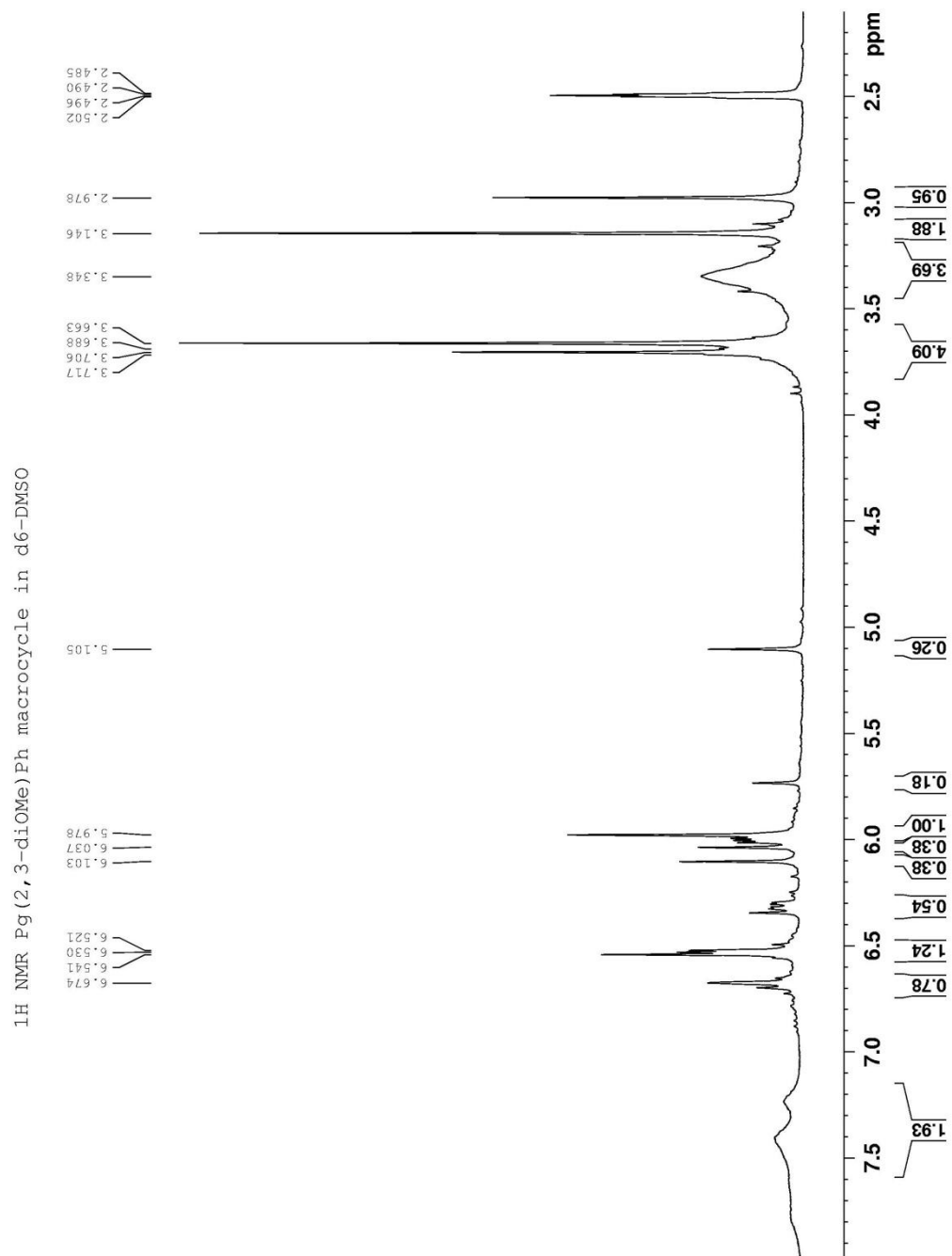
0.936
0.961
0.986
1.027

1.619
1.642
1.666
1.689
1.713
1.737

2.497

3.334

3.734
3.756
3.778
3.811
3.834
3.855

5.370

5.594

5.950

6.438
6.466
6.492
6.521
6.564
6.589
6.637
6.655

7.381
7.536
7.690
7.825

ppm

14.92

9.84

6.05

26.86

8.47

33.87

1.0
1.5
2.0
2.5
3.0
3.5
4.0
4.5
5.0
5.5
6.0
6.5
7.0
7.5
8.0

C-2,3-methoxyphenylpyrogallol[4]arene 2.12

1H NMR Pg(2,3-diOMe)Ph macrocycle in d6-DMSO

_C_-3,4,5-trimethoxyphenylpyrogallol[4]arene 2.18

1H NMR Pg(3,4,5-triOMe)Ph in d6-DMSO

Peaks: 2.267, 2.461, 2.499, 2.551, 2.726, 3.269, 3.351, 3.384, 3.441, 5.360, 5.541, 5.948, 7.231, 7.521, 7.655, 7.681

Integrations: 0.80, 0.88, 1.88, 4.03, 1.19, 0.45, 1.00, 1.85, 0.79, 0.13, 2.94
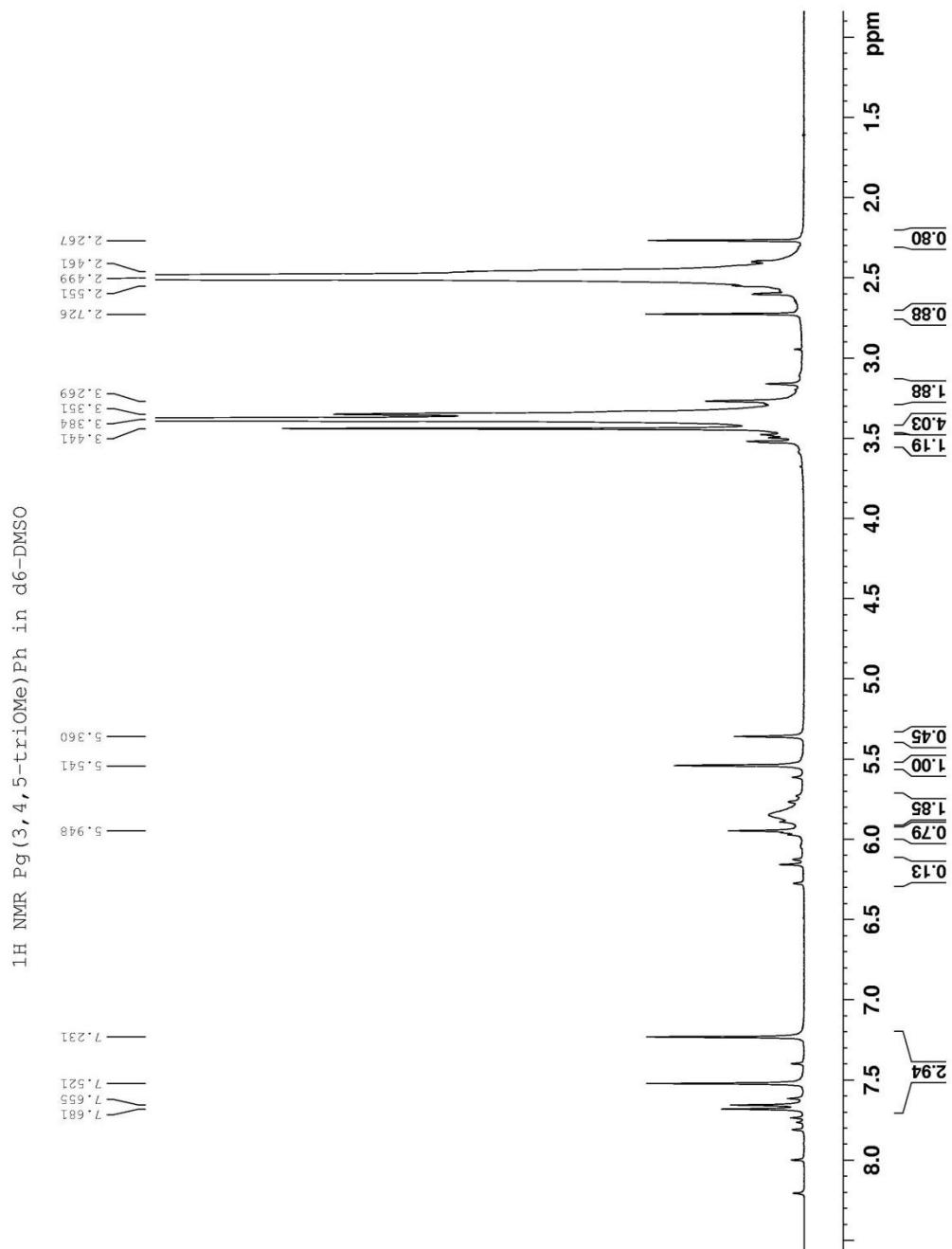
[Zn₈(*C*-phenylpyrogallol[4]arene)₂(Pyridine)₈⊂(Pyridine)] 3.2

1H NMR
ZnPgCC6H5 Dimer Pyr

Current Data Parameters
NAME   AKM1-28-08
EXPNO   1
PROCNO   1

F2 - Acquisition Parameters
Date_   20080128
Time   14.51
INSTRUM   DRX300
PROBHD   5 mm Multinucl
PULPROG   zg30pad
TD   32768
SOLVENT   Acetone
NS   16
DS   2
SWH   7183.908 Hz
FIDRES   0.219235 Hz
AQ   2.2807028 sec
RG   228.1
DW   69.600 usec
DE   6.00 usec
TE   300.0 K
D1   1.00000000 sec
D31   0.00000000 sec

======== CHANNEL f1 ========
NUC1   1H
P1   7.05 usec
PL1   0.00 dB
SFO1   300.1324010 MHz

F2 - Processing parameters
SI   32768
SF   300.1301033 MHz
WDW   EM
SSB   0
LB   0.30 Hz
GB   0
PC   1.30

References

[1] J.-M, Lehn, *Proc. Nat. Acad. Sci.*, 2002, **99**, 4763-4768.

[2] J. W. Steed, J. L. Atwood, "*Supramolecular Chemistry*". New York; Wiley and Sons. 2009 p. 2.

[3] L. R. MacGillivray, J. L. Atwood, *Angew. Chem. Int. Ed.*, 1999, **38**, 1018-1033.

[4] D. M. Haddleton, R. N. Perutz, *J. Chem. Soc. Chem. Commun.*, 1985 1372.

[5] E. P. Kyba, R. C. Helgeson, K. Madan, G. W. Gokel, T. L. Tranowski, S. S. Moore, and D. J. Cram, *J. Am. Chem. Soc.*, 1977, **99**, 2564-2571.

[6] J. Rebek Jr., *Acc. Chem. Res.,* 1999, **32**, 278-286.

[7] P. A. Gale, R. Quesada, *Coord. Chem. Rev.*, 2006, 3219.

[8] B. T. Nguyen, S. L. Wiskur, E. V. Anslyn, *Org. Lett.*, 2004, **15**, 2499-2501.

[9] S. L. Wiskur, E. V. Anslyn, *J. Am. Chem. Soc.,* 2001, **123**, 10109.

[10] H. Ait-Haddou, S. L. Wiskur, V. M. Lynch, E. V. Anslyn, *J. Am. Chem. Soc.*, 2001, **123**, 11296.

[11] S. L. Tobey, E. V. Anslyn, *Org. Lett.,* 2003, 5**,** 2029.

[12] K. Niikura, A. P. Bisscon, E. V. Anslyn, *J. Chem. Soc., Perkin Trans.*, 1999, **2**, 1111.

[13] S. L. Wiskur, H. Ati-Haddou, J. J. Lavinge, E. V. Anslyn, *Acc. Chem. Res*., 2001, **34**, 963.

[14] Z. Zhong, E. V. Anslyn, *J. Am. Chem. Soc.,* 2002, **124**, 9014.

[15] J. J. Lavinge, E. V. Anslyn, *Angew. Chem., Int. Ed.,* 1999, **38**, 3666.

[16] F. Hapiot, S. Tilloy, E. Monflier, Chem. Rev., 2006, **106**, 767

[17] J. Szejtli, *Chem. Rev*., 1998, **98**, 1743

[18] R. Breslow, S. D. Dong, *Chem. Rev.*, 1998, **98**, 1997.

[19] A. Harada, Y. Takashima, H. Yamaguchi, *Chem. Soc. Rev.*, 2009, **38**, 875.

[20] F. Sallas, R. Darcy, *Eur. J. Org. Chem.*, 2008, 957-969.

[21] R. Wyler, J. Demendoza, J. Rebek Jr., *Angew. Chem. Int. Ed. Engl.*, 1993, **32**, 1699-1701.

[22] K. Kim. N. Selvapalam, Y. H. Ko, K. M. Park, D. Kim, J. Kim, *Chem. Soc. Rev.*, 2007, **36**, 267-279.

[23] V. Sindelar, S. Silvi, A. E. Kaifer, *Chem. Commun.*, 2006, 2185.

[24] Y. J. Jeon, S. Y. Kim, Y. H. Ko, S. Sakamoto, *Organic&Biomolecular Chemistry*, 2005, **3(11)**, 2122.

[25] D. R. Turner, M. J. Paterson, J. W. Steed, *J. Org. Chem.*, 2006, **71**, 1598-1608.

[26] J. P Mathis, J. F. Stoddart, *Chem. Soc. Rev.*, 1992, **21**, 215-225.

[27] W. H. Powell, *Pure Appl. Chem.,* 1998, **70**, 1513-1545.

[28] H. A. Favre, D. Hellwinkel, W. H. Smith, S. S. C. Tsay, *Pure and Appl. Chem.*, 2002, **74**, 809-834.

[29] K. T. Holman, M. M. Halihan, J. W. Steed, S. S. Jurisson, J. L. Atwood, *J. Am. Chem. Soc.*, 1995, **117**, 7848-7849.

[30] J. W. Steed, P. C. Junk, J. L. Atwood, *J. Am. Chem. Soc.*, 1994, **116**, 10346-10347.

[31] D. J. Cram, J. Weiss, R. C. Helgeson, C. B. Knobler, A. E. Dorigo, K. N. Houk, *J. Chem. Soc., Chem. Commun.*, 1988, 407-409.

[32] A. Zinke, R. Kretz, E. Leggewie, K. Hossinger, *Monatsh.*, 1952, **83**, 1213.

[33] J. B. Niedler, H. J. Vogel, *J. Am. Chem. Soc.*, 1940, **62**, 2521.

[34] J. W. Cornforth, E. D. Morgan, K.T. Potts, and R. J. W. Rees, *Tetrahedron*, 1973, **29**, 1659.

[35] C. D. Gutsche, A.E. Gutsche, A. I. Karaulov, *J. Inclusion Phenom.*, 1985, **3**, 447.

[36] C. D. Gutsche, Calixarenes: An introduction, Monographs in Supramolecular Chemistry, 2nd Edition; J. F. Stoddart, Ed.; The Royal Society of Chemistry: Cambridge, 2008.

[37] C. D. Gutsche, R. Muthukrishnan, *J. Org. Chem.*, 1978, **43**, 4905.

[38] W. Sliwa, C. Kozlowski, Calixarenes and Resorcinarenes: Synthesis, Properties, and Applications; Wiley-VCH: Weinheim, 2009.

[39] F. Hajek, E. Graf, M. W. Hosseini, X. Delaigue, A. DeCian, J. Fissher, *Tetra. Lett.*, 1996, **37**, 1401-1404.

[40] H. Li, F. Qu, *J. Mater. Chem.*, 2007, **17**, 3536.

[41] S. G. Bott, A. W. Coleman, J. L. Atwood, *J. Am. Chem. Soc.*, 1986, **108**, 1709-1710.

[42] A. Ikeda, H. Tsuzuki, S. Shinkai, *J. Chem. Soc., Perkin Trans.*, 1994, **2**, 2073-2080.

[43] F. ArnaudNeu, Z. Asfari, B. Souley, J. Vicens, *New J. Chem.*, 1996, **20**, 453-463.

[44] S. J. Dalgarno, P. K. Thallapally, L. J. Barbour, J. L. Atwood, *Chem. Soc. Rev.*, 2007, **36**, 236-245.

[45] D. C. Jeunesse, D. Matt, L. Toupet, *Angew. Chem., Int. Ed.*, 2006, **45**, 5810.

[46] a) G. J. Yang, J. J. Xu, K. Wang, H. Y. Chen, *Electroanalysis*, 2006, **18**, 282.

[47] C. Y. Liu, G. H. Lu, L. Y. Jiang, L. P. Jiang, X. C. Zhou, *Electroanalysis*, 2006, **18**, 291.

[48] H. Liu, G. Zhao, L. Wen, B. Ye, *J. Anal. Chem.*, 2006, **61**, 1104.

[49] Ch. Liu, Z. Fu, H. Yu, H. Xu, L. Wang, Y. Zhou, *J. Luminescence*, 2007, **126**, 747.

[50] A. Jasat, J. C. Sherman, *Chem. Rev.*, 1999, **99**, 931-967.

[51] L. J. Prins, J. Huskens, F. de Jong, P. Timmerman, D. N. Reinhoudt, *Nature*, 1999, **398**, 498-502.

[52] L. R. MacGillivray, J. L Atwood, *Nature*, 1997, **389**, 469-472.

[53] E. V. Anslyn, D. A. Dougherty, *Modern Physical Organic Chemistry*, University Science Books, Sausalito, CA, USA, 2006, pp.162-241.

[54] I. Dane, 'π-π Interactions: Theory and Scope', in *Encyclopedia of Supramolecular Chemistry*, J. L., Atwood, J. W. Steed, eds, Marcel Dekker; New York, 2004; vol. 2, pp. 1076-1079.

[55] O. B. Berryman, V. S. Bryantsev, D. P. Stay, D. W. Johnson, B. P. Hay, *J. Am. Chem., Soc.*, 2007, **129**, 48.

[56] Y. S. Rosokha, S. V. Lindeman, S. V. Rosokha, J. K. Kochi, *Angew. Chem., Int. Ed.*, 2004, **43**, 4650.

[57] C. A. Deakyne, M. Mautner, *J. Am. Chem. Soc.*, 1999, **121**, 1546-1557.

[58] F. Perret, A. N. Lazar, O. Shkurenko, K. Suwinska, N. Dupont, A. Navaza, and A. W. Coleman, *CrystEngComm.*, 2006, **8**, 890-894.

[59] A. N. Lazar, N. Dupont, A. Navaza, and A. W. Coleman, *Chem. Commun.,* 2006, 1076-1078.

[60] L. Mahalakshmi, P. P. Das, T. N. Guru Row, *J. Chem. Sci.,* 2008, **120**, 39-44.

[61] L. J. Hubble, T. E. Clark, M. Makha, and C. L. Raston, *J. Mater. Chem.,* 2008, **18**, 5961-5966.

[62] O. V. Kulikov, M. M. Daschbach, C. R. Yamnitz, N. Rath, and G. W. Gokel, *Chem. Commun.,* 2009, 7497-7499.

[63] S. J. Dalgarno, J. E. Warren, J. Atesberger, T. E. Glass, and J. L. Atwood, *New J. Chem.,* 2007, **31**, 1891-1894.

[64] S. Kennedy, and S. J. Dalgarno, *Chem. Commun.,* 2009, 5275-5277.

[65] Y. Rudzevich, V. Rudzevich, and V. Böhmer, *Chem. Eur. J.,* 2010, 4541-4549.

[66] N. P. Power, S. J. Dalgarno, and J. L. Atwood, *Angew. Chem., Int. Ed.,* 2007, **46**, 8601.

[67] A. K. Maerz, H. M. Thomas, N. P. Power, C. A. Deakyne, and J. L. Atwood, *Chem. Commun.,* 2010, **46**, 1235-1237.

[68] Dalgarno, T. Szabo, A. Siavosh-Haghighi, C. A. Deakyne, J. E. Adams, and J. L. Atwood, *Chem. Commun.,* 2009, 1339-1341.

[69] B. Schnatwinkel, I. Stoll, A. Mix, M. V. Rekharsky, V.V. Borovkov, Y. Inoue, and J. Mattay, *Chem. Commun.,* 2008, 3873-3875.

[70] E. S. Barrett, T. J. Dale, J. Rebek Jr., *JACS,* 2008, **130**, 2344-2350.

[71] M. W. Heaven, G. W. V. Cave, R. M. McKinlay, J. Antesberger, S. J. Dalgarno, P. K. Thallapally, and J. L. Atwood, *Angew. Chem., Int. Ed.,* 2006, **45**, 6221-6224.

[72] A. G. S. Hogber, *J. Am. Chem. Soc.* 1980 **102** 6046-6050.

[73] L. M. Tunstad, J. A. Tucker, E. Dalcanale. J. Weiser, J. A. Byrant, J. C. Sherman, R. C. Helgeson, C. B. Knobler, D. *J. Cram, J. Org. Chem.* 1989 **54** 1305-1312.

[74] P. Timmerman, W. Verboom, D. N. Reinhoudt, *Tetrahedron* 1996 **52** 2663-2704.

[75] J. B. Niederl, H. J. Vogel, *J. Am. Chem. Soc.,* 1940, **62**, 2512.

[76] B. Nilsson, *Acta Chem. Scand.,* 1968, **22**, 7321.

[77] A. G. S. Hogberg, *J. Am. Chem. Soc.,* 1980, **102**, 6046.

[78] H. Erdtman, S. Hogberg, S. Abrahamsson, B. Nilsson, *Tetrahedron Lett.,* 1968, 1679.

[79] K. J. Palmer, R. Y. Wong, L. Jurd, K. Stevens, *Acta. Cryst.,* 1976, *B32*, 847.

[80] L. M. Tunstad, J. A. Tucker, E. Dalcanale, J. Weiser, J. A. Bryant, J. C. Sherman, R. C. Helgeson, C. B. Knobler, D. J. Cram, *J. Org. Chem.*,

1989, **54**, 1305.

[81] S. F. Alshahateet, F. Kooli, M. Messali, Z. M. A. Judeh, A. S. ElDouhaibi, *Mol. Cryst. Liq. Cryst.,* 2007, **474**, 89.

[82] B. Schnatwinkel, I. Stoll, A. Mix, M. V. Rekharsky, V. V. Borokov, Y. Inoue, J. Mattay, *Chem. Commun.,* 2008, 3873.

[83] T. Harada, F. Ohseto, S. Shinkai, *Tetrahedron*, 1994, **50**, 13377-13394.

[84] O. Morikawa, E. iyama, T. Oikawa, K. Kobayashi, H. Konishi, *J. Phys. Org. Chem.,*(2006, **19**, 214.

[85] J. P. Kass, C. H. Zambrano, M. Zeller, A. D. Hunter, E. E. Dueno, *Acta Cryst.* 2006 **E62** o3179.

[86] C. H. Zambrano, J. P. Kass, E. E. Dueno, Y. Ke, H. C. Zhou, *J. Chem. Cryst.*, 2006, **1**, 67.

[87] J. Han, X. Song, L. Liu, C. Yan, *J.Inclusion Phenom.Macrocyclic Chem.,* 2007, *59*, 257.

[88] C. Yan, W. Chen, J. Chen, T. Jiang, Y. Yao, *Tetrahedron,* 2007, **63**, 9614.

[89] T.Gerkensmeier, C.Agena, W.Iwanek, R.Frohlich, S.Kotila, C.Nather, J.Mattay, *Z.Naturforsch.,B: Chem.Sci.,* 2001, **56**, 1063.

[90] A. K. Maerz, H. M. Thomas, N. P. Power, C. A. Deakyne, J. L. Atwood, *Chem. Commun*., 2010, **46**, 1235-1237.

[91] This was a joint collaboration project with Dr. Haunani Thomas whereby all the computational calculations were performed by Dr. Haunani Thomas.

[92] Gaussian Reference: M.J. Frisch, *et al.* Pople, Gaussian 03, Revision C.02, Gaussian, Inc., Wallingford CT, 2004.

[93] S. Tsuzuki, K. Honda, T. Uchimaru, M. Mikami, K. Tanabe, *J. Am. Chem. Soc.,* 2002, **124**, 104.

[94] M.O. Sinnokrot, E.F. Valeev, C.D. Sherrill, *J. Am. Chem. Soc.,* 2002, **124**, 10887.

[95] S. Miertuš, E. Scrocco, and J. Tomasi, *Chem. Phys.*, 1981,**55**, 117-29.

[96] S. Miertuš and J. Tomasi, *Chem. Phys.*, 1982, **65**, 239-245.

[97] J. L. Pascual-Ahuir, E. Silla, and I. Tuñón, *J. Comp. Chem.*, 1994, **15**, 1127-38.

[98] T. Gerkensmeier, W. Iwanek, C. Agena, R. Frohlich, S. Kotila, C. Nather, J. Mattay, *Eur. J. Org. Chem.,*1999, 2257.

[99] N. P. Power, S. J. Dalgarno, J. L. Atwood, *Angew. Chem. Int. Ed.,* 2007, **46**, 8601.

[100] C. Schiel, G. A. Hembury, V. V. Borovkov, M. Klaes, C. Agena, T. Wada, S. Grimme, Y. Inoue, J. Mattay *J. Org. Chem.,* 2006, **71**, 976.

[101] V. I. Maslennikova, O. S. Serkova, M. Gruner, S. Goutal, I. Bauer, W. D. Habicher, K. A. Lyssenko, M. Y. Antipin, E. E. Nifantyev, *Eur. J. Org. Chem.*, 2004, 4884-4893.

[102] S. Miao, R. D. Adams, D. Guo, Q. Zhang, *J. Mol. Struct.*, 2003, **659**, 119-128.

[103] N. K. Beyeh, K. Rissanen, *Tetra. Lett*., 2009, **50**, 7369-7373.

[104] Most of the solid-state structures were refined by fellow co-worker Drew. A. Folwer, however because all synthesis was performed by the author, the author will only comment on the solid-state structural analysis and not the refinement parameters.

[105] E. S. Barrett, T. J. Dale, J. Rebek, Jr., *J. Am. Chem. Soc*., 2008, **130**, 2344-2350.

[106] L. Avram, Y. Cohen, *Org. Lett*., 2003, **5**, 3329-3332.

[107] D. B. Bassil, S. J. Dalgarno, G. W. V. Cave, J. L. Atwood, S. A. Tucker, *J. Phys. Chem. B*, 2007, **111**, 9088-9092.

[108] L. Avram, Y. Cohen, *J. Am. Chem. Soc.*, 2003, **125**, 16180-16181.

[109] E. Kalenius, N. K. Beyeh, J. Janis, K. Rissanen, *Chem. Commun.*, 2001, **47**, 2649-2651.

[110] B. Schnatwinkel, I. Stoll, A. Mix, M. V. Rekharsky, V. V. Borokov, Y. Inoue, J. Mattay *Chem. Commun.,* 2008, 3873.

[111] S. J. Dalgarno, N. P. Power, J. L. Atwood, *Coord. Chem. Rev.,* 2008, **252**, 825.

[112] A. Sasat, J. C. Sherman, *Chem. Rev.*, 1999, **99**, 931-967.

[113] L. R. MacGillivray, J. L. Atwood, *Nature* 1997, **389**, 469.

[114] D. J. Cram, S. Karback, Y. H. Kim, L. Baczynskyj, G. W. Kalleymeyn, *J. Am. Chem. Soc.*, 1985, **107**, 2575-2576.

[115] J. R. Fraser, B. Borecka, J. Trotter, J. C. Sherman, *J. Org. Chem.*, 1995, **60**, 1207-1213.

[116] P. Timmerman, W. Verboom, F. Vanveggel, W. P. Vanhoorn, D. N Reinhoudt, *Angew. Chem., Int. Ed. Engl.*, 1994, **33**, 1292-1295.

[117] P. Timmerman, W. Verboom, F. Vanveggel, W. P. Vanhoorn, D. N Reinhoudt, *Angew. Chem., Int. Ed. Engl.*, 1994, **33**, 1292-1295.

[118] R. G. Chapman, G. Olovsson, J. Trotter, J. C. Sherman, *J. Am. Chem. Soc.*, 1998, **120**, 6252-6260.

[119] P. Jacopozzi, E. Dalcanale, *Angew. Chem. Int. Ed. Engl.*, 1997, **36**, 613-614.

[120] O. D. Fox, N. K. Dalley, R. G. Harrison, *J. Am. Chem. Soc.*, 1998, **120**, 7111-7112.

[121] P. Neri, A. Bottino, F. Cunsolo, M. Piattelli, E. Gavuzzo, *Angew. Chem. Int. Ed.*, 1998, **37**, 166-169.

[122] R. K. Castellano, D. M. Rudkevich, J. Rebek, Jr. *J. Am. Chem. Soc.,* 1996, **118**, 10002.

[123] N. P. Power, S. J. Dalgarno, and J. L. Atwood, *New J. Chem.*, 2007, **31**, 17-20.

[124] P. Jin, S. J. Dalgarno, J. E. Warren, S. J. Teat, J. L. Atwood, *Chem. Commun.,* 2009, 3348.

[125] T. Gerkensmeir, W. Iwanek, C. Agena, R. Frohlich, S. Kotila, C. Nather, J. Mattay, *Eur. J. Org. Chem.,* 1999, 2257.

[126] Synthesis and Purification of PgC_1 was carried out by a fellow co-worker Andy V. Mossine.

[127] M. Karas, R. Kruger, *Chem. Rev.*, 2003, **103**, 427-439.

[128] C. Schiel, G. A. Hembur, V. V. Borovkov, M. Klaes, C. Agena, T. Wada, S. Grimme, Y. Inoue, and J. Mattay, *J. Org. Chem.*, 2006, **71**, 976-982.

[129] M. W. Wong, M. J. Frish, and K. B. Woberg, *J. Am. Chem. So.*, 1991, **113**, 4782-4791.

[130] T. Gerkensmeier, J. Mattay, and C. Nather, *Chem. Eur. J.*, 2001, **7**, 465-473.

[131] X. Ni, Y. Zhang, J. Song, and H. Zheng, *J. Crystal Growth,* 2007, **299**, 365-368.

[132] D. Chopra, T. P. Mohan, K. S. Rao, and T. N. G. Row, *CrystEngComm.*, 2005, **7**, 374-379.

[133] N. Prabhu, and K. Sharp *Chem. Rev.*, 2006, **106**, 1616-1623.

[134] S. Scheiner, and T. Kar *J. Phys. Chem. B*, 2005, **109**, 3681-3689.

[135] V. Rudzevich, Y. Rudzevich, and V. Böhmer, *Synlett*, 2009, **12**, 1887-1904.

[136] S. Sameni, C. Jeunesse, D. Matt, and J. Harrowfield, *Chem. Soc. Rev.*, 2009, **38**, 2117-2146.

[137] L. J. Prins, P. Timmerman, and D. N. Reinhoudt, *Pure & Appl. Chem.*, 1998, **70**, 1459-1468.

[138] P. Timmerman, W. Verboom, and D. N. Reinhoudt, Resorcinarenes, *Tetrahedron*, 1996, **8,** 2663.

[139] L. Avram, and Y. Cohen, *Org. Lett.*, 2008, **10**, 1505-1508.

[140] S. J. Dalgarno, T. Szabo, A. Siavosh-Haghighi, C. A. Deakyne, J. E. Adams, and J. L. Atwood, *Chem. Commun.*, 2009, 1339-1341.

[141] B. Schnatwinkel, I. Stoll, A. Mix, M. V. Rekharsky, V.V. Borovkov, Y. Inoue, and J. Mattay, *Chem. Commun.*, 2008, 3873-3875.

[142] E. S. Barrett, T. J. Dale, J. Rebek Jr., *J. Am. Chem. Soc.*, 2008, **130**, 2344-2350.

[143] M. W. Heaven, G. W. V. Cave, R. M. McKinlay, J. Antesberger, S. J. Dalgarno, P. K. Thallapally, and J. L. Atwood, *Angew. Chem., Int. Ed.*, 2006, **45**, 6221-6224.

[144] Y. Rudzevich, V. Rudzevich, and V. Böhmer, *Chem. Eur. J.*, 2010, 4541-4549.

[145] N. P. Power, S. J. Dalgarno, and J. L. Atwood, *Angew. Chem., Int. Ed.*, 2007, **46**, 8601.

[146] A. K. Maerz, H. M. Thomas, N. P. Power, C. A. Deakyne, and J. L. Atwood, *Chem. Commun.*, 2010, **46**, 1235-1237.

[147] S. J. Dalgarno, J. Antesberger, R. M. McKinlay, and J. L. Atwood, *Chem. Eur. J.*, 2007, **13**, 8248-8255.

[148] F. Perret, A. N. Lazar, O. Shkurenko, K. Suwinska, N. Dupont, A. Navaza, and A. W. Coleman, *CrystEngComm.*, 2006, **8**, 890-894.

[149] A. N. Lazar, N. Dupont, A. Navaza, and A. W. Coleman, *Chem. Commun.*, 2006, 1076-1078.

[150] L. Mahalakshmi, P. P. Das, T. N. Guru Row, *J. Chem. Sci.*, 2008, **120**, 39-44.

[151] L. J. Hubble, T. E. Clark, M. Makha, and C. L. Raston, *J. Mater. Chem.*, 2008, **18**, 5961-5966.

[152] O. V. Kulikov, M. M. Daschbach, C. R. Yamnitz, N. Rath, and G. W. Gokel, *Chem. Commun.*, 2009, 7497-7499.

[153] S. J. Dalgarno, J. E. Warren, J. Atesberger, T. E. Glass, and J. L. Atwood, *New J. Chem.*, 2007, **31**, 1891-1894.

[154] S. Kennedy, and S. J. Dalgarno, *Chem. Commun.*, 2009, 5275-5277.

[155] J. L. Atwood, L. J. Barbour, and A. Jerga, *Proc. Nat. Acad. Sci.*, 2002, **99,** 4837-4841.

[156] J.B. Niederl and H. J. Vogel, *J. Am. Chem. Soc.*, 1940, **62**, 2512-2514.

[157] M. O. Vysotsky, O. Mogck, Y. Rudzevich, A. Shivanyuk, V. Böhmer, M. S. Brody, Y. L. Cho, D. M. Rudkevich, and J. Rebek Jr., *J. Org. Chem.*, 2004, **69**, 6115-6120.

[158] R. K. Castellano, and J. Rebek Jr., *J. Am. Chem. Soc.*, 1998, **120**, 3657-3663.

[159] R. K. Castellano, C. Nuckolls, and J. Rebek Jr., *J. Am. Chem. Soc.*, 1999, **121**, 11156-11163.

[160] Y. L. Cho, D. M. Rudkevich, A. Shivanyuk, K. Rissanen, and J. Rebek Jr., *Chem. Eur. J.*, 2000, **6**, 3788-3796.

[161] Y. Rudzevich, V. Rudzevich, and V. Böhmer, *Chem. Eur. J.*, 2010, **16**, 4541-4549.

[162] H. Mansikkamaki, S. Busi, M. Nissinen, A. Ahman, and K. Rissanen, *Chem. Eur. J.*, 2006, **12**, 4289-4296.

[163] S. J. Dalgarno, G. W. V. Cave, and J. L. Atwood, *Angew. Chem., Int. Ed.*, 2006, **45**,

570-574.

[164] The program X-Seed was used for crystallographic modeling and molecular graphics. Interior void space was calculated by MSRoll, interfaced with X-Seed, using a 1.5Å probe radius. L. J. Barbour, "X-Seed – A software tool for supramolecular crystallography" *J. Supramol. Chem.* **2001***, 1,* 189-191; Connolly, M. L. *J. Mol. Graph.* **1993**, 11, 139-141.

VITA

Andrew K. Maerz was born on April 2nd, 1985 at Boone County Hospital in Columbia, Missouri. He is the only son of R. Michael Maerz and Myrna K. Maerz. He attended David H. Hickman High School in Columbia Missouri from 2000-2003. He would then graduate with a Bachelors of Science from Truman State University in Kirksville Missouri in 2007. Since August 2007, he has attended graduate school at the University of Missouri-Columbia in the Department of Chemistry where he received his doctor of Philosophy in Chemistry. Andrew has worked under the supervision of Prof. Jerry L. Atwood in the area of supramolecular chemistry working specifically on *C*-arylpyrogallol[4]arenes and metal-organic nanocapsules. After graduation, Andrew will be moving to St. Louis, Missouri with his wife, Tanya M. Maerz, continuing his education with a post doc position or finding a job in industry.